Dissertation

On

EMPIRICAL MODELING FOR A SUBMERGED ARC WELDING PROCESS FOR PREDICTING THE WELD BEAD GEOMETRY AND MICROSTRUCTURE

Submitted in the partial fulfillment of requirement for the award of the degree of

MASTER OF ENGINEERING

IN

PRODUCTION AND INDUSTRIAL ENGINEERING

Submitted by

Parveen Kumar
Regn.No:80782007

Under the Guidance of

Dr. Ajay Batish
Associate Professor, MED
Thapar University, Patiala

Mr. R.K. Duvedi
Lecturer, MED
Thapar University, Patiala

DEPARTMENT OF MECHANICAL ENGINEERING

THAPAR UNIVERSITY

PATIALA -147004, INDIA

ACKNOWLEDGEMENT

Primarily, I acknowledge this moment of time, which has gone just forever, but made my mind to write the words for those who have been with me with their ever-whelming gestures throughout this assignment.

Best of my words are for my respected supervisor ***Dr. Ajay Batish*** *and Co-supervisor* ***Mr. R. K. Duvedi****, whose mere presence has shown that "whatsoever it is, if we do it, it can happen". Their clarity of mind, intelligence and attitude for quest for perfection encouraged me to put the drop of my hypothesis in the ocean of laws and phenomena's.*

I thank our head of department ***Dr. S. K. Mohapatra****, whose excellent leadership and administration made this research project very convenient in terms of required stuff and nice working conditions. I am extremely thankful to members of distinguished faculty.*

The non teaching staff Mr.Trilok Singh, Mr. Surender Kumar, Mr. Surender Suri, Mr. A.S. Cheema, Mr.Roshan, Mr.Kuldeep, Mr. Deshraj, Mr. Manoj Kumar and Mr. Purshotam Kumar deserves special thanks for their help during the period of this work. My assignment would not have been successful without noted help from Mr. Lalit Kumar who helped and guided me as his younger brother and succumbed to all of my requirements.

Some friends were never too busy to give me a hand whenever they were needed. No words acknowledge the support I received from Baljeet, Rajesh, Sameer, Vivekpal, Manmeet, Davinder, Kuldeep, Nischint, Narinderpal, Talwinder Sir, Vivek, Ashish, Lalit for their valorous help and co-operation. I thank all my juniors for their support and affection.

I would also like to thank all the members and employees of Mechanical Engineering Department, Thapar University Patiala for their everlasting support.

I would like to thank to all the members and employees of Mechanical Engineering Department, Thapar University Patiala for their everlasting support.

Parveen Kumar

Registration no. 80782007

DECLARATION

I hereby declare that the thesis entitled "**EMPIRICAL MODELING FOR A SUBMERGED ARC WELDING PROCESS FOR PREDICTING THE WELD BEAD GEOMETRY AND MICROSTRUCTURE**" is an authentic record of my study carried out as requirements for the award of degree of **ME (Production and Industrial Engineering)** at **Thapar University**, Patiala, under the guidance of **Dr. Ajay Batish**, Associate Professor and **Mr. Ravinder Kumar Duvedi** Lecturer, Department of Mechanical Engineering, Thapar University, Patiala during **July 2008 to June 2009**. The matter embodied in this thesis has not been submitted in part or full to any other university or institute for the award of any degree.

Parveen Kumar

Registration no. 80782007

This is to certify that above declaration made by the student concerned is correct to the best of my knowledge & belief.

(Dr. Ajay Batish)
Associate Professor,
Mechanical Engineering Department,
Department,
Thapar University,
Patiala, 147004

(Mr. Ravinder Kumar Duvedi)
Lecturer,
Mechanical Engineering
Department,
Thapar University,
Patiala, 147004.

Countersigned by:

(Dr. S.K. MOHAPATRA)
Professor and Head,
Mechanical Engineering Department,
Thapar University,
Patiala, 147004.

(Dr. R.K.SHARMA)
Dean of Academic Affairs,
Thapar University,
Patiala, 147004.

CONTENTS

LIST OF TABLES

LIST OF FIGURES

ABBREVATIONS

SAW	-	Submerged Arc Welding
ANOVA	-	Analysis of variance
HAZ	-	Heat Affected Zone
DOF	-	Degree of Freedom
S/N	-	Signal to Noise
DC	-	Direct Current
AC	-	Alternating Current

Abstract

The present study has been done to study the effect of different input parameters on the desired responses in the submerged arc welding process. Partial factorial technique has been used for the design of experiments. The effects of flux, current, travel speed and voltage have been evaluated on the bead height, bead width, depth of penetration, micro hardness and microstructure of the heat affected zone. The effect of all the input parameters on the output responses have been analyzed using the analysis of variance (ANOVA) and empirical modeling. The effect of variation in input parameters has been studied on the microstructure of the heat affected zone. Plots of significant factors, S/N ratio and empirical modeling have been used to determine the best-fit relationship between the response and the model parameters.

CHAPTER 1

SUMBERGED ARC WELDING-AN OVERVIEW

1.1 Introduction

During the earlier times several attempts were made to mechanize the arc welding process. Developing a continuous coated electrode as an extension of the manual metal-arc welding electrode was ruled out for some reasons. Since the coating is non-conducting, arranging electrical contact with the electrode is not practicable. The coating is likely to peel off when the electrode is coiled, and the coating is also likely to get crushed when fed through the feed rolls. In one of the methods attempted, the work piece was painted with a thin slag flux, while feeding of the bare wire and arc travel were mechanized. Many methods were tried out to provide flux coating in mechanized welding, but all efforts led to failure. The idea of placing a thick layer of dry granular flux on the joint ahead of the carbon electrode was conceived and successfully developed in the *U.S.A*. and later applied to the welding of penstocks and water conduits in California. Submerged-arc welding was the next logical step and the process became a commercial success both in the *U.S.A*. and the *U.S.S.R*. by the middle and late *1930's*.

1.2 The Submerged Arc Welding Process

The modern submerged arc welding *(SAW)* is an arc welding process, in which one or more arcs formed between one or more bare wire electrodes and the work piece provides the heat for coalescence. The flux is supplied through a funnel located ahead of the filler wire which is fed continuously. The flux exercises a shielding function. During welding, part of it is converted into a readily removable slag. In fully-automatic welding, the flux is fed mechanically to the joint ahead of the arc, the wire is fed automatically to the welding head, the arc length is automatically controlled and the traverse of the arc or the workpiece is also mechanized. Flux feed may be by gravity flow, through a nozzle concentric with the electrode from a small hopper a top the gun, or it may be through a concentric nozzle connected to an air-pressurized flux tank. Flux may also be applied in advance of the welding operation or ahead of the arc from a hopper run along the joint. **(S.V. Nadkarni [1])**

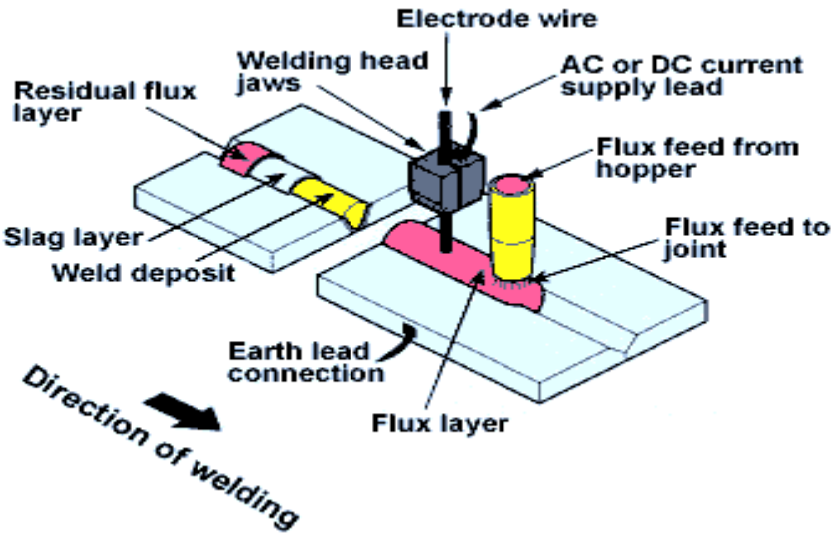

Figure 1.1 - Mechanism of Submerged Arc Welding [1]

During welding, the intense heat of the arc simultaneously melts the tip of the bare wire electrode and part of the flux as shown in Figure 1.1. The electrode tip and the welding zone are always surrounded and protected by molten flux, while all of them are covered by the top layer of unfused flux. As the arc progresses along the joint, the molten metal settles down while the lighter molten flux rises from the puddle in the form of slag. The weld metal, having a-higher melting point, solidifies first while the slag above it takes some more time to solidify. The solidified slag continues to protect the weld metal while it is still hot, and is capable of reacting with atmospheric oxygen and nitrogen. The submerged arc welding process can provide higher deposition rates and faster travel speeds, and the process is known to produce a very smooth bead with good penetration and excellent fusion. And as with other welding processes, it lends itself to creative applications.

R Quintana [2] observed a peculiarity of the submerged arc welding process is that, where the electric arc meets the slag covered welding area; both the welding pool and the welding cord of the same material are protected. This limits oxidation of the alloyed metal elements, with relatively small losses of fluxes agglomerated with vitreous, ceramic and pseudo ceramic matrices, which are molten at *1,350* ^{0}C and not very volatile in the electric arc conditions. In addition, during this process *95–98 %* of the wire-electrode and a high percentage of the alloyed load is deposited, and almost the entire matrix *(>96 %)*

contributes to slag formation. One of the more important characteristics of *SAW* is the high utilization of the energy of the electric arc, since there are no losses due to radiation or projection. The calorific yield has been determined as between *80* and *90 %.*

1.3 Applications

Applications cover pressure vessels, line pipe, storage tanks, heavy structurals, ships, railway wagons and coaches, surfacing and build-up work.

1.4 Basic Equipment

The typical set up for submerged arc welding equipment is shown in Figure 1.2, it essentially consists of:

- A wire feeder to drive the electrode to the work through the contact tube of a welding gun or welding head.
- A welding power source to supply electric current to the electrode at the contact tube.
- An arrangement for holding the flux and feeding it ahead of the arc.
- A means of traversing the weld joint.

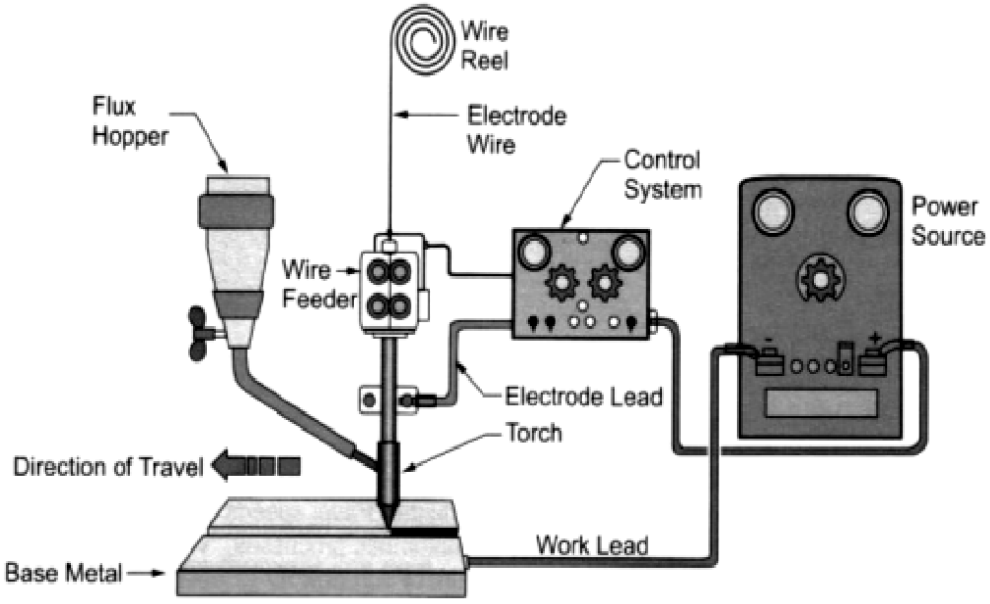

Figure 1.2: Equipment set-up for Single Wire Submerged Arc Welding

Typical welding outfits

A typical semi-automatic outfit consists of:

a) Power source
b) Wire feeder
c) Torch with flux hopper
d) Set of cables for connecting wire feeder to power source, comprising control cable, welding cable with end lugs and welding cable with end lug and ground clamp.

(a) Power source: It is a *DC* welding rectifier giving maximum welding current of *600 amps 60%* duty cycle and *500 amps at 100*% duty cycle. It has constant potential characteristics, giving a constant arc, voltage, while the current is determined by the wire-feed rate. The rectifier has a drip-proof casing with the following built-in components: transformer, silicon rectifier, and reactance coil, and fan, safety device against ventilation failure, control transformer and welding contactor.

(b) Wire feeder: The wire feeder for submerged arc welding is shown in Figure 1.3, with an arrow pointing towards it. It consists of a *DC* wire drive motor, reduction gearbox, four-roll drive mechanism and a wire spool holder. Wire-feed rate is continuously variable in the range of *0.5-2.5 m/min.* The wire sizes which can be accommodated in the available equipment are of *2.5-5.0 Ø mm.*

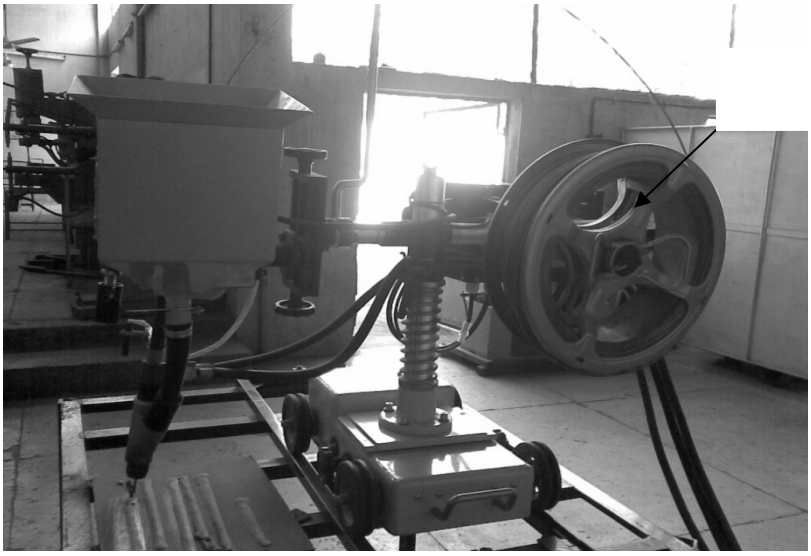

Figure 1.3: Wire feeder of a Semi-Automatic SAW unit

(c) Torch with flux hopper: Welding torch with flux hopper has been shown in Figure 1.4. It is a self-contained unit with bent torch head; it has a long hose, flux hopper which can take up to kilograms of flux, and a suitable coupler for connection to the wire feeder. The flux is fed around the electrode from a cylindrical tunnel along with the electrode.[1]

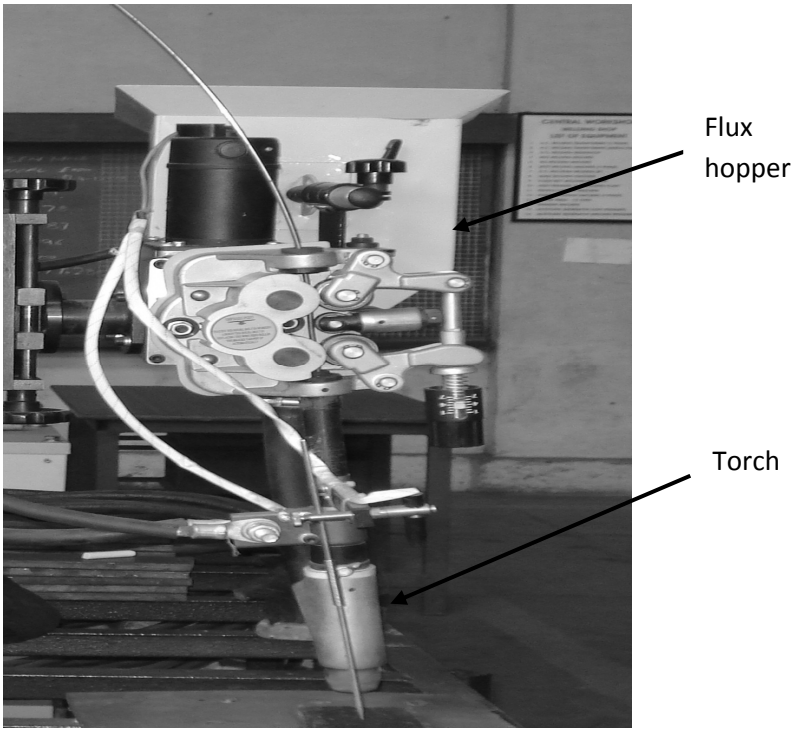

Figure 1.4: Torch with Flux Hopper for SAW Welding Tractor

1.5 Types of fluxes

SAW flux basically performs the same functions as the coating of a manual electrode. Additionally, it must satisfy certain special conditions demanded by the nature of the process. The flux protects the molten pool and the arc against atmospheric oxygen and nitrogen by creating an envelope of molten slag. The slag also cleanses the weld metal (i.e. deoxidizes it and removes impurities such as sulphur) modifies its chemical composition and controls the profile of the weld bead. The molten slag also provides favorable conditions for very high current densities, which together with the insulating properties of the flux; concentrate intense heat into a relatively small welding zone. This result in a deeply penetrating arc, which makes narrower and shallower welding grooves practicable, thus reducing the amount of weld metal, required to comp1ete the joint. It also results in higher welding speeds. The properties of the flux enable submerged arc weld-to be made

over a wide range of welding currents, voltage and speeds, each of which can be controlled independently of the other. Thus one can obtain welded joints of desired shape, chemistry and mechanical and metallurgical properties by using an appropriate welding procedure.
Nowadays, two main types of submerged arc fluxes are available, depending on the method of manufacture *i.e***.** fused and agglomerated. Sintered fluxes have been produced in some countries but their properties and welding characteristics have been rarely reported in the literature.

1.5.1 Fused fluxes

Typical ingredients are quartz, manganese ore or slag, dolomite, potassium felspar and clay. These minerals are ground and mixed in a definite proportion and melted. Melting is carried out in a magnesia or fireclay crucible if heating is by gas or in a graphite crucible if electricity is used. Electric melting is started by heating with an arc between the electrode and crucible and continued by resistance heating with the electrode submerged in the molten flux, which is an electrical conductor. After fusion, the melt is solidified rapidly by quenching into water or pouring into cell steel chills to produce small fragments of flux. These are dried and crushed to the required size; sieved, sized and packed in bags or drums.

Fused Flux Features:

- Non-hygroscopic
- Fully Reacted
- Chemically homogenous
- Contain no metallic deoxidizers
- Glass-like appearance, high grain strength

Fused Flux Benefits:

- Particles are non-hygroscopic and do not absorb moisture, therefore only a low temperature *(300°F/150°C)* drying cycle is required to remove surface moisture/condensation, providing increased protection against hydrogen cracking.
- Provide smooth, stable performance even welding currents (up to *2,000 amps).*
- Flux particles are chemically consistent welds.

Fused fluxes are less susceptible to particle breakdown due to flux recycling, reducing the creation of fine dust particles.

1.5.2 Agglomerated fluxes

For producing an agglomerated flux, finely powdered ingredients are mixed and ground dry in a mixer. The mix is steadily moistened by spraying with a solution of alkaline silicate and the mixing is continued. The mixer blades are suitably designed to assist agglomeration. The silicate solution initially fills the spaces between the pores of the particles. When subsequently dried, the water evaporates, leaving the binder as bridges between particles. After baking, the flux is graded to a specified granule size by sieving, and packed in water-proof containers.

Bonded Flux Features:

- Contain metallic deoxidizers
- May contain alloying agents
- Flat, low gloss, or dry particle appearance
- Each flux particle has a unique chemistry.

Bonded Flux Benefits:

- Presence of deoxidizers provides good performance over rust and mill scale and helps prevent weld porosity.
- Usually provides better peeling properties than fused fluxes.
- Alloying elements can be added to provide improved chemical and mechanical properties.
- Usually exhibit lower flux consumption than a fused flux welded at the same current and voltage

1.5.3 Sintered fluxes

They are produced by grinding the dry charge together, pressing into small balls, and heating to *1,000-1,100°C* (just below melting point) in gas-fired furnaces. The solid mass produced then has the characteristics of a fused flux. It is crushed to the desired fineness, sieved, sized and packed in suitable containers.

1.5.4 Flux Storage: To prevent contamination of weld by hydrogen, the flux must be kept dry and free from oils and other hydrocarbons. If flux becomes damp, it must be redried. Excessive levels of hydrogen in some steels can cause porosity. In hardable steels, even small amount of hydrocarbon can cause underline cracking. Commercially available dryers are the best method of drying flux. Do not dry flux by using direct flame. This may fuse the flux together; at the same time, the flame produces water that might condense on the flux. (**Larry Jeffus** [3]).

1.6 Parameters

In SAW, the weld deposit quality is determined by the type of flux, grade of wire and the following parameters:

- Welding current
- Arc voltage
- Speed of arc travel
- Size of electrode
- Electrode stick-out
- Heat input rate

To get optimum results, one must know their effects and how to select and control them properly.

1.6.1 Welding Current

It controls the melting rate of the electrode and thereby the weld deposition rate. It also controls the depth of penetration and thereby the extent of dilution of the weld metal by the base metal. Too high a current causes excessive weld reinforcement which is wasteful, and burn-through in the case of thinner plates or in badly fitted joints, which are not provided with proper backing. Excessive current also produces a high narrow bead and undercut. Excessively low current gives an unstable arc, inadequate penetration and overlapping. SAW equipment is usually provided with an ammeter to monitor and control the welding current.

1.6.2 Arc-Voltage

Arc voltage, also called welding voltage, means the electrical potential difference between the electrode wire tip and the surface of the molten weld puddle. It is indicated by the voltmeter provided on the equipment. It hardly affects the electrode melting rate, but it determines the profile and surface appearance of the weld bead. As arc voltage increases, the weld bead becomes wider and flatter, and the penetration decreases.

The effects of changing voltage are explained as follows:

1) *Increasing voltage:*

a) Produces a flatter and wider bead.
b) Increases flux consumption.
c) Increases resistance to porosity caused by rust or scale.
d) Helps bridge gaps when fit-up is poor.
e) Increases pickup of alloy from the flux: this can be used to advantage to raise the alloy content of the weld when welding is performed with alloy or hard surfacing fluxes. If excessive, it can reduce ductility and increase crack sensitivity, particularly in the making of multiple-pass welds.

- Produces a hat-shaped bead that is subject to cracking.
- Produces poor slag removal in groove welds.
- In multiple-pass welds, increases the normal alloy pickup from the flux.
- Produces a concave fillet weld that may be subject to cracking
- Increases undercut on fillet welds.

3) Lowering the voltage produces a stiffer arc needed for getting penetration in a deep groove and to resist arc blow on high-speed work.

4) An excessively low voltage produces a high, narrow bead with poor slag removal.

1.6.3 Speed of Arc Travel

For a given combination of welding current and voltage, increase in the welding speed or the speed of arc travel results in lesser penetration, lesser weld reinforcement and lower heat input per unit length of weld. Excessively high travel speeds decrease fusion between the weld deposit and the parent metal, and increase tendencies for undercut, arc blow, porosity and irregular bead shape. As the travel speed is decreased, penetration and weld reinforcement increase. But too slow a speed results in poor penetration, because under this condition, the weld puddle is directly under the electrode tip and the force of the arc is cushioned by the weld puddle. Excessively slow speeds also produce a convex bead shape, which results in an uneven weld bead with slag inclusions.

1.6.4 Size of Electrode

As in the case of SAW, the electrode size is selected according to the plate thickness and the desired size of weld. With increase in electrode size, welding current can be increased so as to get higher deposition rates, deeper penetration and increased weld size. At a given welding current, changing over to a larger electrode results in a wider, less penetrating bead. Hence in joints with poor fit-up, a larger electrode is preferred to a smaller one for bridging the root gap. For a given electrode size, a high current density (i.e. welding current in amps divided by the cross-section of the wire, expressed in amps/ mm^2) results in a strong, penetrating arc, while a lower current density gives a soft arc which is less penetrating.

1.6.5 Electrode Stick-Out

It is also termed electrode extension. It refers to the length of the electrode, between the end of contact tube and the arc, which is subject to resistance heating (also called I^2R heating) at the high current densities used in the process. The longer the stick-out, the greater the amount of heating and the higher the deposition rate. Increased electrode stick-out reduces to some extent the energy supplied to the arc, resulting in lower arc voltage and a different bead shape. Hence when the electrode stick-out is increased to obtain higher deposition rate, the voltage setting on the equipment must be increased to maintain correct arc length. Deposition rates can be increased by as much as *25-50%* by increasing electrode stick-out, but the technique is little used in industry. This may be due to the following factors:

(a) Insulated guide is needed to direct the hot wire to the weld pool.

(b) Penetration is reduced by about *10%.*

(c) Excessive overheating of the wire leads to electrode pulsation, arc instability and stubbing.

Also termed arc energy, it is calculated by using the formula:

$$HIR = \frac{V \times I \times 60}{S \times 100}$$

HIR=heat input rate in kilojoules per mm *(kJ/mm)*

V= arc voltage

A=welding current

S=arc travel speed in *mm/ min.*

For a given joint thickness, the higher the heat input rate, the lower is the cooling rate of the weld metal and heat affected zone *(HAZ)* of the parent metal, and vice versa. Heat input rate has an important bearing on the weld metal microstructure and the final microstructure of the *HAZ.* [1]

1.7 Advantages of SAW

The growth in the use of *SAW* has been due to its major advantages, as follows:

- *Minimum operator protection required* – The heavy blanket of granular flux covers all of the arc light except for an occasional flash. The absence of the light means that many welders can work close to each other without the problem of arc flash. The welder does not have to wear a welding helmet, so visibility and safety are improved. The granular flux also prevents most of the welding smoke from escaping. Even with a large number of welders operating in confined spaces, forced ventilation is virtually eliminated. The heating and cooling costs of the shops are lessened because the amount of ventilation required is greatly reduced.
- Highest deposition rate-using large diameter wires, more than *40 lb/hr (18kg/hr)* can be deposited. This rate is nearly two times the rate of flux cored arc welding and

four times the SMAW. No process other than the electro slag welding can come close to this deposition rate.

- Efficient use of materials-with SAW, there is no spatter to waste metal and cause cleanup problem. All of the electrodes is transferred and becomes weld deposit. Only the melted flux needed for the weld is lost. Unfused granular flux can be retrieved and reused. The amount of flux consumed can be controlled by varying the arc length, which is done by changing the arc voltage.
- Weld size-flat groove or fillet welds as large as *1 inch (254 mm)* can be made in one pass using a single electrode. Larger sizes are possible with multiple electrodes.
- Easily adapted-with the process, the flux and wire are purchased separately. The flux can be used to change the alloys in the weld metal deposited from the electrode. By changing the flux, the properties of the weld are altered. Two or more fluxes can be mixed or granulated metal can be added to a flux or mixture to meet individual needs.
- High quality welds-many codes permit saw to be used on structural iron, pressure vessels, cryogenic cylinders, and many other critical applications.

1.8 Disadvantages of SAW

As with other processes, the submerged arc processes have several disadvantages:

- *Restricted to flat position and horizontal fillets*- Because the fluxes needed for submerged arc welding flow easily, welding is restricted to those positions in which the flux can produce a self–supporting blanket.
- *Welding parameters need careful control*- Because the flux hides the weld pool, welding conditions must be preset on the basis of experiments or with proven tabular information, including thee contact tip-to-work distance, the current, travel speed and the voltage. Arc voltage must be carefully controlled to ensure the proper weld profile. Equally important, deviations in arc voltage can cause significant changes in the weld compositions when using the fluxes as the sources of alloys.
- *Mechanical guidance is necessary*- Without some sort of guidance, the arc could easily move away from the joint being welded. To take advantage of the deep penetration possible with the process, accurate positioning is very important. This need can become an expensive complication with other than perfectly straight

joints. Even with good guidance systems, positioning problems can develop if the wire does not have a large and uniform cast (or little band) and a negligible (twist). Significant variations in cast or large helix will cause an arc to wander. [1]

1.9 Organization of Study

Whole study has been divided into seven chapters.

Chapter1: This chapter gives the introduction of the submerged arc welding and the process parameters. This chapter also includes the brief description of various types of fluxes. It also includes the advantage and disadvantage of submerged arc welding processes.

Chapter 2: This chapter includes the literature review of submerged arc welding process. The total work literature has been categorized into four categories. It also includes the summary of literature and objective of the study.

Chapter 3: This chapter gives the description of design of experiments and experimental design of the study. The experimental set up, process parameters levels and orthogonal array for experiment.

Chapter 4: This chapter includes the observation tables of the responses and also includes the analysis of the observed data using ANOVA. It gives us the idea about the significant and non significant input factors. The optimal design is also included in this chapter.

Chapter 5: This chapter includes the regression analysis of the observed data. It also includes the regression equations developed after the analysis and residual analysis for each of the response.

Chapter 6: This chapter includes the iron carbide phase diagram and different microstructure obtained during the phase transformation. It also includes the micrographs of heat affected zone for all the experiments.

Chapter 7: This chapter includes all the observations and results obtained in the study.

Chapter 2

LITERATURE REVIEW

2.1 Review of Literature

A lot of work has been done in the area of submerged arc welding. The available literature can be categorized in the following broad classifications.

1. Study of heat affected zone.
2. Improvement in weld property with flux modifications.
3. Process optimization of *SAW* process.
4. Effect of welding parameters on weld properties.

The subsequent sections in this chapter describe extensive literature review on the above classifications**.**

2.2. Study of Heat Affected Zone

Heat affected zone is that zone of work material which is affected by the heat generated due to the spark. The properties of the metal changes due to immense of heat.

Eroglu M [4] *et al.,* observed high heat input welding processes (submerged arc, shielded metal arc welding, electro slag welding) are commonly used for welding of thick sections. Weld thermal cycles associated with the high heat input processes are known to affect both the macro and microstructure of *HAZ* and weld metal which in turn influence the mechanical properties of the joint.

C. S. Lee [5] *et al.,* discussed the effect of welding parameters on the size of the heat affected zone *(HAZ)* and its relative size as compared to the weld bead of submerged arc welding. The effect of submerged arc welding parameters on the size of the heat affected zone and *HAZ* size to bead size ratio has been studied. They concluded that the size of the *HAZ* is influenced by *SAW* parameters; however different parameters have different degrees of influence. Among the welding parameters, the welding current has the greatest influence on *HAZ* size and *HAZ* size to bead size ratio; higher current causes smaller *HAZ* and *HAZ* to bead size ratio. Other welding parameters like heat input and polarity also affect *HAZ* to bead size ratio while voltage, electrode diameter and stick out have no significant effect on it.

Vera Lu´cia [6] *et al.,* tried to evaluate the effect of a post weld heat treatment *(PWHT*) on the microstructure and mechanical properties of the base metal, heat-affected zone *(HAZ),* and weld metal of a submerged arc welded pressure vessel steel. The plate studied, welded with a heat input of *22.8 kJ/cm* in the *SAW* process. They presented the reduced tensile properties for the base metal. However, both yield strength and tensile strength were slightly above slightly lower limits established by ASTM. This reduction was expected based on the literature. Higher toughness for the weld metal and a reduction of this property for the *HAZ* and base metal. This trend was probably observed due to a difference in the characteristics (intensity and location) of the precipitation in these regions.

Keshav Prasad [7] *et.al,* investigated the influence of the submerged arc welding *(SAW)* process parameters (welding current and welding speed) on the microstructure, hardness, and toughness of *HSLA* steel weld joints. Attempts have also been made to analyze the results on the basis of the heat input. The weld joints were prepared using comparatively high heat input *(3.0 to 6.3 KJ/mm)* by varying welding current *(500–700 A*) and welding speed *(200–300 mm/min)*. Results showed that the increase in heat input coarsens the grain structure both in the weld metal and heat affected zone *(HAZ)*. The hardness has been found to vary from the weld centre line to base metal and peak hardness was found in the *HAZ*. The hardness of the weld metal was largely uniform. The hardness reduced with the increase in welding current and reduction in welding speed (increasing heat input) while the toughness showed mixed trend. The increase in welding current from *500 A* to *600 A* at a given welding speed *(200 mm/min or 300 mm/min)* increased toughness and further increase in welding current up to *700 A* lowered the toughness. Scanning electron microscopy of the fractured surfaces of impact test specimen was carried out to study the fracture modes.

2.3 Improvement in Weld Property with flux modifications

A lot of work has been done in this field with the change in flux compositions we can improve the weld chemical properties resulting in strengthening of weld.

T.W. Eagar [8] *et al.,* observed that the mechanical properties of weld metal is primarily the result of the weld metal chemical composition, microstructure and the cooling rate. The cooling rate experienced by weld metal deposit is controlled by a combination of heat

input and heat extraction. Under identical condition of welding, viz. joint design and plate thickness, heat extraction may be assumed to remain same. Therefore, weld metal chemical composition and heat input controlling microstructure are the governing factors responsible for the mechanical properties of weld metal. The weld metal *YS, UTS* and impact toughness increases with increase in alloying elements, viz. carbon *(up to 0.10 wt%),* manganese *(up to 1.5 wt%),* silicon *(up to 0.5 wt%)* and nickel *(up to 3.5 wt%)* by various mechanisms such as (i) solid solution hardening, (ii) grain refinement and (iii) refinement of microstructure, etc. The basic requirements of improved toughness in low alloy steel weld metal are associated with the amount of acicular ferrite in the microstructure.

P. Kanjilal [9] *et al.,* predicted the results that polarity, speed and flux–parameter interactions have profound influence on the weld metal chemical composition. The final weld metal chemical composition is a result of combining actions of several mechanisms, viz. slag metal reaction, electrochemical reaction, weld metal dilution which operate simultaneously within the molten weld pool. The mechanical properties of weld metal are primarily the result of the weld metal chemical composition**,** microstructure and the cooling rate. The cooling rate experienced by weld metal deposit is controlled by a combination of heat input and heat extraction. Under identical condition of welding, viz. joint design and plate thickness, heat extraction may be assumed to remain same. Therefore, weld metal chemical composition and heat input controlling microstructure are the governing factors responsible for the mechanical properties of weld metal. The weld metal *YS, UTS* and impact toughness increases with increase in alloying elements, viz. carbon *(upto0.10 wt%),* manganese *(up to 1.5 wt%),* silicon *(up to 0.5 wt%)* and nickel *(upto 3.5 wt%)* by various mechanisms such as (i) solid solution hardening, (ii) grain refinement and (iii) refinement of microstructure, etc. The basic requirements of improved toughness in low alloy steel weld metal is associated with the amount of acicular ferrite in the microstructure .Weld metal mechanical properties are primarily dependent on: (i) welding parameters, (ii) mixture related variables (MRV), (iii) interaction effects, viz. (a) interaction between MRVs and (b) interaction between MRV and welding parameters.

R.Quintana [10] *et al.* said that to obtain metal coatings with complex chemical compositions and phases, as well as differing mechanical properties, the Submerged Arc Welding *(SAW)* process is often used, employing a great variety of types of agglomerate

fluxes. All agglomerate fluxes consist of two fundamental parts: the matrix and the alloyed load. The ratio of matrix to the alloyed load can vary greatly, from *9:1* to *2:1*. The two constituents of the flux aggregate, by various processes, with the help of agglomerating agents. Agglomeration by granulation (pelletizing) using liquid sodium and/or potassium glass is the most common and widely used for these types of fluxes, despite their hygroscopic character. One of the most significant profitability characteristics of an agglomerate flux is the efficiency of the transfer of the chemical element of the alloyed load of the flux to the deposited metal by particular wire–flux systems and welding regimens. The aim of this study was to evaluate the capacity of various agglomerate fluxes to transfer to the welding bath the elements *Cr, Mn* and *C* from alloy loads formed with different ratios of *FeCr, FeMn* and graphite. To do this, a vitreous matrix was synthesized and melted in an electric arc furnace, using a formulation of the minerals, and alloyed loads were formed with different ratios of the components established using a McLean Anderson experimental design.

P. Ambroza [11] *et.al.,* carried out the experiment using *WC-8%Co* powder spread on low carbon structural steel surface and then melted by arc under the flux, containing graphite powder. The test results showed that by using for overlaying welding under flux *WC-8%Co* powder, it is possible to obtain layers with large amount of carbides phase (about *90%)*; formation of carbides was influenced by both amount of *WC-8%Co* powder spread over the structural steel surface, and amount of graphite powder, mixed with flux. Electric arc between welding wire and base metal resulted, due to high temperature, melting of *WC* carbide in powder and formation of Fe_3W_3C carbide during cooling, because the iron into welding bath came from both melted welding wire and structural steel surface. The microstructure was obtained in which carbides are bonded by the matrix, having alloyed steel composition. The matrix is composed of martensite, troostite and retained austenite. Amount of those phases depends on the amount of alloying elements (*W, Co, Mn* and *Si)*, and amount of carbon, as well as heat treatment.

A. Cruz [12] *et al.,* carried out research to characterize manganese ore to define its use in the synthesis of fluxes for submerged arc welding. Fluxes consisting of a system of oxides with high contents of silica and manganese are among those most widely used in welding carbon steels, because they possess good technological properties. In Cuba, fluxes of this type have mainly been used in the metal mechanical and agricultural sectors. In Cuba

there are deposits of manganese ores which could be used in the development of fluxes of this type, and there are also ores with appreciable quantities of silica, calcium magnesium and aluminum, which are all suitable for use as raw materials in flux production.

J. Jang [13] *et al.,* Bead-on-plate welds were produced using twenty four fused reagent grade submerged arc welding fluxes, selected from three flux systems, SiO_2-*MnO-FeO,* *MnO-*CaF_2 and SiO_2-*CaO-*CaF_2. The welds were processed using *AISI 1010* steel coupons, and a Lincoln *L-50 AWS type A5.17)* welding wire with a constant heat input of *3.0 kJ mm*. The three flux systems were selected because of their different oxygen potentials and their ability to produce welds with a wide oxygen range *(70 to 1400 ppm).* Qualitative and quantitative metallography and chemical analysis were performed on the welds. Inclusion morphology and volume fraction are observed to be affected by flux composition Inclusions of $1\mu m$ in size and greater are associated with grain boundary and blocky proeutectoid ferrites, while inclusions $0.64\mu m$ and smaller are linked with the presence of acicular ferrite.

Ana Ma [14] *et al.,* studied the effect of active and non active fluxes on the mechanical properties and microstructure in submerged-arc welds .They observed the effect of flux composition on the weld material property and microstructure. Equiaxed ferrite grains and pearlite colonies are the main constituents of the microstructure corresponding to flux *A* (without *Cr* and *Mo*). On the other hand, the microstructures of the welds corresponding to fluxes having *Cr* and *Mo* compositions (flux *B* and *C)* are mainly composed of acicular ferrite with an abundant dispersion of fine carbides, presumably composed of *Cr* and *Mo.* This micro structural behavior seems to indicate that the mechanical properties of the welds corresponding to fluxes *B* and *C* are expected to be higher than those corresponding to flux *A*. It has been observed that the engineering yield, ultimate tensile strengths and hardness increases as the *Cr* and *Mo* contents increase. This behavior agrees with the weld microstructures. In contrast, the charpy *V-notch* impact test energy at room temperature, and the elongation and area reduction values were higher in the welds corresponding to flux not having *Cr* and *Mo*. This behavior can be attributed to the formation of pearlite and ferrite in the weld.

2.4 Process Optimization of SAW

Now a day's quality and cost are the top most priorities. *SAW* is a process which can be optimized to meet above objectives.

Bendell A [15] *et al.,* Taguchi method is a powerful Design of Experiments *(DOE)* tool. It provides a simple, efficient, and systematic approach to optimize designs for performance, quality, and cost. The methodology is valuable when process Parameters are qualitative and discrete. The parameter design based on the Taguchi method can optimize the quality characteristics through the settings of process parameters and reduce the sensitivity of the system performance to sources of variation. In recent years, a number of applications of the Taguchi method have been used in a worldwide range of industries and nationalities.

Unal R [16] *et al.,* suggested that Taguchi's philosophy is an efficient tool for the design of high quality manufacturing systems. Dr. Genichi Taguchi, a Japanese quality management consultant, has developed a method based on orthogonal array experiments, which provide much-reduced variance for the experiment with optimum setting of process control parameters. Thus the integration of design of experiments *(DOE)* with parametric optimization of process is achieved in the Taguchi method. This will provide desired results. The desired results refer to the acceptable quality parameters of the product. For welded joint, this will mean desired mechanical properties of the joint, which-in turn-depend on bead geometry. Again, control of the process parameters will lead to optimal bead. An orthogonal array *(OA)* provides a set of well-balanced (minimum experimental runs) experiments and Taguchi's signal-to-noise ratios *(S/N),* which are logarithmic functions of desired output, serve as objective functions for optimization. This helps in data analysis and prediction of optimum results.

EA. Elsayed [17] *et al.,* said that parameter design, based on the Taguchi method, can optimize the performance characteristic through the setting of process parameters and can reduce the sensitivity of the system performance to sources of variation. However, most published Taguchi applications to date have been concerned with the optimization of a single performance characteristic. Handling the more demanding multiple performance characteristics are still an interesting research problem.

H.L. Tsai [18] *et al.,* suggested the desired welding parameters are determined based on experience or handbook values. However, this does not ensure that the selected welding

parameters result in optimal or near optimal welding performance for that particular welding machine and environment. Therefore, several mathematical models have been developed to correlate welding performance, such as deposition rate and dilution, with welding parameters. To select welding parameters, an objective function with constraints is formulated to solve optimal welding parameters using optimization techniques.

Y. S. Tarng [19] *et al.,* observed that the desired welding parameters are determined based on experience or handbook values. However, it does not ensure that the selected welding parameters result in optimal or near optimal welding performance for that particular welding machine and environment. In recent years, several mathematical models have been developed to correlate welding performance with welding parameters. To properly select welding parameters, an objective function with constraints is formulated to solve optimal welding parameters using optimization techniques. However, considerable knowledge and experience are required to use this approach. Furthermore, numerous welding experiments have to be performed to build the mathematical models. In this paper, an alternative approach based on the Taguchi method is used as an efficient method to determine the optimal welding parameters.

Tarng Y.S [20] *et al.,* said that the use of fuzzy logic in the Taguchi method to optimize the submerged arc welding process with multiple performance characteristics. An orthogonal array, the signal-to-noise ratio, multiresponse performance index, and analysis of variance are employed to study the performance characteristics in the submerged arc welding process. The process parameters, namely arc current, arc voltage, welding speed, electrode protrusion, and preheat temperature are optimized with considerations of the performance characteristics, including deposition rate and dilution. In this study, the use of fuzzy decision-making logic to perform fuzzy reasoning of multiple performance characteristics has been studied. It is shown that optimization of multiple performance characteristics can be transformed into optimization of a single performance index through fuzzy logic. As a result, the integration of fuzzy logic with the Taguchi method can be used to solve the optimization of the multiple performance characteristics. In this paper, the optimization of the submerged arc welding *(SAW)* process, with the multiple performance characteristics, is studied using the proposed approach. This paper has presented an application of fuzzy logic using the Taguchi method for the optimization of the submerged arc welding process with multiple performance characteristics. As a result,

the performance characteristics such as deposition rate and dilution can be simultaneously considered and improved through this approach instead of using engineering judgment. Experiments were conducted to confirm this approach.

Moi S.C. [21] *et al.,* introduced the concept of using *slag-mix%* as a process variable. The percentage of slag, in the mixture of fused flux and fresh flux, has been denoted as *slag mix%.* The main effect of using slag-mix and interactive effects of process parameters *(*including *slag-mix%)* on features of bead geometry and *HAZ*, in terms of bead height, depth of penetration, bead width and *HAZ* width have been evaluated through analysis of variance (ANOVA) method. However, their work did not provide the optimal factor combination to yield acceptable weldments and the maximum *slag-mix%* that can be used during *SAW* process without adversely affecting bead geometry as well as *HAZ* dimensions. They, however, carried out microstructure studies for comparing the results of conventional *SAW* and *SAW* with a mixture of fresh flux and fused slag.

Myers R. [22] *et al.,* in submerged arc welding, process parameters interact in a complicated manner that influences various features of quality characteristics of the weld bead. Quadratic response surface methodology is an efficient approach to represent these relationships through mathematical equations

Saurav Datta [23] *et al.,* observed that in most of the cases the optimization has been performed using single objective function. For a multi-response process, while applying the optimal setting of control factors, it can be observed that, an increase/ improvement of one response may cause change in another response, beyond the acceptable limit. Thus, for solving the multicriteria optimization problem, one must convert all the objectives into an equivalent single objective function. This equivalent objective function, which is the representative of all the quality characteristics of the product, is to be optimized (maximized). Research related to this technique can also be found in literature. This approach converts each of the responses (objectives) into their individual desirability value (that varies from *0* to *1*). These individual desirability values are then accumulated to compute overall desirability function, which is to be optimized (maximized) next. But in doing so, it is frequently experienced that, within experimental domain, either the function becomes too insensitive or the optimum solution may occur at a saddle point. To overcome this, a trial-and-error technique is adopted to yield satisfactory results. Taguchi's optimization approach is very efficient in this context. This method can

evaluate the optimal setting by using a limited number of experimental runs. However, the general Taguchi method cannot solve multi-objective optimization problems; therefore, the Taguchi method coupled with grey relational analysis is the appropriate option. Literature reveals that the use of recycled slag would be a new area of research because of less work is done so far in this respect.

Saurav Datta [24] *et al.,* studied how to obtain optimal parametric combinations to achieve desired weld bead geometry and dimensions related to the heat affected zone *(HAZ),* such as *HAZ* width in the present case, in submerged arc welding. The philosophy and methodology proposed by Dr. Genichi Taguchi can be used for continuous improvement in products that are produced by submerged arc welding. This approach highlights the causes of poor quality, which can be eliminated by self adjustment among the values of the process variables if they tend to change during the process. Depending on functional requirements of the welded joint, an acceptable weldment should confirm maximum penetration, minimum reinforcement, minimum bead width, minimum *HAZ* width, minimum bead volume, etc. to suit its area of application. Based on Taguchi's approach, the present study has been aimed at integrating statistical techniques into the engineering process. Taguchi's L_9 (3*3) orthogonal array design has been adopted and experiments have been accordingly conducted with three different levels of conventional process parameters using welding current and flux basicity index to obtain bead-on plate weld on mild steel plates. Features of bead geometry and HAZ in terms of bead width, reinforcement, depth of penetration and HAZ width have been measured for each experimental run. The slag, generated during welding, has been consumed in further runs by mixing it with fresh unmelted flux. The percentage of slag in the mixture of fused flux (slag) and fresh flux has been defined as *slag mix%.* Welding has been performed by using varying *slag mix%,* treated as another process variable, in order to obtain the optimum amount of slag-mix that can be used without any alarming adverse effect on features of bead geometry and *HAZ.*

Saurav Datta [25] *et al.,* said that quality has now become an important issue in today's manufacturing world. Whenever a product is capable of conforming to desirable characteristics that suit its area of application, it is termed as high quality. Therefore, every manufacturing process has to be designed in such a way that the outcome would result in a high quality product. Therefore, there exists an increasing need to search for the

optimal conditions that would fetch the desired yield. Apart from process optimization, the work has been initiated to develop mathematical models to show different bead geometry parameters, as a function of process variables. Hence, optimization has been performed to determine the maximum amount of slag–flux mixture that can be used without sacrificing any negative effect on bead geometry, compared to the conventional SAW process, which consumes fresh flux only. Experiments have been conducted using welding current, slag-mix percentage and flux basicity index as process parameters, varied at four different levels. After measuring bead width, depth of penetration and reinforcement; based on simple assumptions on the shape of bead geometry, other relevant bead geometry parameters: percentage dilution, weld penetration shape factor, weld reinforcement form factor, area of penetration, area of reinforcement and total bead cross sectional area. All these data have been utilized to develop mathematical models between predictors and responses. Response surface methodology *(RSM),* followed by the multiple linear regression method, has been applied to develop these models. The effects of selected process parameters on different responses have been represented graphically. Finally grey relational analysis coupled with the Taguchi method (with Taguchi's orthogonal array) has been applied for parametric optimization of this welding technique.

Patnaik A. [26] *et.al*. studied the submerged arc welding *(SAW)* process finds wide industrial application due to its easy applicability, high current density and ability to deposit a large amount of weld metal using more than one wire at the same time. It is highly emphasized in manufacturing especially because of its ability to restore worn parts. SAW is characterized by a large number of process parameters influencing the performance outputs such as deposition rate, dilution and hardness, which subsequently affect weld quality. An exhaustive literature survey indicates that five control factors, viz., arc current, arc voltage, welding speed, electrode stick-out and preheat temperature, predominantly influence weld quality. The relationship between control factors and performance outputs is established by means of nonlinear regression analysis, resulting in a valid mathematical model. Finally, Genetic Algorithm *(GA),* a popular evolutionary approach, is employed to optimize the welding process with multiple objectives.

2.5 Effect of welding parameters on weld properties

Welding parameters have a great influence over the properties of weld materials. Welding parameters can change the mechanical properties and microstructures of the weld materials**.**

W. Troyer [27] *et al.,* had shown that by adding the powder in *SAW*, a better use of heat can be made. Thus, for a given heat input, the number of passes required to fill a joint can be reduced and therefore, the total energy supplied to the joint can be reduced. Alternatively, the same bead size or deposition rate can be achieved by lowering heat input per pass. Welds made with lower heat input experience higher cooling rates, and thermal gradients are steeper; hence, the width of the *HAZ* is also less. Additionally, the time spent above the peak temperature is reduced; the combined effect of this results in a narrow *HAZ* that cools faster and has smaller grain growth. Weld metals produced under faster cooling rates are also superior in mechanical properties. Thus, the process of powder addition has potential not only for producing welds that are cost effective but metallurgically superior too and they may become attractive for welding *HSLA* and *HY* steels.

J. Tanaka [28] *et al.* compared the measured and expected composition of weldments, where the latter is based on the composition of the electrode, the base metal, and on weld dilution. They proposed that the transfer of a particular element from the slag to the weld metal and vice versa depends on the overall flux composition and/or the flux basicity index *(B.I.)*. They have reported details for many elements, including manganese, silicon, carbon, sulphur and phosphorus. They have also introduced a parameter, defined by *AM*, which is the difference between the measured and the expected composition of the weld metal. When *AM* for a particular element is greater than zero, that element is supposed to be transferred from the slag to the weld metal.

M.L.E. Devis [29] *et al.,* worked with ten fluxes of different bases, found that the measured and the expected composition were not identical and also studied a three flux system and reported that weld-metal carbon content appeared to be independent of fluxes and reported that the change in silicon content of the weld metal is influenced by the value of basicity index and that degree of influence is greater when the value of basicity index is less than *2*.

N.D. Pandey [30] *et al.,* studied the influence of submerged arc welding *(SAW)* parameters and flux basicity index on the weld chemistry and transfer of elements manganese, silicon, carbon and sulphur has been investigated, five fluxes and different values of the welding parameters being used for study. The welds were produced as a bead on a mild-steel plate. The weld-metal composition showed, in general, gain of silicon and loss of carbon, manganese and sulphur elements. The results show that welding current and voltage have an appreciable influence on element transfer, as well as on weld composition. On the other hand, except for weld-metal silicon, the basicity index of the fluxes has only a minor influence. Weldments properties such as strength, toughness and solidification cracking behavior are affected by chemical composition.

N.A. McPherson [31] *et al.,* observed that direct submerged arc welding of *316LN* stainless steel to mild steel can result in unacceptable welds, due to localized areas of high hardness or areas having low ferrite numbers. Altering the position of the consumable wire toward the stainless steel side of the preparation produces an acceptable weld, when used in conjunction with a high ferrite consumable. Variables used in this work were the position of the consumable wire in the weld preparation and the ferrite number of the consumable wire. Abnormally high hardnesses were measured in some regions of the welds. These were related to the central position of the consumable wire in the weld preparation. Undesirably low ferrite numbers were related to the ferrite number of the consumable wire and also to the central position of the consumable wire in the weld preparation. The position of the consumable wire in the weld preparation controlled the relative dilution from the parent plates, and when the dilution from the *316LN* steel was increased by off-setting the wire to that side of the weld preparation, the high hardness regions were no longer found. Similar optical microstructures were found to have significantly different hardnesses. Martensite was observed by transmission electron microscopy *(TEM)* in some of the regions of high hardness. The presence of *M23C6* was due to the effects of high heat input or reheating of areas by subsequent passes. Some of the martensitic areas were confirmed to contain twins. The use of *309* type consumables, in this case, does not produce acceptable welds. Reducing the dilution from the mild steel resulted in acceptable levels of hardness across the weld. The use of image analysis to measure ferrite number in dissimilar welds has been shown to be unreliable.

R. S. Chandel [32] *et al.,* observed that many variants of *SAW* such as twin arc, tandem arc, multiple wire, strip electrodes, etc., are now available and widely used for specific applications. With the use of proper parameters and *SAW* variant, it is now possible to achieve deposition rates in excess of *50 kg/hr*. The increase in deposition rate in most cases is, however, achieved by increasing welding current and hence the heat input, which tends to impair joint toughness.

Abilio Manuel Pinho De Jesus [33] *et al.* did a comparison between the low and high cycle fatigue behaviours of a base metal, the *P355NL1* steel and a weld material resulting from the automated submerged arc welding was carried out based on stress- and strain-controlled fatigue tests of smooth specimens. A comparison of the crack propagation behaviours between the *BM, WM* and *HAZ* was also performed using results from fatigue tests of cracked specimens. Energy-life relations were derived from the strain-life data. These relations indicate that the fatigue resistance of the *WM*, defined in terms of the strain energy density of the cycle, is lower than observed for the *BM*. The *BM* presents slightly higher crack growth rates than *WM* and *HAZ*, for null stress ratio. For stress ratios equal to *0.5* and *0.7*, the differences between crack growth rates are almost negligible. The influence of stress ratio is small. In general, crack growth rates obtained for the three materials (three distinct microstructures) and stress ratios fall in a narrow band, which is in agreement with results published in literature for this type of materials and weldments.

S. Datta [34] *et.al,* developed nonlinear mathematical models in order to reveal the direct and interactive effects of process parameters on mechanical properties of butt weldments by Submerged Arc Welding *(SAW).* Based on factorial design without replication, experiments were conducted with different levels of process parameters (welding current, electrode stick-out and voltage on mild steel plates) to obtain butt welds. Various bead quality and performance parameters like hardness, toughness, yield strength and ultimate tensile strength were measured for each of the butt welds made in the experimental runs. Multiple linear regression method was used to calculate the coefficients of the models. The significance of the coefficients for each of the factors in the models was calculated by Analysis of Variance (ANOVA) Method. The predictions as given by the models have been represented graphically to show the influence of the process control parameters on bead quality in terms of mechanical properties associated with the weldments.

2.6 Literature Summary

After studying the literature it can be concluded that a lot of work has been done in the field of submerged arc welding, in one way or another. Some investigators like [4], [5], [6], [7] have studied the various responses like bead geometry, width of heat affected zone, hardness etc. The value and nature of the responses depends upon the range and selection of the input parameters *i.e.* current, voltage, electrode stick out, flux, travel speed, polarity etc. Some other researchers [9], [10], [11], [12] investigated different flux composition depending upon the requirement of the weld properties and their effect on the weld have been studied. Different kinds of fluxes have been designed to strengthen the weld joint by mixing the metal constituents in flux [13]. Many studies *e.g.*[20], [21], [23], have been reported optimizing the submerged arc welding process using the optimisation techniques. These optimisation techniques include Taguchi design of experiment, response surface methodology, grey relational analysis, fuzzy logic etc. Some of the researchers like [30], [31], [32] have also studied the effect on physical properties of weld by changing the chemical composition of flux and electrode material. Many studies have been done to improve the surface properties of weld by changing the flux composition and input parameters. The metal loaded in the flux gets mixed with the fused weld metal resulting in betterment of weld joints.

2.7 Objective of the Study

After observing the literature available regarding the submerged arc welding, it was concluded that many researchers have done the optimisation of submerged arc welding process taking the various parameters as input factors. But was found out that study of bead geometry influenced by flux variation, current, voltage, travel speed all together have not been reported. So, in the present thesis work it is proposed to study the effect of flux variation, current, voltage and travel speed on the bead geometry and micro hardness and microstructure of heat affected zone. The effect of variation in input factors has been studied using ANOVA and regression analysis.

Chapter 3

EXPERIMENTAL DESIGN

3.1 Introduction

Submerged arc welding *(SAW)* is a common arc welding process. It requires a continuously fed consumable solid or tubular (flux cored) electrode. The molten weld and the arc zone are protected from atmospheric contamination by being "submerged" under a blanket of granular fusible flux consisting of lime, silica, manganese oxide, calcium fluoride, and other compounds. When molten, the flux becomes conductive and provides a current path between the electrode and the work. This thick layer of flux completely covers the molten metal thus preventing spatter and sparks as well as suppressing the intense ultraviolet radiation and fumes that are a part of the *SMAW* (shielded metal arc welding) process. *DC* or *AC* power can be utilized, and combinations of *DC* and *AC* are common on multiple electrode systems. The objective of this research is to study the effect of input factors on the various weld bead properties. The input factors which could be varied in the submerged arc welding are current, voltage, travel speed, flux, electrode stick out, electrode diameter polarity etc. whole of the study has been done on the submerged arc welding machine. FD1X-200TZ welding tractor with TORNADO SAW M-800 transformer was used for the study. The welding set up has a maximum current and voltage range of *800 amp* and *110 volts* respectively.

3.2 Pilot Experimentation

In order to study the contributing factors that affect the response parameters, pilot experimentation was carried out on the machine. For the pilot experiment current, voltage, travel speed, flux and electrode stick out were varied at two levels each. For this purpose an L_8 Taguchi design was used to study the effect of contributing factors shown in Table 3.1.

Table 3.1: Table for Pilot Experiment Factors

Exp.no.	**Flux**	**Current**	**Travel speed**	**voltage**	**Electrode Stick out**
1.	I	350	27	28	15

2.	I	350	27	32	20
3.	I	450	31	28	15
4.	I	450	31	32	20
5.	II	350	31	28	20
6.	II	350	31	32	15
7.	II	450	27	28	20
8.	II	450	27	32	15

Based on the above experiment it was observed that electrode stick out had no impact on optimal conditions for *SAW*. Hence only four factors were taken up for the detailed experiment. Taguchi design has been used for the design of experiments, because it reduces the number of iterations and used to optimize the known parameters. It helps to select the best out of goods.

3.3 Orthogonal Array

To select an appropriate orthogonal array for experiments, the total degrees of freedom must be computed. The degrees of freedom are defined as the number of comparisons between process parameters that must be made to determine which level is better and, specifically, how much better it is. For example, a two-level process parameter counts for one degree of freedom. The degrees of freedom associated with interaction between two process parameters are given by the product of the degrees of freedom for the two process parameters. In the present study, the interaction between the welding parameters is neglected. Therefore, there are five degrees of freedom owing to the five sets of welding parameters in the submerged arc welding process. Once the degrees of freedom are known, the next step is to select an appropriate orthogonal array to fit the specific task.

The degrees of freedom for the orthogonal array should be greater than, or at least equal to, those for the process parameters. In this study, an L_{18} orthogonal array with four columns and eighteen rows was used. This array has seven degrees of freedom and it can handle four process parameters. Each welding parameter was assigned to a column and eighteen welding parameter combinations were tested. Therefore, only eighteen experiments are required to study the entire welding parameter space using the L_{18}

orthogonal array. The experimental layout for the welding parameters using the L_{18} orthogonal array is shown in Table 3.4.

3.3.1 Selection of Orthogonal Array and Factor Assignment

In this experimental study, three factors were varied to three levels each and one factor at two levels. The degree of freedom *(DOF)* to a three level parameter is *2* and for two level parameter is *1* (because *DOF=number of levels-1),* hence total *DOF* for the experiment is *7*. So the Orthogonal Array *(OA)* which could be used were L_9 and L_{18}. But L_9 could not be used due to its limitation of input factor levels. So, to overcome this problem L_{18} was used. Degree of freedom allocated to various factors is given in Table 3.2.

Table 3.2: DOF Allocated to Various Factor Combinations

Parameter	**Units**	**DOF**
Flux (A)		1
Current (B)	Ampere	2
Travel speed (C)	m/hr	2
Voltage(D)	volts	2
Total		7

3.4 Description of Machine

The experiments have been conducted on **Submerged Arc Welding Machine *i.e.*** Tornado Saw M-800 transformer and FD 10-200T welding tractor available at Central Workshop, Thapar University, Patiala.

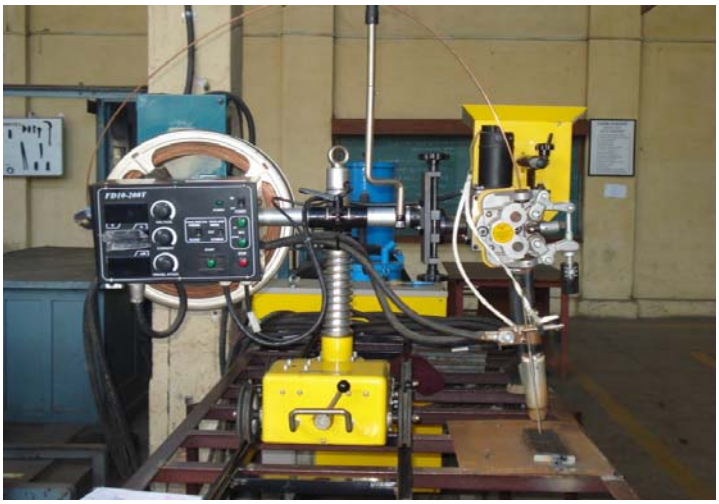

Figure: 3.1 SAW Used for Experimentation

SAW machine used for the experiments is shown in the Figure 3.1. The main parts of the machine are control box panel, electrode wire, wire spool and flux hopper. The welding current, welding voltage and welding speed can be regulated, displayed and preset on the panel of the tractor for the convenience of the operator. The function of inch wire feeding and withdrawing makes it convenient for the welder to preset the operating position of the welding wire. Control is provided on the machine for the movement of the tractor on the platform. The movement can be manual or can be automatic. There is also welding head site adjustment function it make the gun move vertically and vertically. Main technical parameters of the tractor are given in Table 3.3.

Table 3.3: Main Technical Parameters of Welding Tractor

Travel speed	20-60 m/hr
Wire feeding rate	0.5 m/min - 2.5 m/min
Wire diameter	2.4 mm -5 mm
Rated current value	800 amp
Rated voltage	110 volts
Tractor weight	54 kg

As stated earlier, the working of the machine is controlled by control box provided on the machine. There are parameter indication and control devices on the panel of control box. The detail of the controls has been discussed under next heading.

Figure 3.2: Control Box Panel

3.5 Switches, Knobs and Buttons on Control Panel

3.5.1 Travel mode

- *Manual*: In this mode tractor is not under the welding program. Direction of travel depends upon the decision of operator.
- *Automatic*: Welding program controls the behavior of tractor. The choice of travel direction switch decides the travelling direction.
- *Stop*: Tractor stops when stop button is pushed.

Travel direction is decided by the reverse/forward choice of the operator.

3.5.2 Knobs

- *Welding voltage:* Knob shown in Figure 3.2 shows the knob for voltage adjustment. The voltage can be adjusted by wringing the welding voltage knob on panel.
- *Welding current:* This knob is used for adjusting the welding current by just wringing it to desired value of current.
- *Welding speed:* This knob is used for setting the tractor's travelling speed, and the adjustment range is 20m/h-62 m/h.

3.5.3 Buttons

- *Inch wire feeding and wire drawing:* The inch wire feeding button is used for feeding the wire before welding. When the wire reliably contacts the work piece the feeding stops automatically. The inch wire button is used for drawing the wire during the off time of welding.
- *Start and Stop:* The start button is used for starting control of welding process. When it is pressed, drawing striking arc is automatically executed and the welding process begins. The stop button is used for compulsorily cease the welding process.

3.5.4 Display Indication

- *Welding voltage and current:* The two meters are used for displaying welding voltage and current. The preset voltage and current are displayed before welding begins.
- *Welding speed:* The welding speed meter is used for displaying the travelling speed of the tractor with a unit of m/h.
- *Power indicator:* The power indicator is used for indicating the on/off of the tractor's system power source. The light up of the indicator indicates the power source is ON, and the going out of the indicator indicates the power source is OFF

3.6 Experimental Set Up

As stated earlier L_{18} array has been selected for the experimentation. Flux, current, travel speed and voltage have been chosen as the factors of interest. L_{18} array with actual factors level is shown in Table 3.4.

The values of the input process parameters for the SAW are as below:

Flux used	'A'	:	I, II (with Basicity Index of 0.8 and 1.6)
Current	'B'	:	350, 400, 450 amperes
Travel speed	'C'	:	27, 29, 31 meter/hour
Voltage	'D'	:	28, 30, 32 volts

Table no 3.4 Orthogonal Array for Experimentation.

Exp no.	flux	Current (amp)	Travel speed(m/hr)	Voltage (volts)
1.	I	350	27	28
2.	I	350	29	30
3.	I	350	31	32
4.	I	400	27	28
5.	I	400	29	30
6.	I	400	31	32
7.	I	450	27	30
8.	I	450	29	32
9.	I	450	31	28
10.	II	350	27	32
11.	II	350	29	28
12.	II	350	31	30
13.	II	400	27	30
14.	II	400	29	32
15.	II	400	31	28
16.	II	450	27	32
17.	II	450	29	28
18.	II	450	31	30

The three input factors were varied up to three levels each and one factor up to two levels. Welding was done in the form of weld on bead. The mild steel plate of *12mm* thickness was used as work material for the experiment (composition given in Table 3.6). The dimensions of the work piece sample taken was $12 \times 75 \times 200$ *mm*. Figure 3.3 shows the mild steel plate after welding.

Figure 3.3: Work Plate after Welding

Two types of fluxes were used for the experimentation. The concentrations of the different compounds available in the flux are given in Table 3.5. The electrode material and composition is provided in Table 3.7.

Table 3.5: Concentrations of the Different Compounds available in the Flux

Flux	Al_2O_3+MnO_2	CaO+MgO	SiO_2+TiO_2	CaF_2
I	55	5	30	5
II	35	25	20	15

Table 3.6 Composition of Mild Steel Work piece

Base Metal Composition	Fe%	C%	Si%	Cr%	Ni%	Cu%	V%
	98.3	0.328	0.501	0.159	0.0857	0.175	0.074

Table no 3.7 Composition of Mild Steel Electrode

Mild Steel Electrode	C%	Si%	Mn%	S%	P%	Ni%	Cr%
	0.44	0.40	1.65	0.01	0.017	0.09	0.152

Schematic diagram of the weld joint is shown in Figure 3.4. The three physical measurements bead height, depth of penetration and bead width were measured after each experiment.

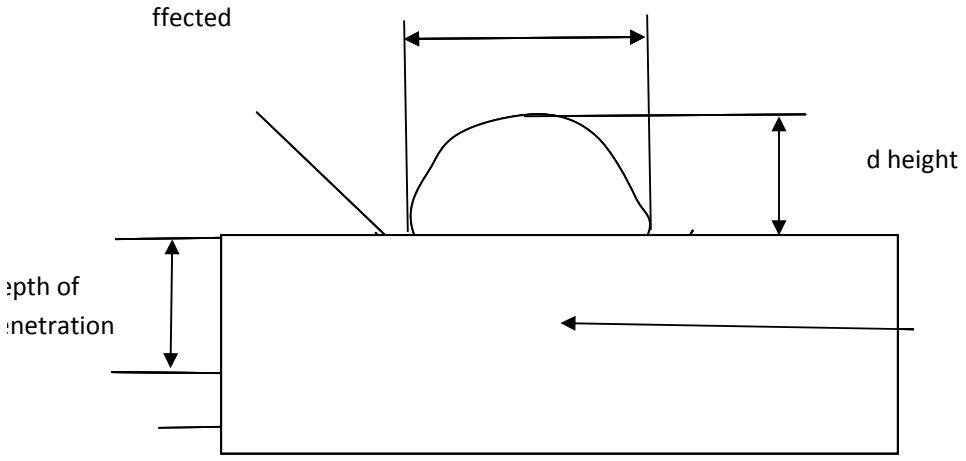

Figure 3.4: Schematic diagram of Weld Bead

Welding bead was formed on the work pieces as per the required parameter settings. After welding the samples were cut out from the work piece to measure the various characteristics shown in Figure 3.5.

Figure 3.5: Sample cut out for Analysis

The samples were cut out using power hack saw. After this samples were ground on the belt grinder. The surfaces were further smoothened using sand grinders of fine grit sizes. After polishing Micro hardness was measured, samples were etched with *2%* Nital solution. Bead geometry and micro hardness were measured after the etching the sample surface.

3.7 Analysis of Variance

ANOVA is a statistical technique which can infer some important conclusions based on analysis of the experimental data. The method is very useful for revealing the level of significance of influence of factor(s) or interaction of factors on a particular response. It separates the total variability of the response (sum of squared deviations about the grand mean) into contributions rendered by each of the parameter/ factor and the error. Thus

$$SS_T = SS_F + SS_e$$

where $SS_T = \sum_{j=1}^{p} (\gamma_j - \gamma_m)^2$

Where SS_T= Total sum of squared deviations about the mean.

γ_j Mean response for *jth* experiment.

γ_m Grand mean of the response.

SS_F Sum of squared deviations due to each factor.

SS_E Sum of squared deviations due to error

In the ANOVA table mean square deviation is defined as:

$$MS = \frac{SS(Sum\ of\ squared\ divison)}{DF(Degree\ of\ freedom)}$$

F-value of Fisher's F ratio (Variance ratio) is defined as:

$$F = \frac{MS\ for\ a\ term}{MS\ for\ the\ error\ term}$$

Depending on *F* value, *P*-value (probability of significance) is then calculated. If *P*-value for a term appears less than *0.05* (For *95%* confidence level) then it can be concluded that the effect of the factor(s)/ interaction of factors is significant on the selected response[MINITAB release *15.0* **(**user manual)].

In the ANOVA table, the degrees of freedom are used to calculate the mean square (*MS).* In general, the degrees of freedom measure how much "independent" information is available to calculate each sum of squares (*SS).*

Total DF = DF for all factors + DF for all interactions +DF for error

Where *n* is the total number of observations and ,

DF for factor = k−1

Where *k* is the number of the factor levels.

DF for Interaction = $(k_1-1) \times (k_2-1)$

Where k_1 is the number of levels of factor one, and k_2 is the number of levels of factor two. The same rule applies to interactions of more than two factors. In the present study, the interaction of factors has not been studied. The sequential sum of squares for each term in the model (factor or interaction) measures the amount of variation in the response that is explained by adding each term to the model sequentially in the order listed under source. Thus, the sequential sums of squares for terms are specific to the order of the terms specified in the linear model. The adjusted sum of squares for a term in the model (factor or interaction) measures the amount of additional variation in the response that is explained by the term, given that all the other terms are already in the model. Thus, the values for the adjusted sums of squares do not depend on the order of the terms listed under source. The adjusted mean square for a term is simply the adjusted sum of squares (*Adj. SS*) divided by the degrees of freedom.

3.8 Regression Analysis

Regression analysis is used to establish relationship between two variables. The response variable *y* is the independent variable or variable of interest, and the predictor variable *x* is the dependent variable. An objective of regression analysis is to develop a regression model, relating *y* to *x* that can be used to predict values of the response variable. As in case of the simple linear regression model relating *y* to *x* is

$$y = \beta_0 + \beta_1 x + \epsilon$$

The two parameters of the model are β_0, the *y*-intercept, and β_1, the slope of the line. β_0 is the mean value of *y* when *x* is zero. β_1 is the change in the mean value of *y* for one unit change in *x*. The random error ϵ, accounts for the variability in *y* that is not explained by the independent variable *x*. This variability could be due to other important independent variables or to some random phenomenon. The model assumes

that errors are independent, that is, the error associated with any one observation has no effect on the error associated with any one observation. The model also assumes a normal probability distribution of ϵ, with zero mean and constant variance σ^2 for all values of general linear model. In this experiment more than one variable is significantly affecting the response variable, and a multiple linear regression model may better estimate or predict the value of a response variable. The general form of linear regression model is:

$$y = \beta_0 + \beta_1 x_1 + \beta_2 x_2 + \ldots\ldots\ldots\ldots\ldots \beta_k x_k + \epsilon$$

Where $\beta_0, \beta_1, \ldots\ldots\ldots, \beta_k$ are the parameters we wish to estimate and ϵ is the random error term.

3.9 Signal-to-Noise Ratio

In the Taguchi method, there are three categories of performance characteristic in the analysis of the signal-to-noise ratio, that is, the lower-the-better, the higher-the-better, and the nominal the better. The change in quality characteristic of a product under investigation in response to a factor introduced in the experimental design is the 'signal' of the desired effect. The effect of the external factors (uncontrollable factors) on the outcome of quality characteristic is termed as 'noise'. The objective of any experiment is to achieve the best possible S/N ratio.

Finding a correct objective function to maximize in an engineering design problem is very important. Depending upon the type of response, the following three types of S/N ratios are employed in practice:

- ***Higher the Better:***

$(S/N)_{HB} = -10 \log (MSD_{HB})$

Where $MSD_{HB} = \frac{1}{R}\sum_{j=1}^{R}\left(\frac{1}{y_j^{\,2}}\right)$

MSD_{HB} = Mean Square Deviation for higher-the-better response.

- ***Lower the Better:***

$(S/N)_{LB} = -10 \log (MSD_{LB})$

Where $MSD_{LB} = \frac{1}{R}\sum_{j=1}^{R}\left(y_j^{\,2}\right)$

MSD_{HB} = Mean Square Deviation for Lower-the-better response.

- ***Nominal the Best:***

$(S/N)_{NB} = -10 \log (MSD_{NB})$

Where $MSD_{NB} = \frac{1}{R}\sum_{j=1}^{R}\left(y_j - y_0\right)^2$

MSD_{HB} = Mean Square Deviation for Lower-the-better response.

And, Y_j = Observed value of the response characteristic

Y_0 = nominal or target value of the results

R = Number of repetitions

3.10 Signal-to-Noise Ratio for Response Characteristics

The parameters that influence the output can be categorized into two classes, namely controllable (or design) factors and uncontrollable (or noise) factors. Controllable factors are those factors whose values can be set and easily adjusted by the designer. Uncontrollable factors are the sources of variation often associated with operational environment. The best settings of control factors as they influence the output parameters are determined through experiments. For smaller-the-better type, target value is zero. For larger-the-better, inverse of each large value becomes a small value and again the target value is zero.

For this experimental work, the following response characteristics have been studied:

1.	Response Name	:	Depth of penetration
	Response type	:	Higher-the-better
	Units	:	mm.
2	Response Name	:	Reinforcement
	Response type	:	Lower-the-better
	Units	:	mm.

3. Response Name : Weld bead width

   Response type : Lower the better

   Units : mm.

4. Response Name : Microhardness of HAZ

   Response type : Nominal-the-best

   Units : HVN

3.11 Measuring Equipment

1) **Microhardness Tester:** Microhardness tests were conducted on the computer interfaced micro hardness tester manufactured by Metatech industries, Pune, India. Microhardness measured is dependent on the diameter of indentation on the samples. The indentations were measured by the Quantimet software. The indents formed by pyramid shaped indenter were measured with the help of software. There are two eyepieces available in the instrument of 10X and 40X. Eyepiece of 40X was used for the experiments. The diameter of indent is measured with the software, which gives the direct number for micro hardness.
2) **Optical Microscope:** Micrographs were taken with the optical microscope manufactured by Beuhler, Germany available in R and D centre, Thapar University, Patiala. The instrument has many eyepieces of different magnifications of 10X, 20X, 50X,100X,200X and 500X. 200X magnification were used to take the micrographs.
3) **Digital Vernier Caliper:** Bead dimensions were measured with the help of profile projector and vernier caliper manufactured by Mitutoyo, Japan. The dimensions can be measured from the projected image of the specimen. This instrument mounts a digital clock which gives the measurement value. Measurements can be taken in inches and mm units.

Chapter4

RESULTS AND ANALYSIS

4.1 ANOVA Analysis

Results obtained from the experiments were analyzed using the ANOVA, which helps in predicting the significance of input parameter for any desired response function. It indicates which is the most influencing factor or parameter. A confidence interval of *95%* has been taken for this analysis. Significance of all the dependent variables has been completed using statistical software MINITAB 15. These dependent variables studied in this study are (1) bead height (2) depth of penetration (3) bead width (4) micro hardness.

4.2 ANOVA for Bead Height

The results observed for the height of bead are shown in the Table 4.1. The table consists of the values of bead height for the eighteen trials with one replication. The mean value of the bead height is also given in Table 4.1. The experimental results for bead height were analyzed using ANOVA and is given in the Table 4.2. The *p* value given in the last column of ANOVA table suggests the significance of the factors on the desired characteristics. The principle behind significance value is that the *p* value should be lesser than *0.05* (considering confidence level of *95%*). The principle of *F* test is that, the *F* value should be large compared to e-pooled; larger the *F* value more is the significance of factor. An ANOVA Table 4.2 show that *p* value for current is *0.014 i.e.* less than *0.05* indicates thereby that current is the most significant factor for the bead height. The mean value for all four variables is given in Table 4.3. In last row of Table 4.3 ranks have been given to various factors. Higher is the rank, higher is the significance. In Table 4.3 Current with the highest rank *1* and is the most significant factor and voltage with its lowest rank is least significant in affecting the bead geometry. Main effect plots are shown in Figure 4.1 shows the variation in the bead height with the change in the input factors *i.e.* flux, current, travel speed and voltage. It could be seen from the Figure 4.1 that current causes the most significant change in the bead height with change in current value. The flux change also has some effect on the variation in the bead height. Travel speed and voltage have no affect on the bead height.

Table 4.1: Results for Bead Height

Exp. no.	Flux	Current	Travel Speed	Voltage	Heightof Bead		Mean Height	S/N Ratio
					I	II		
1.	I	350	27	28	3.80	3.01	3.405	-10.7004
2.	I	350	29	30	3.66	2.74	3.200	-10.1918
3.	I	350	31	32	3.79	3.49	3.640	-11.2294
4.	I	400	27	28	4.05	4.10	4.075	-12.2027
5.	I	400	29	30	3.48	3.83	3.655	-11.2677
6.	I	400	31	32	3.26	3.53	3.395	-10.6237
7.	I	450	27	30	4.09	4.30	4.195	-12.4574
8.	I	450	29	32	4.65	4.53	4.590	-13.237
9.	I	450	31	28	3.52	3.77	3.645	-11.2391
10.	II	350	27	32	2.63	2.87	2.750	-8.79492
11.	II	350	29	30	3.14	3.29	3.215	-10.146
12.	II	350	31	30	2.96	3.02	2.990	-9.51386
13.	II	400	27	30	3.72	4.30	4.010	-12.0855
14.	II	400	29	32	3.64	3.72	3.680	-11.3175
15.	II	400	31	28	3.97	3.91	3.940	-11.9102
16.	II	450	27	32	3.56	3.81	3.685	-11.3337
17.	II	450	29	28	3.67	3.57	3.620	-11.175
18.	II	450	31	30	3.63	3.75	3.690	-11.3417

Table 4.2: Analysis of Variance for Means

Analysis of Variance for Means

Source	DF	Seq SS	Adj SS	Adj MS	F	P
flux	1	0.27380	0.27380	0.273800	2.14	0.174
current	2	1.71875	1.71875	0.859376	6.72	**0.014**
travel speed	2	0.06298	0.06298	0.031489	0.25	0.786
voltage	2	0.00284	0.00284	0.001422	0.01	0.989
Residual Error	10	1.27804	1.27804	0.127804		
Total	17	3.33641				

Table 4.3: Response Table for Means of Bead Height

Level	flux	current	travel speed	voltage
1	3.756	3.200	3.687	3.650
2	3.509	3.792	3.660	3.623
3		3.904	3.550	3.623
Delta	0.247	0.704	0.137	0.027
Rank	2	1	3	4

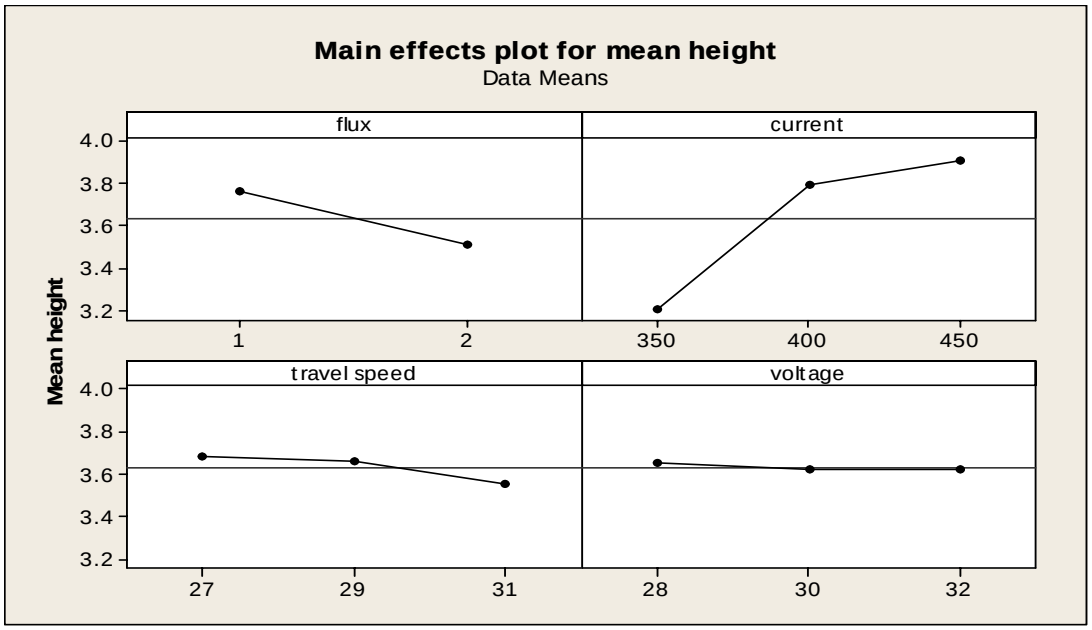

Figure 4.1: Main Effect Plot for Bead Height

4.3 Analysis of S/N Ratio for Bead Height

The signal to noise ratio gives an idea about the variations present in the process. The ANOVA table for S/N ratio has been shown as Table 4.4. ANOVA table for S/N ratio also advocates the significance of current with *p* value of *.012*. Main effects plot for S/N ratio are shown in Figure 4.2.

Table 4.4: Analysis of Variance for SN ratios

Source	DF	Seq SS	Adj SS	Adj MS	F	P
flux	1	1.6994	1.6994	1.69939	2.39	0.153
current	2	10.2262	10.2262	5.11309	7.19	**0.012**
travel speed	2	0.2882	0.2882	0.14408	0.20	0.820
voltage	2	0.0594	0.0594	0.02972	0.04	0.959
Residual Error	10	7.1086	7.1086	0.71086		
Total	17	19.3818				

Table 4.5: Response Table for Signal to Noise Ratios of Bead Height

Response Table for Signal to Noise Ratios

Smaller is better

Level	flux	current	travel speed	voltage
1	-11.44	-10.07	-11.25	-11.22
2	-10.84	-11.56	-11.21	-11.12
3		-11.79	-10.97	-11.08
Delta	0.60	1.73	0.27	0.13
Rank	2	1	3	4

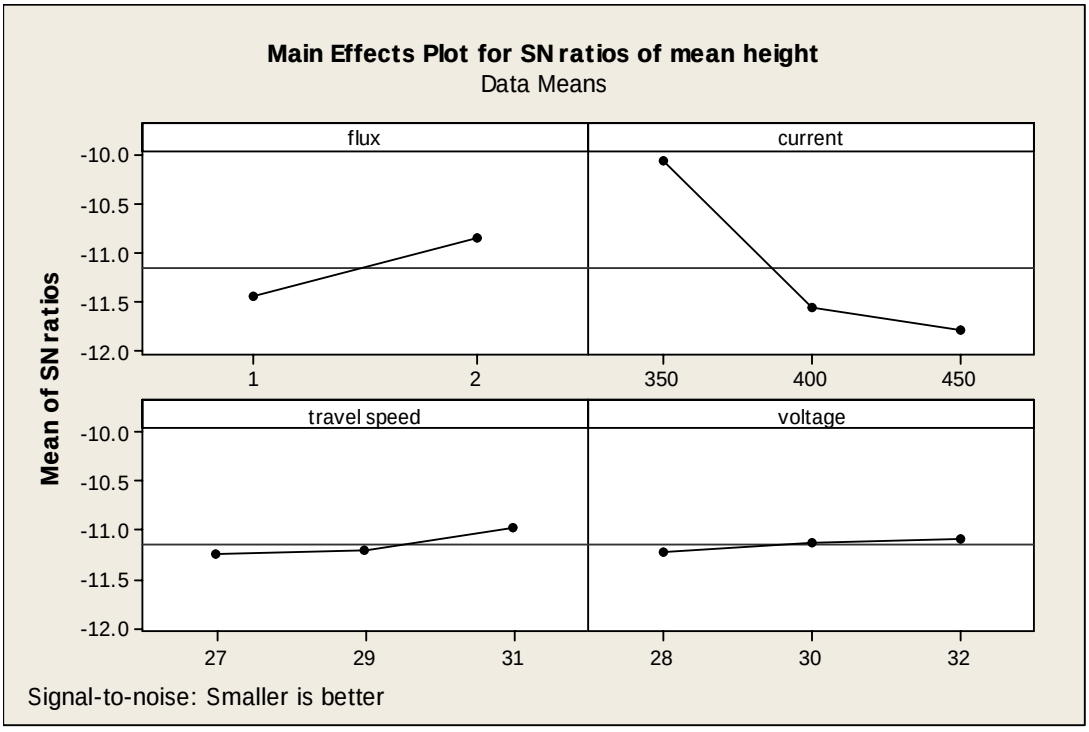

Figure 4.2: Main effect plots for S/N ratios of bead height

4.4 Optimal Design for bead height

In this experimental analysis, the main effect plot in figure 4.1 has been used to estimate the bead height in optimal conditions. From Table 4.2, it can be concluded that current and flux are two significant factors. In order to obtain minimum height of the bead, the lower levels of current input *(350 Amp)* and flux type II (Basicity Index-1.6) has been chosen.

Mean value of bead height for low levels

$\mu_{A2B1}=\bar{A}_2+\bar{B}_1-\bar{T}$

3.509 + 3.200 - 3.96 = 2.749 mm

Confidence Interval around the estimated mean bead height

$$C.I.=\sqrt{\frac{f_{\alpha:v1:v2}\times v_e}{n_{eff}}}$$

Where $F_{\alpha:\, v:;v2}$ = *F ratio*

$\alpha = risk$ (0.05) $\qquad\qquad$ $confidence = 1-\alpha$

v_1=*dof for mean (which is always 1)*

v_2= *dof for error*

varience= $v_e = \frac{SS\ of\ e\ pooled}{dof\ of\ e\ pooled} = 0.016$

n_{eff} = number of tests performed using participating factors

$n_{eff} = \frac{18}{1+d.o.f._{A2B1}} = 4.5$

C.I=0.165

So the confidence interval around bead height is given by *2.749 ±.165 mm.*

4.5 ANOVA for Depth of Penetration

Results observed for the height of bead are shown in the Table 4.6. The table consists of the mean depth of penetration for the eighteen trials with one replication. The mean of the bead height is also given in Table 4.7. ANOVA table for depth of penetration is given in Table 4.7. ANOVA table indicates the significance value of various input factors. If the *p* value given in the last column of ANOVA table is less than 0*.05*, this means the factor corresponding to that value of *p* is significant. In present study the *p* value for current and voltage are *0.002* and *0.037* respectively coming lesser than *0.05*. *F* value given in ANOVA table also indicates the significance of factors, higher the *F* value higher is the significance of that factor. Table 4.8 gives mean value of the response has been given at all levels of input parameters. In the last row of this table, factors are ranked as per their degree of significance. Current is the most significant factor with rank *1*. Main effect plot for depth of penetration is shown in Figure 4.3. Mean value of the depth of penetration is taken along the *y*-axis and levels of contributing factors are taken along the *x*- axis. The plots indicate that with change in value of current and voltage, the mean value of depth of penetration varies. Flux and travel speed does not have any significant effect on mean value of depth of penetration.

Table 4.6: Results for Depth of Penetration

Exp. no.	flux	current	Travel speed	voltage	Depth of penetration		Mean depth	S/N Ratios
					I	II		
1.	I	350	27	28	4.80	5.03	4.915	13.8233
2.	I	350	29	30	5.26	5.11	5.185	14.2922
3.	I	350	31	32	4.82	5.16	4.990	13.9469
4.	I	400	27	28	5.19	5.07	5.130	14.2006
5.	I	400	29	30	5.58	5.81	5.695	15.1046
6.	I	400	31	32	5.83	5.50	5.665	15.0529
7.	I	450	27	30	6.72	6.85	6.785	16.6298
8.	I	450	29	32	6.69	6.72	6.705	16.5279
9.	I	450	31	28	4.74	4.88	4.810	13.6401
10.	II	350	27	32	4.12	4.80	4.460	12.9109
11.	II	350	29	30	4.47	4.41	4.440	12.9471
12.	II	350	31	30	5.07	5.10	5.085	14.1257
13.	II	400	27	30	4.89	5.03	4.960	13.9070
14.	II	400	29	32	6.06	6.45	6.255	15.9119
15.	II	400	31	28	4.40	5.18	4.790	13.5202
16.	II	450	27	32	7.20	7.57	7.385	17.3588
17.	II	450	29	28	6.22	5.88	6.050	15.6248
18.	II	450	31	30	6.43	6.24	6.335	16.0320

Table 4.7: Table for Analysis of Variance for Means

Analysis of Variance for Means

Source	DF	Seq SS	Adj SS	Adj MS	F	P
flux	1	0.0008	0.0008	0.0008	0.00	0.958
current	2	6.8715	6.8715	3.4358	**12.65**	**0.002**
travel speed	2	0.6319	0.6319	0.3159	1.16	0.351
voltage	2	2.5359	2.5359	1.2679	**4.67**	**0.037**
Error	10	2.7163	2.7163	0.2716		
Total	17	12.7564				

Table 4.8: Response Table for Means of Depth of Penetration

Level	flux	current	travel speed	voltage
1	5.681	4.931	5.691	5.107
2	5.529	5.538	5.722	5.674
3		6.345	5.402	6.032
Delta	0.152	1.414	0.320	0.925
Rank	4	1	3	2

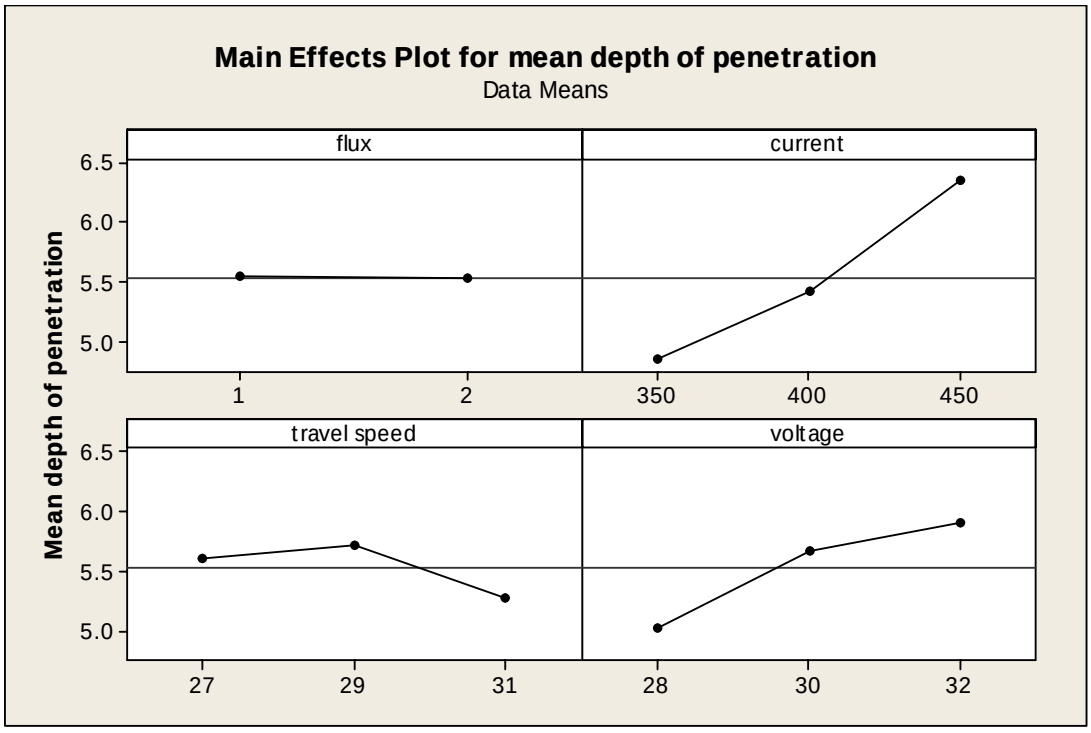

Figure 4.3: Main effect plots for mean depth of penetration

4.6 Analysis of S/N Ratio for Depth of Penetration

Larger depth of penetration is the desirable property of the weld joint. So in case of depth of penetration, larger the better option has been chosen for calculation of S/N ratio. ANOVA for S/N ratio is given in Table 4.9. Mean value at each level of parameters is given in Table 4.10. Table 4.10 also indicates the ranks given to input parameters according to their order of significance. The main effect plot for S/N ratio is given in Figure 4.4

Table 4.9: Analysis of Variance for SN ratios

Source	DF	Seq SS	Adj SS	Adj MS	F	P
flux	1	0.0430	0.0430	0.04301	0.06	0.804
current	2	15.9638	15.9638	7.98191	**11.99**	**0.002**
travel speed	2	1.4187	1.4187	0.70933	1.07	0.381
voltage	2	5.8892	5.8892	2.94460	**4.43**	**0.042**
Residual Error	10	6.6544	6.6544	0.66544		
Total	17	29.9691				

Table 4.10: Response Table for Signal to Noise Ratios

Larger is better

Level	flux	current	travel speed	voltage
1	15.02	13.83	14.96	14.12
2	14.73	14.81	15.07	15.02
3		15.97	14.58	15.48
Delta	0.29	2.14	0.49	1.36
Rank	4	1	3	2

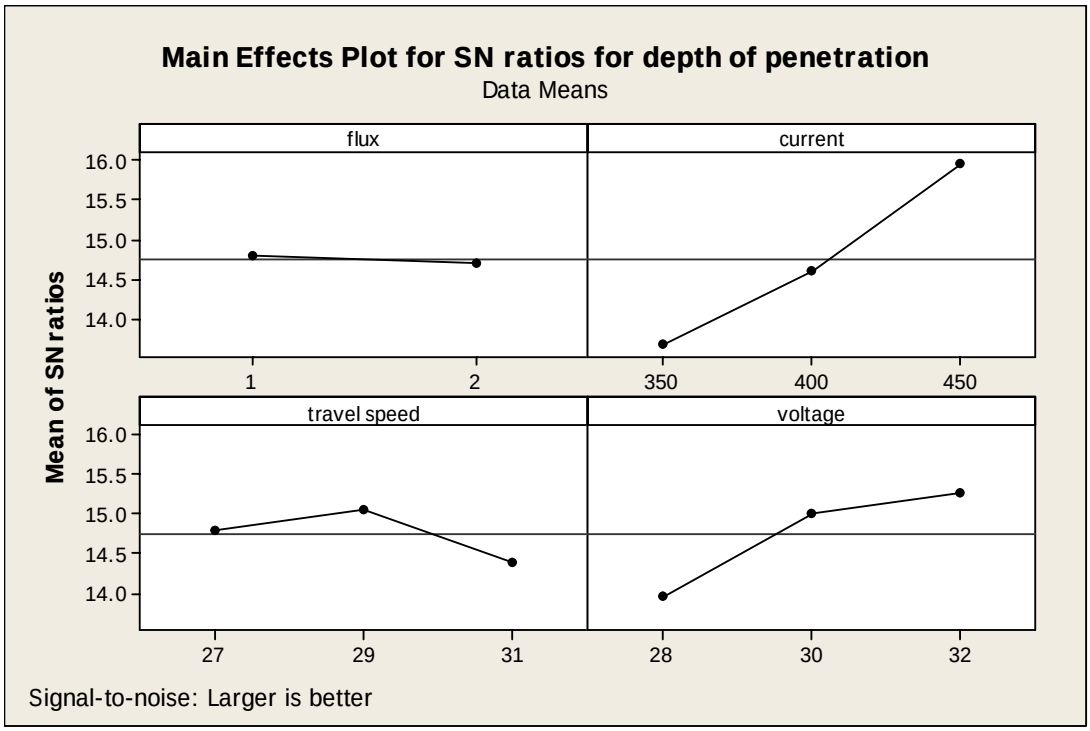

Figure 4.4: Main Effects Plot for S/N Ratios

4.7 Optimal design for Depth of Penetration

In this experimental analysis, a higher average response is better *(HB)* has been chosen so as to have a higher depth of penetration. From Figure 4.3 it can be concluded that current and voltage are two significant factors. For depth of penetration higher the better option has been selected .So, for higher depth of penetration maximum level of both the significant factors has been chosen *i.e.450 amp* and *32 volts*. Confidence interval predict with *95%* confidence that value of depth of penetration at optimal design conditions would be *6.847±1.537mm*.

Mean value of depth of penetration is given by:

$\mu_{B3D3} = \overline{B_3} + \overline{D_3} - \bar{T}$

6.345 + 6.032 - 5.53 = *6.847 mm*

Confidence Interval around the estimated mean depth of penetration:

$$n_{eff} = \frac{18}{1 + dof_{B3D3}}$$

$n_{eff} = 3.6$

$$C.I. = \sqrt{\frac{F_{\alpha:V1:V2} \times v_e}{n_{eff}}}$$

C.I. =1.537

So the confidence interval around the estimated depth of penetration is *6.847±1.537 mm*.

4.8 ANOVA for Bead Width

The results for bead width are shown in the Table 4.11. The table consists of the values of bead width for the eighteen trials with one replication. The mean value is also given in last column of Table 4.11. ANOVA table for means is given in Table 4.13. ANOVA table indicates that *p* value for voltage is minimum when bead width is taken as response. *P* value for voltage is *0.030,* which is lesser than *0.05. F* value for the voltage is also maximum, which indicates that it is a significant factor contributing to the response, which includes the ranks of the contributing factors. In the present study voltage is the most significant factor. Main effect plots showing the variation in the bead width with change in input factors have been shown in Figure 4.5. It is clear from Figure 4.5 that bead width increases almost linearly with increase in voltage. On the other hand bead width decreases with increase in travel speed.

Table 4.11: Results for Bead width

Exp. no.	Flux	Current	Travel speed	Voltage	Bead width		Mean Width	S/N ratios
					I	II		
1.	I	350	27	28	12.27	12.20	12.235	-21.7521
2.	I	350	29	30	12.23	13.18	12.705	-22.0856
3.	I	350	31	32	14.19	14.54	14.365	-23.1468
4.	I	400	27	28	12.35	12.68	12.515	-21.9494
5.	I	400	29	30	14.41	14.47	14.440	-23.1914
6.	I	400	31	32	14.25	14.84	14.545	-23.2561

7.	I	450	27	30	14.15	13.83	13.990	-22.9169
8.	I	450	29	32	14.85	14.65	14.750	-23.376
9.	I	450	31	28	13.25	13.41	13.330	-22.4968
10.	II	350	27	32	17.74	16.18	16.960	-24.5977
11.	II	350	29	30	13.78	13.78	13.780	-22.785
12.	II	350	31	30	12.66	12.30	12.480	-21.9252
13.	II	400	27	30	14.66	13.43	14.045	-22.9588
14.	II	400	29	32	13.64	13.75	13.695	-22.7313
15.	II	400	31	28	12.43	13.09	12.760	-22.1199
16.	II	450	27	32	14.64	14.77	14.705	-23.3494
17.	II	450	29	28	13.23	12.95	13.090	-22.3393
18.	II	450	31	30	13.78	13.85	13.815	-22.807

Table 4.12: Analysis of Variance for Means

Source	DF	Seq SS	Adj SS	Adj MS	F	P
flux	1	0.1233	0.1233	0.12334	0.14	0.720
current	2	0.1311	0.1311	0.06555	0.07	0.931
travel speed	2	1.5603	1.5603	0.78016	0.86	0.453
voltage	**2**	**9.2702**	**9.2702**	**4.63509**	**5.10**	**0.030**
Residual Error	10	9.0846	9.0846	0.90846		
Total	17	20.1696				

Table 4.13: Response Table for Means

Level	flux	current	travel speed	voltage
1	13.77	13.75	14.25	13.14
2	13.94	13.84	13.76	13.58
3		13.96	13.55	14.84
Delta	0.17	0.21	0.70	1.69
Rank	4	3	2	1

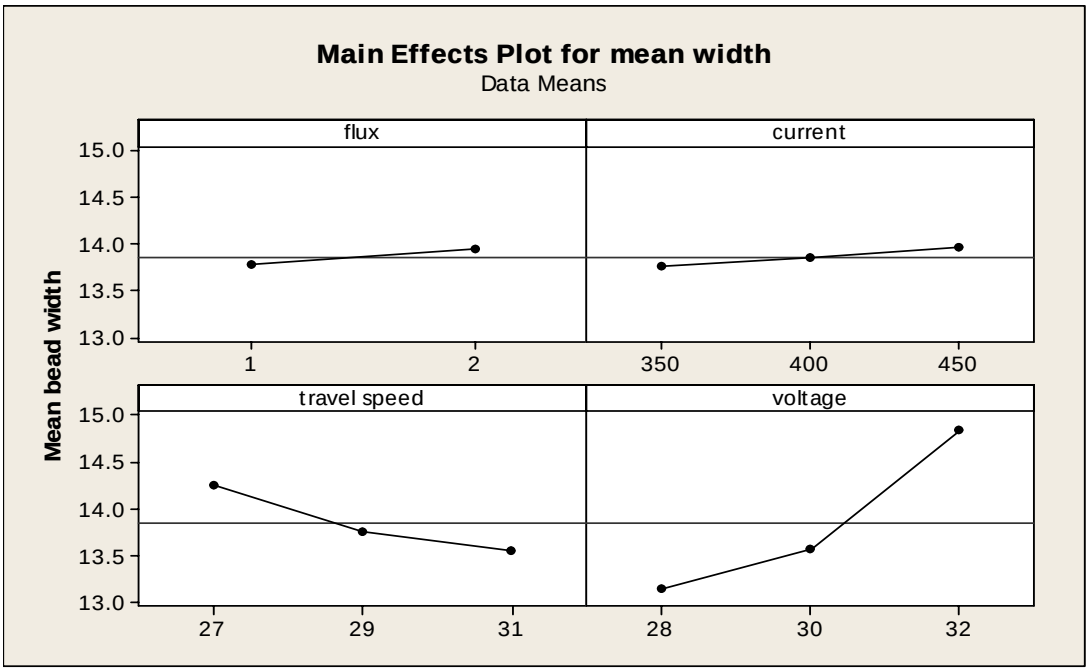

Figure 4.5: Main effect plots for Mean of Bead Width

4.9 Analysis of S/N Ratio for Bead Width

Higher bead width is an undesirable property of the weld bead joint. Because it does not provide any strength to the weld joint. So, for bead width, lower the better option is chosen for signal to noise ratio calculations. Table 4.15 shows the response table for means. Main effect plots are shown in Figure 4.6. Significant change in bead width can be seen from the figure with change in the levels of input factors voltage and travel spee

Table 4.14: Analysis of Variance for S/N ratios

Source	DF	Seq SS	Adj SS	Adj MS	F	P
flux	1	0.03559	0.03559	0.03559	0.11	0.751
current	2	0.09401	0.09401	0.04701	0.14	0.871
travel speed	2	0.53136	0.53136	0.26568	0.79	0.479
voltage	2	3.48376	3.48376	1.74188	5.**20**	**0.028**
Residual Error	10	3.35137	3.35137	0.33514		
Total	17	7.49609				

Table 4.15: Response Table for Signal to Noise Ratios

Smaller is better

Level	flux	current	travel speed	voltage
1	-22.76	-22.71	-23.04	-22.37
2	-22.85	-22.82	-22.76	-22.64
3		-22.89	-22.62	-23.41
Delta	0.09	0.18	0.41	1.04
Rank	4	3	2	1

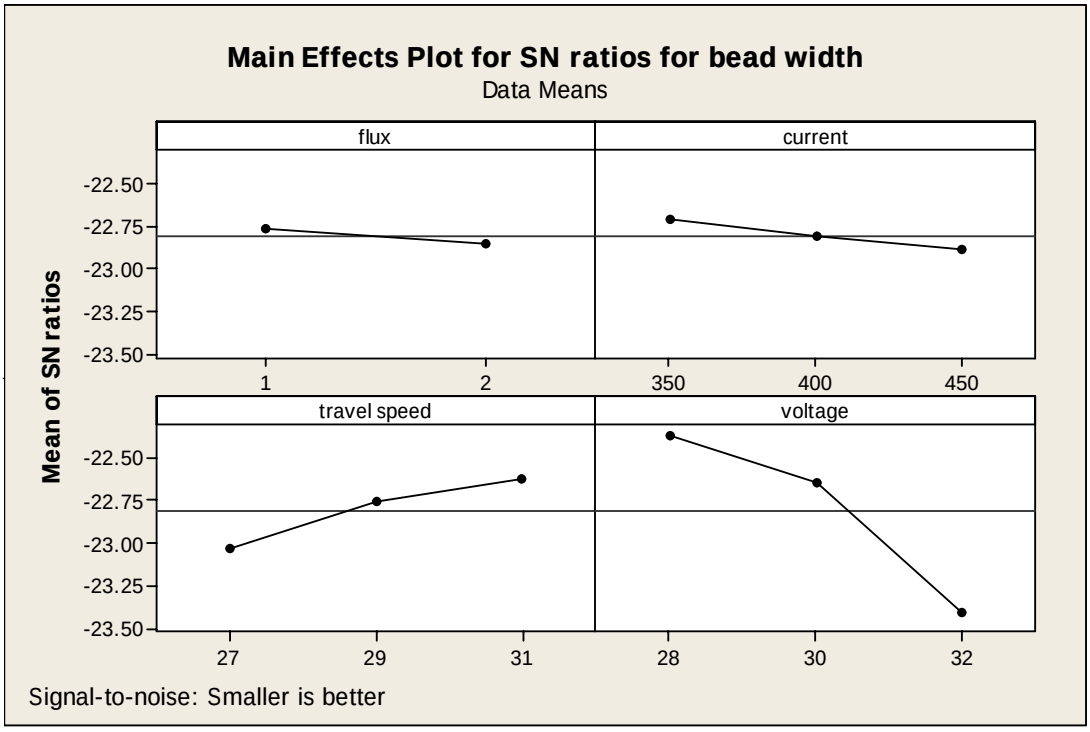

Figure 4.6: Main effect plot for S/N ratios of Bead Width

4.10 Optimal design for bead width

The signal to noise ratio calculations have been computed using the 'lowest the better' option for bead width. For bead width lower the better option is desired. The main effect plots shown in figure 4.5 indicate that travel speed and voltage are two significant contributing factors. So, in order to minimize the bead width, higher travel speed and lower voltage are the two desired input parameters for optimal design. Confidence interval predicts with 95% confidence that value of bead width at optimal design conditions would *12.90 ±.424 mm.*

Mean bead width is given by:

$\mu_{C3D1}=\overline{C_3}+\overline{D_1}-\bar{T}$

13.55 + 13.11 - 13.789 = *12.90 mm.*

Variance =v_e= *0.084*

n_{eff}= number of tests under that condition using the participating factors

$$n_{eff} = \frac{18}{1 + dof_{C3D1}}$$

n_{eff}=3.6

$$C.I. = \sqrt{\frac{F_{\alpha:V1:V2} \times v_e}{n_{eff}}}$$

Substituting the *F* values from the statistical tables and variance, value of C.I. comes out to be *0.424*.

So the confidence interval around the estimated bead width is *12.90 ±.424 mm.*

4.11 ANOVA for Microhardness

The results observed for the mean hardness are shown in the Table 4.16. The table consists of the values of micro hardness for the eighteen trials with one replication. The last column of Table 4.16 displays the mean value of micro hardness. Micro hardness of heat affected zone changes due to recrystallisation of metal grains. This recrystallisation of metal grains occurs due to the high temperature of weld pool. Flux also plays a big role in deciding the hardness of the fusion zone and heat affected zone. ANOVA analysis has been shown in the Table 4.17. From Table 4.17, it can be concluded that current and fluxes are two significant factors affecting the micro hardness. *P* value for flux and current being *0.010* and *0.005* respectively. Mean values for all parameters at different levels has been given in Table 4.18. Main effect plots are given in Figure 4.7. From Figure 4.7, it can be seen that micro hardness decreased, with change in basicity of flux. S/N ratios are calculated taking 'nominal the best' with target value of *23.5 hvn* (mean value of parent metal micro hardness).

Table 4.16: Results for Micro Hardness of HAZ

Exp. No.	Flux	Current	Travel Speed	Voltage	Micro Hardness		Mean Hardness	S/N Ratios
					I	II		
1.	I	350	27	28	28.530	25.56	27.045	22.1969
2.	I	350	29	30	39.700	38.53	39.115	33.4934
3.	I	350	31	32	49.650	51.25	50.450	32.9851
4.	I	400	27	28	43.320	44.85	44.085	32.2023
5.	I	400	29	30	49.310	50.32	49.815	36.8711
6.	I	400	31	32	41.440	42.68	42.060	33.6193
7.	I	450	27	30	56.550	53.26	54.905	27.4586
8.	I	450	29	32	56.769	54.55	55.659	30.9979
9.	I	450	31	28	65.930	63.34	64.635	30.9537
10.	II	350	27	32	36.840	35.14	35.990	29.5250
11.	II	350	29	30	32.240	33.52	32.880	31.2047
12.	II	350	31	30	32.710	34.12	33.415	30.5047
13.	II	400	27	30	32.601	35.10	33.850	25.6463
14.	II	400	29	32	39.028	37.50	38.264	30.9836
15.	II	400	31	28	39.870	38.19	39.030	30.3321
16.	II	450	27	32	44..116	43.82	43.968	46.4472
17.	II	450	29	28	47.557	48.66	48.108	35.8032
18.	II	450	31	30	40.360	42.58	41.470	28.4379

Table 4.17: Analysis of Variance for Microhardness

Analysis of Variance for Means

Source	DF	Seq SS	Adj SS	Adj MS	F	P
flux	**1**	**362.11**	**362.11**	**362.110**	**9.90**	**0.010**
current	**2**	**702.81**	**702.81**	**351.406**	**9.61**	**0.005**
travel spee	2	88.92	88.92	44.459	1.22	0.337
voltage	2	17.28	17.28	8.638	0.24	0.794
Residual Error	10	365.79	365.79	36.579		
Total	17	1536.90				

Table 4.18: Response Table for Means for Micro Hardness

Response Table for Means

Level	flux	current	travel speed	voltage
1	47.52	36.48	39.97	42.63
2	38.55	41.18	43.96	42.10
3		51.45	45.18	44.39
Delta	8.97	14.97	5.20	2.29
Rank	2	1	3	4

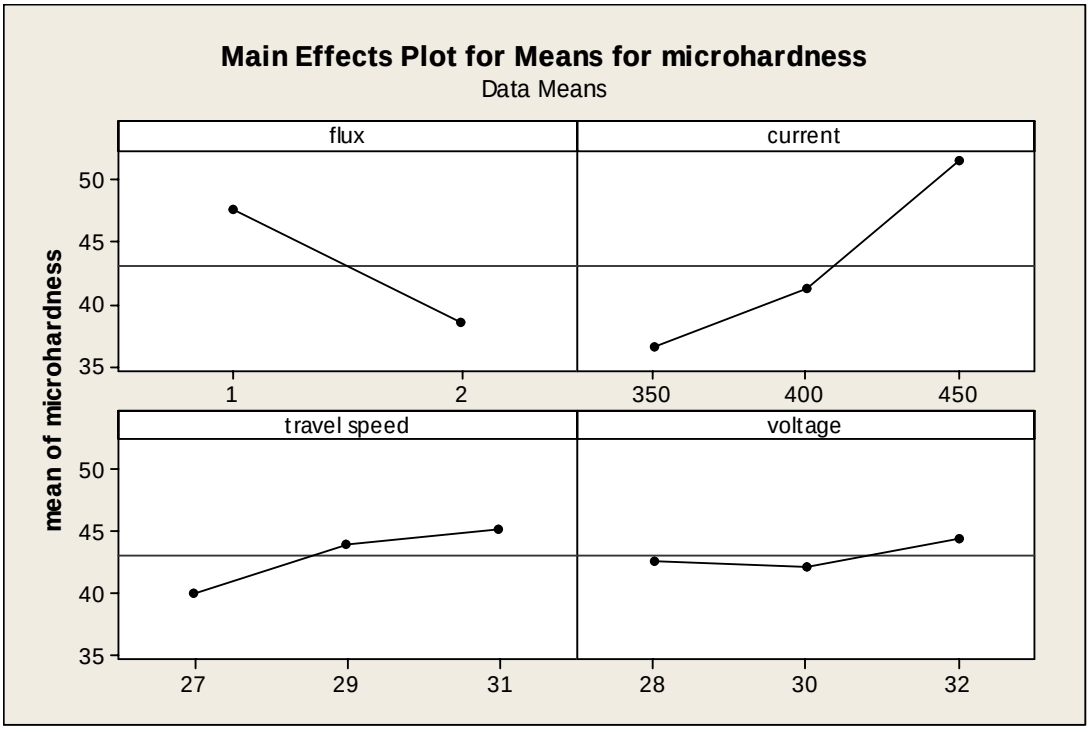

Figure 4.7: Main effects plot for Mean Micohardness

4.12 Analysis of S/N Ratio for Micro Hardness

ANOVA analysis for signal to noise ratio has been given in Table 4.19, from where it can be concluded that flux and current are the two most significant factors impacting micro hardness with *p* value less than *0.05*. Response table for signal to noise ratio also given at Table 4.20. Main effect plots for S/N ratios are shown in Figure 4.8.

Table 4.19.: Analysis of Variance for S/N Ratios

source	DF	Seq SS	Adj SS	Adj MS	F	P
flux	1	362.11	362.11	362.110	**9.90**	**0.010**
current	2	702.81	702.81	351.406	**9.61**	**0.005**
travel speed	2	88.92	88.92	44.459	1.22	0.337
voltage	2	17.28	17.28	8.638	0.24	0.794
Residual Error	10	365.79	365.79	36.579		
Total	17	1536.90				

Table 4.20: Response Table for Signal to Noise Ratios for Micro Hardness

Nominal is best (10*Log10 (Ybar**2/s**2))

Level	flux	current	travel speed	voltage
1	31.25	29.98	30.58	30.45
2	32.10	31.61	33.30	30.40
3		33.43	31.14	34.17
Delta	0.85	3.44	2.72	3.77
Rank	4	2	3	1

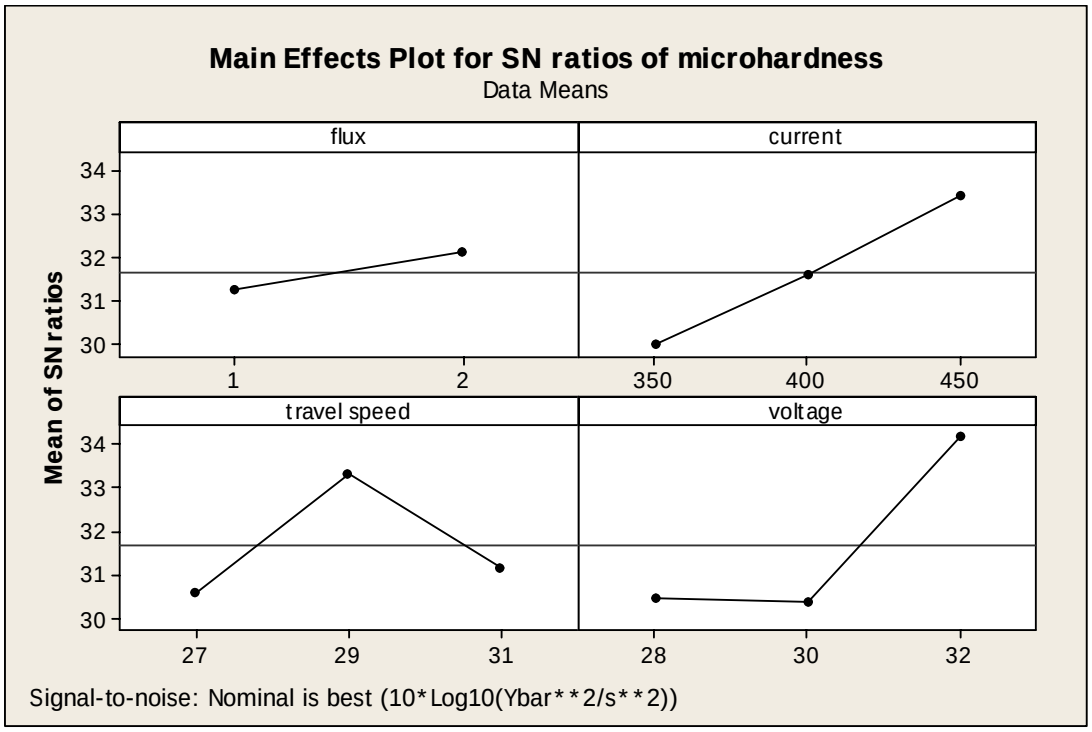

Figure 4.8: Main Effect Plots for S/N Ratios

4.13 Optimal Design for Microhardness

Main effects plot shown in Figure 4.7 shows that flux and current have the significant effect on micro hardness of heat affected zone. Nominal micro hardness is the desired response parameter. For optimization of response first type of flux and third level of current *i.e. 450 amp* has been chosen for optimal design. Confidence interval predict with *95%* confidence that value of micro hardness at optimal design conditions would be *55.93 ± 6.74.*

Mean Micro Hardness is given by:

$$\mu_{A2B3} = \overline{A_2} + \bar{B}_3 - \bar{T}$$

38.55 + 51.45- 43.04 = 46.96

$$n_{eff} = \frac{18}{1 + dof_{A2B3}}$$

$$C.I. = \sqrt{\frac{F_{\alpha:V1:V2} \times v_e}{n_{eff}}}$$

n_{eff} = 4.5

v_e = 46.96

Substituting the values of variance and n_{eff} in equation for C.I.:

Value of *C.I.* comes out to be *9.35.*

Confidence interval around the mean micro hardness comes out to be *46.96 ± 9.35 hvn.*

4.14 Further Analysis

Observing the Table 4.1, it can be concluded that minimum bead height occurs at minimum at minimum level of current, *e.g.* bead height in trial 1^{st},10^{th} ,12^{th} , the bead height is very low as compared to remaining trials. The bead height shows a great change when current is raised from *350 amp* to *400 amp,* whereas further rise to *450 amp* shows lesser effect. The depth of penetration has a direct relation with heat input. Table 4.6 provides the evidence for previous statement. It is clear from table 4.6 that maximum depth of penetration is obtained only in those trials where current and voltage has maximum values. Flux has nil effect on the depth of penetration. From table 4.11 it is clear that bead width is maximum in those trials where the voltage input is maximum *i.e. 32 volts.* For example in 3^{rd} , 8^{th} ,10^{th} trials bead width has higher values irrespective of level of other input factors. The micro hardness of the heat affected zone shows the significant effect of current input. The mean value is maximum at the highest level of current input *i.e.450 amp.* Table 4.21 gives a concise view of ANOVA for mean values and ANOVA for S/N ratios for all the input factors.

Table 4.21: Significant Factors in ANOVA and S/N ratios Analysis

Response Name	**Significant Factors Affecting Mean Values**	**Significant Factors Affecting S/N Ratios**
Bead Height	Current	Current
Depth Of Penetration	Current, Voltage	Current, Voltage
Bead Width	Voltage	Voltage
Microhardness	Flux, Current	Flux, Current

Chapter 5

Empirical Modeling

5.1 Regression Analysis

Regression analysis is done to establish the relationship between two variables. Regression analysis indicates the relationship among the dependent variable and independent variables. Value of dependent variable can be predicted only by putting the desired value of independent variable in the regression equation. Regression analysis has been done using statistical software MINITAB 15.

5.2 Regression Analysis for Bead Height

Equation 5.1 is the regression equation obtained from the regression analysis. ANOVA for regression has been given in Table 5.1. Regression table also suggests that current is the most significant factor. Table 5.1 indicates that p value for regression equation is significant.

The regression equation is

$$\text{mean height} = 2.38 - 0.247f + 0.00704c - 0.0342\,t.s. - 0.0067v \quad \ldots \text{(Equation 5.1)}$$

Where
f = flux
c = current
t.s. = travel speed
v = voltage

Table 5.1: Regression Table for Mean Bead Height

Predictor	Coef	SE Coef	T	P
Constant	2.376	2.218	1.07	0.303
flux	-0.2467	0.1610	-1.53	0.150
current	0.007042	0.001972	**3.57**	**0.003**
travel speed	-0.03417	0.04930	-0.69	0.501
voltage	-0.00667	0.04930	-0.14	0.895

S = 0.341590 R-Sq = 54.5% R-Sq(adj) = 40.5%

Table 5.2: Analysis of Variance Table for Bead Height

Analysis of Variance

Source	DF	SS	MS	F	P
Regression	**4**	**1.8195**	**0.4549**	**3.90**	**0.027**
Residual Error	13	1.5169	0.1167		
Total	17	3.336			

5.2.1 Residual Analysis

The residual is the difference between the observed and fitted value of the response. there are four plots available in Figure 5.1. These plots are normal probability plot, histogram, versus fits and versus order. The *x*-axis of histogram plot indicates the residuals and *y*-axis indicates the frequency of occurrence of that residual. The normal probability plot and histogram suggests approximate normal distribution of residuals. In residual plot of fits *x*-axis represent the bead height response and *y*-axis the residuals. Straight horizontal line residual versus fits shows the zero residual or the fitted model line. Which means all the points would have been lying on that if there is zero residual or no residual which is nearly not possible. The scattered points in residual versus fits show the residuals lying away from the fitted value. Absence of any particular trend of residuals in versus fitted value plot shows the good fit of the model.

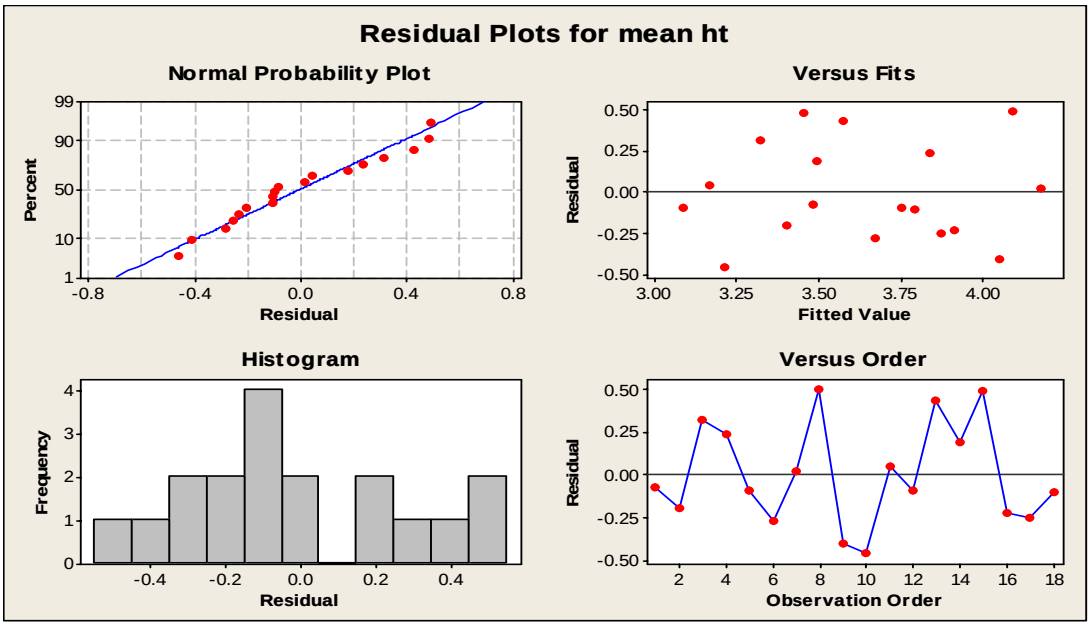

Figure 5.1: Residual Plots for Mean Bead Height

5.3 Regression Analysis for Mean Depth

Regression equation for mean depth has been shown in Equation 5.2. *P* value lesser than *0.05* for current and voltage indicates the significance of these factors. Regression table given in Table 5.3 indicates the *p* value of significant factors. R^2 value given suggests the suitability of the model. In present study model is *68.5 %* suitable.

mean depth = - 4.67 - 0.152 f + 0.0141 c- 0.0723 t.s.+ 0.231 v . . . . **(Equation. 5.2)**

Where

f = flux

c = current

t.s. = travel speed

v = voltage

Table 5.3: Regression Table for Mean Depth

Predictor	Coef	SE Coef	T	P
Constant	-4.665	3.650	-1.28	0.223
flux	-0.1517	0.2650	-0.57	0.577
current	0.01414	0.003245	**4.36**	**0.001**
travel speed	-0.0729	0.08113	-0.89	0.389
voltage	0.23125	0.08113	**2.85**	**0.014**

S = 0.562076 R-Sq = 68.5% R-Sq(adj) = 58.8%

Table 5.4: Analysis of Variance for Regression of Mean Depth

Analysis of Variance

Source	DF	SS	MS	F	P
Regression	4	8.9208	2.2302	7.06	0.003
Residual Error	13	4.1071	0.3159		
Total	17	13.0279			

5.5 Regression Analysis For Bead Width

Equation 5.3 shows the relation how the input parameters are related with mean bead width. *5.17* is the value of mean width when value of all the input parameters is zero. Regression table for the mean width is given in Table 5.6. In regression table voltage has

the minimum value of *p*, *i.e.0.05*. It means voltage is the most significant factor affecting the bead width.

The regression equation is

$$\text{mean width} = 5.17 + 0.166\, f + 0.00208\, c - 0.176\, t.s. + 0.423\, v \quad \text{(Equation 5.3)}$$

Where
f = flux
c = current
t.s. = travel speed
v = voltage

Table 5.6: Analysis of Variance for Regression Analysis

Source	DF	SS	MS	F	P
Regression	4	10.3277	2.5819	3.41	0.041
Residual Error	13	9.8418	0.7571		
Total	17	20.1696			

5.6 Residual Analysis for Mean Width

Residual plot for the mean width has been given in Figure 5.3. For normal probability plot and histogram residuals are taken along the *x*- axis. Percent of residuals and frequency are taken along the *y*-axis respectively. In residual versus fits and residual versus order the residuals are taken along the *y*-axis. The straight horizontal line in residuals versus fits plot is zero residual line. It means if there are no residual in the observations, then all the points would lie on that line. Normal probability curve and histogram follows the approximate normal distribution curve, which is desirable. In residual versus fits plot, most of the residuals lie on the upper side of fit line. No nonrandom pattern occurs in residual versus fits and residual versus order plot.

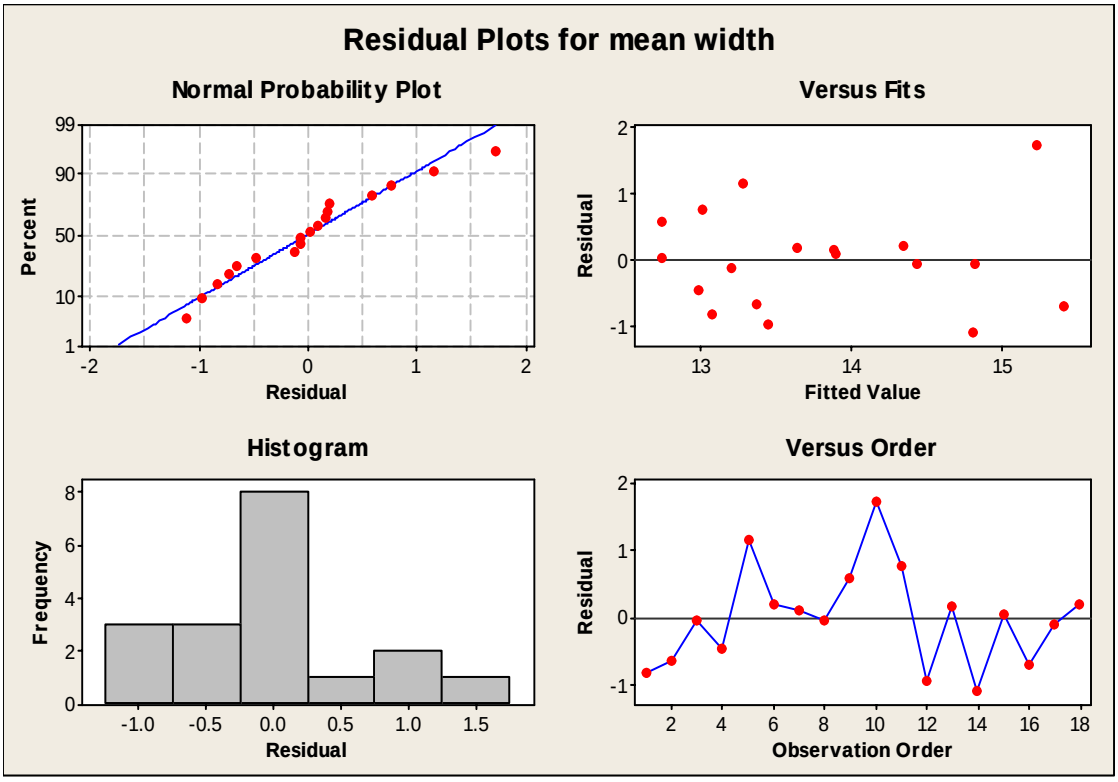

Figure 5.3: Residual plot for Mean Width

5.7 Regression Analysis for Microhardness

Regression analysis for micro hardness is given in Table 5.7. Table 5.7 indicates that flux and current are the significant factors with *p* value *0.005* and *0.000* respectively. Such small *p* value shows very high significance of input parameters. *P* value for travel speed and voltage are not significant but they are participating in regression equation. *P* value for regression is given in Table 5.8, *i.e.0.001*. R^2 value suggests that *73.2%* of variation in micro hardness is explained by the model.

The regression equation is

mean microhardnness = -54.3 -8.97 f+0.150 c+1.30 t.s +0.440 v . . . **(Equation 5.4)**

Where
f = flux
c = current
t.s. = travel speed
v = voltage

Table 5.7: Regression Table for Mean Microhardness

Predictor	Coef	SE Coef	T	P
Constant	-54.27	36.57	-1.48	0.162
flux	**-8.970**	**2.655**	**-3.38**	**0.005**
current	**0.14965**	**0.03252**	**4.60**	**0.000**
travel speed	1.3007	0.8130	1.60	0.134
voltage	0.4395	0.8130	0.54	0.598

S = 5.63260 R-Sq = 73.2% R-Sq(adj) = 64.9%

Table 5.8: Table for Analysis of Variance for Mean Microhardness

Analysis of Variance

Source	DF	SS	MS	F	P
Regression	4	1124.46	281.12	8.86	0.001
Residual Error	13	412.44	31.73		
Total	17	1536.90			

5.8 Analysis of Residual Plot

Figure 5.4 shows the residual plot for mean micro hardness. Residual has been taken along *x* and *y* axis in different plots. Normal probability plot and histogram follows normal distribution approximately. Dispersion around the fitted line is almost symmetrical, only a few point lie away from fitted line i.e. negative side of line. In residual versus order plot curve does not follow any non random pattern.

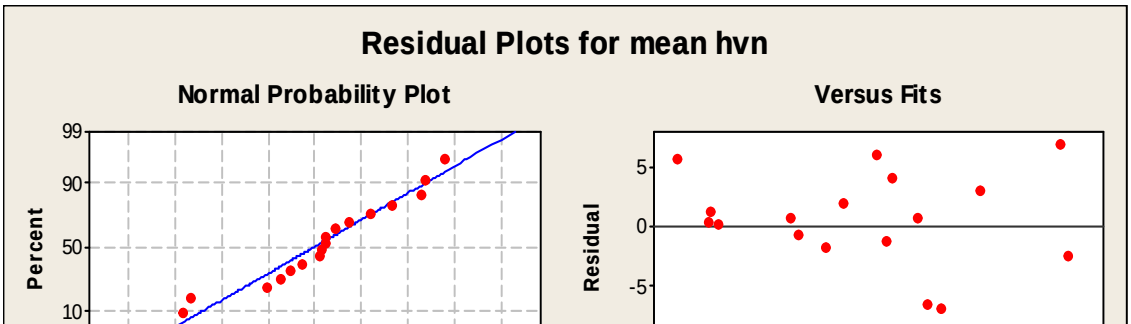

Figure 5.4: Residual Plots for Mean Micro Hardness

Chapter 6

Microstructure Analysis

6.1 Introduction

The present study was carried out to study the effect of current, voltage, travel speed and flux on the microstructure composition of the work material during submerged arc welding. Effect of various input factors on the micro structure were analyzed on the weld. In metal alloys, microstructure is characterized by the type and shape of the grain structure, their proportions, and the manner in which they are distributed or arranged. During welding, the metal converts into molten weld pool. Due to high temperature of molten metal, re-crystallization of the metal grains takes place. Upon cooling of the heated material, a change in microstructure takes place due to the raised temperature and subsequent cooling. The heat input and cooling rate decides the grain shape and properties. The heat input has been varied by changing the input factors value. The present study focuses on the percentage composition change that have occurred in ferrite and pearlite and including the changes in the grain shape of the work material after the submerged arc welding. The term phase equilibrium is often used, in the context of microstructure. This term applies to situation when one or more phase of single material exists.

6.2 Phase Diagram

The microstructure of a particular alloy is conveniently displayed in what is called a phase diagram. Many microstructures develop from the phase transformations. The changes occur between phases when temperature is varied. This transformation may involve the transition from one phase to another or the appearance or disappearance of a phase. Phase diagrams are helpful in predicting phase transformations and the resulting microstructures. Before discussing the microstructure of steel, it is necessary to discuss the iron carbide phase diagram. (**William D. Callister, Jr. [35])**

6.2.1 Iron-Carbide Phase Diagram

Pure iron upon heating, experiences changes in crystal structure before it melts at room temperature the stable form called ferrite or α iron, has a *BCC* crystal structure. Ferrite experiences a polymorphic transformation to *FCC* austenite, or γ iron, at 912^0. This austenite persists to 1394^0, at which temperature the *FCC* austenite reverts back to a *BCC* phase known as δ ferrite, which finally melts at 1538^0. All these changes are apparent along the left vertical axis of the phase diagram. *x*-axis is the composition axis for carbon and limited to maximum limit of *6.70 wt%.* Iron carbide (Fe_3C) is formed at this concentration of carbon. All steels and cast irons have carbon contents less than *6.70 wt%*

C; therefore, it is considered only the iron-iron carbide system. Composition can be expressed in "*wt% C*" rather than "*wt% Fe_3C"; 6.70 wt% C* corresponds to *100 wt% Fe_3C*. Carbon is an interstitial impurity in iron and forms a solid solution with each of α and δ ferrites, and also with austenite, as indicated by the α and δ single phase fields in Figure 6.1.

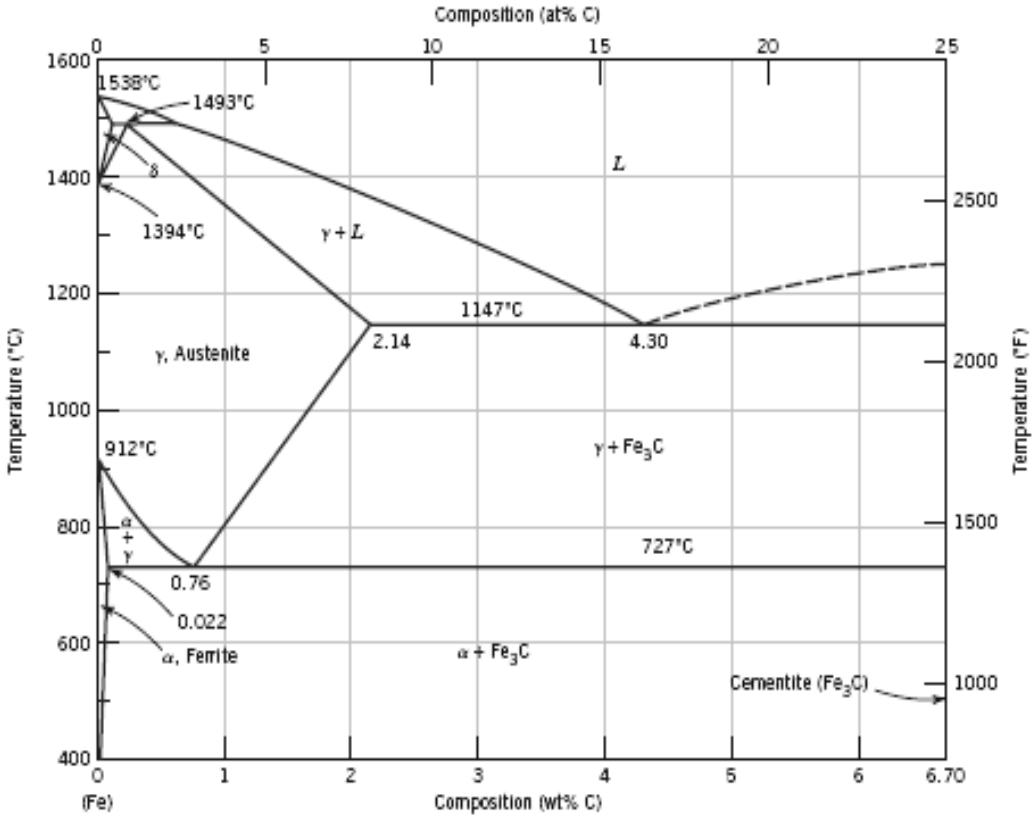

Figure 6.1: Iron-Iron Carbide Phase Diagram[35]

In the *BCC* α ferrite, only small concentrations of carbon are soluble; the maximum solubility is *0.022 wt%* at 727^0C. The austenite, or γ phase of iron, when alloyed with carbon alone, is not stable below 727^0. The maximum solubility of carbon in austenite, *2.14 wt%* occurs at 1147^0C. The ferrite is virtually the same as α ferrite, except for the range of temperatures over which each exists. Since the δ ferrite is stable only at relatively high temperatures, it is of no technological importance. Cementite *(Fe3C)* forms when the solubility limit of carbon in α ferrite is exceeded below 727^0. *Fe3C* will also coexist with the γ phase between 727^0C and 1147^0C. It may be noted that one eutectic exists for the

iron–iron carbide system, at *4.30 wt% C and 1147^{0}C.* For this, eutectic reaction has been given in Equation 6.1.

$$L \underset{\text{heating}}{\overset{\text{cooling}}{\rightleftharpoons}} \gamma + Fe_3C \quad \ldots\ldots \textbf{(Equation. 6.1)}$$

It may be noted that a eutectoid invariant point exists at a composition of 0.*76 wt% C* and a temperature of *727^0*. This eutectoid reaction may be represented by Equation 6.2.

$$\gamma(.76\ wt\%C) \underset{\text{heating}}{\overset{\text{Cooli ng}}{\rightleftharpoons}} (.22wt\%\ C) + Fe_3C(6.7wt\%C) \quad \ldots\ldots \textbf{(Equation 6.2)}$$

Upon cooling, the solid γ phase is transformed into α iron and cementite. Ferrous alloys are those in which iron is the prime component, but carbon as well as other alloying elements may be present. In the classification scheme of ferrous alloys based on carbon content, there are three types: iron, steel, and cast iron. Commercially pure iron contains less than *0.008 wt% C* and is composed almost exclusively of the ferrite phase at room temperature. The iron-carbon alloys that contain between *0.008* and *2.14 wt% C* are classified as steels. In most steels the microstructure consists of both α and Fe_3C phases. The microstructure that develops depends on both the carbon content and heat treatment.

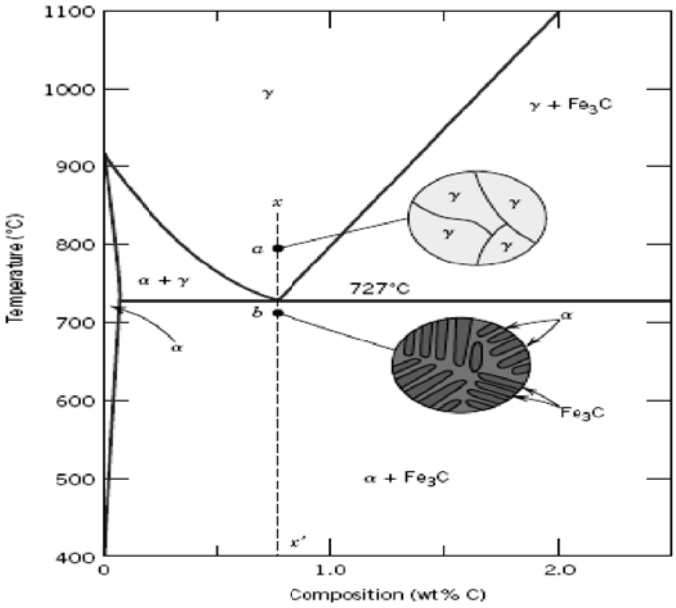

Figure 6.2: Schematic Representations of the Microstructures for an Iron –Carbon Alloy of Eutectoid Composition (0.76 wt%C).

The microstructure for this eutectoid steel that is slowly cooled through the eutectoid temperature consists of alternating layers or lamellae of the two phases (α and Fe_3C) that

form simultaneously during the transformation. In this case, the relative layer thickness is approximately *8* to *1***.** Microstructure, represented schematically Figure 6.2, point *b*, is called pearlite because it has the appearance of mother of pearl when viewed under the microscope at low magnifications**.** The pearlite exists as grains, often termed "colonies"; within each colony the layers are oriented in essentially the same direction, which varies from one colony to another. The thick light layers are the ferrite phase, and the cementite phase appears as thin lamellae most of which appear dark. Many cementite layers are so thin that adjacent phase boundaries are so close together that they are indistinguishable at this magnification, and, therefore, appear dark. Mechanically, pearlite has properties intermediate between the soft, ductile ferrite and the hard, brittle cementite.

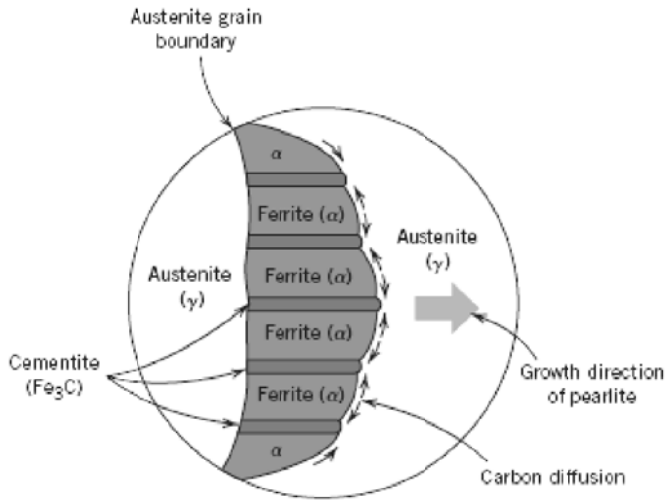

Figure 6.3: Schematic Representation of the Formation of Pearlite from austenite.[35]

6.3 Phase Transformation

Phase transformations occur in the liquid metals by varying the temperature of cooling. Most phase transformations require some finite time to go to completion, and the speed or rate is often important in the relationship between the heat treatment and the development of microstructure.

6.3.1 Transformation Diagrams

Upon cooling, austenite having an intermediate carbon concentration transforms to a ferrite phase, having a much lower carbon content and also cementite with a much higher carbon concentration. The vertical and horizontal axes are respectively temperature and the logarithm of time. Two solid curves shown in the figure 6.4 shows the time required at each temperature for the initiation or start of the transformation and for the transformation conclusion. The dashed curve corresponds to *50%* of transformation completion.

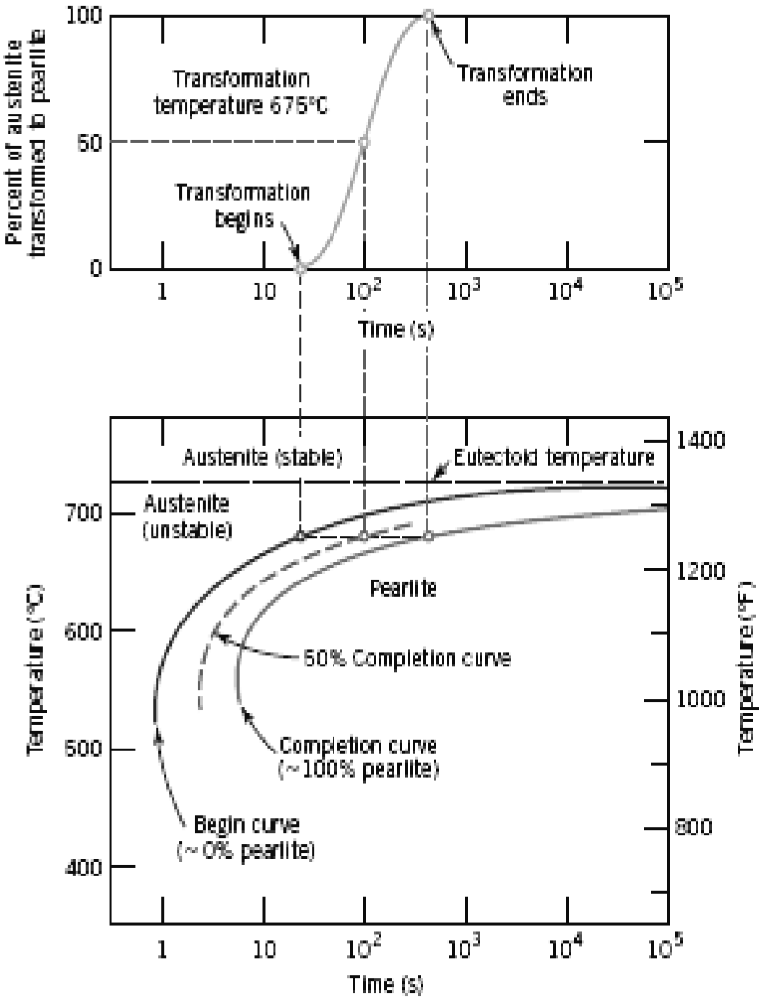

Figure 6.4: Transformations and cooling transformation diagrams[35]

The eutectoid temperature 727^0C is indicated by a horizontal line; at temperatures above the eutectoid and for all the times, only austenite exists. The austenite-to-pearlite transformation will occur only if an alloy is super cooled to below the eutectoid; as indicated by the curves, the time necessary for the transformation to begin and then end depends on temperature. The start and finish curves are nearly parallel, and they approach

the eutectoid line asymptotically. To the left of the transformation start curve, only austenite (which is unstable) will be present, whereas to the right of the finish curve, only pearlite will exist. In between, the austenite is in the process of transforming to pearlite, and thus both micro constituents will be present. The transformation rate at some particular temperature is inversely proportional to the time required for the reaction to proceed to *50%* completion, shorter this time, the higher is the rate. In addition, these plots are accurate only for transformations in which the temperature of the alloy is held constant throughout the duration of the reaction. Conditions of constant temperature are termed isothermal; thus, plots such as are referred to as isothermal transformation diagrams, or sometimes as time-temperature-transformation

(T–T–T) plots.

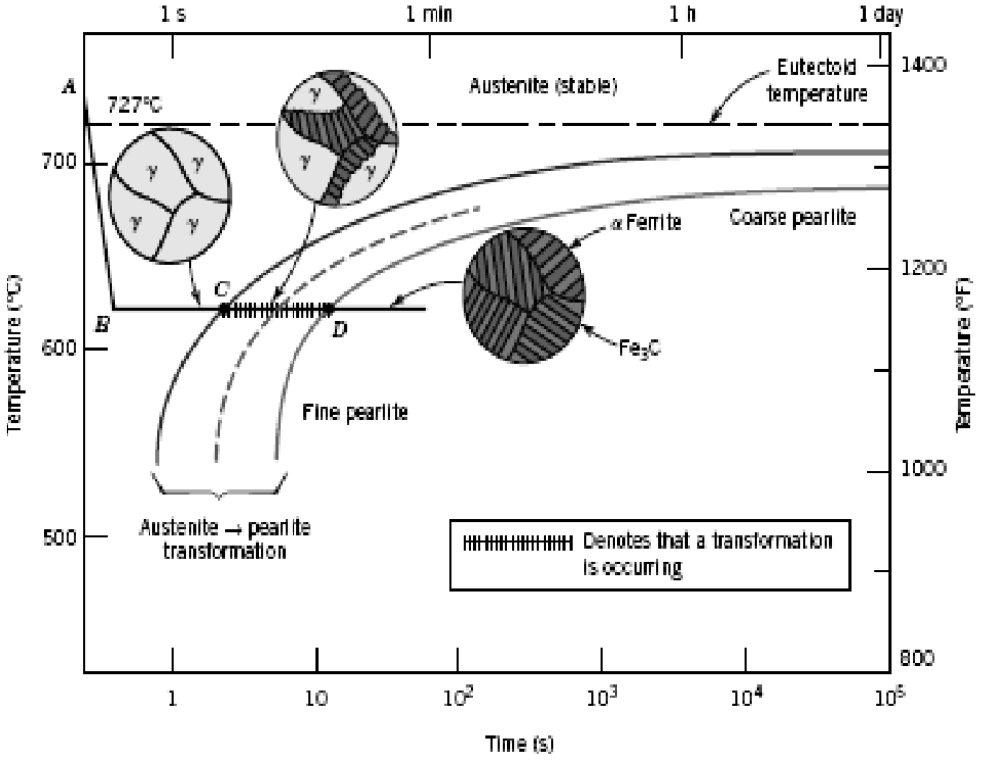

Figure 6.5: Isothermal transformation diagram for a eutectoid iron-carbon alloy[35]

6.4 Pearlite Structure

An actual isothermal heat treatment curve (*ABCD*) is superimposed on the isothermal transformation diagram for a eutectoid iron-carbon alloy in Figure 6.5. Very rapid cooling of austenite to a temperature is indicated by the near-vertical line *AB*, and the isothermal

treatment at this temperature is represented by the horizontal segment *BCD*. Of course, time increases from left to right along this line. The transformation of austenite to pearlite begins at the intersection, point *C* (after approximately *3.5 s*), and has reached completion by about *15 s*, corresponding to point *D*. Figure 6.5 also shows schematic microstructures at various times during the progression of the reaction. The thickness ratio of the ferrite and cementite layers in pearlite is approximately *8* to *1*. However, the absolute layer thickness depends on the temperature at which the isothermal transformation is allowed to occur. At temperatures just below the eutectoid, relatively thick layers of both the ferrite and Fe_3C phases are produced; this microstructure is called coarse pearlite, and the region at which it forms is indicated to the right of the completion curve on Figure 6.5. At these temperatures, diffusion rates are relatively high. This results in the formation of thick lamellae. With decreasing temperature, the carbon diffusion rate decreases, and the layers become progressively thinner. The thin-layered structure produced in the vicinity of 540^0C is termed fine pearlite; this is also indicated in Figure 6.5.

6.4.1 Bainite

In addition to pearlite, other micro constituents that are products of the austenitic transformation exist; one of these is called bainite. The microstructure of bainite consists of ferrite and cementite phases, and thus diffusional processes are involved. Bainite forms as needles or plates, depending on the temperature of the transformation. The time-temperature dependence of the bainite transformation may also be represented on the isothermal transformation diagram. It occurs at temperatures below those at which pearlite forms; begin, end and half-reaction curves are just extensions of those for the pearlitic transformation. whereas pearlite forms above the nose [i.e., over the temperature range of about $540C^0$ to 727^0C, at temperatures between about 215^0C and 540^0C bainite is the transformation product. Pearlitic and bainitic transformations are really competitive with each other, and once some portion of an alloy has transformed to either pearlite or bainite, transformation to the other micro constituent is not possible without reheating to form austenite.

6.4.2 Spheroidite

If a steel alloy having either pearlitic or bainitic microstructures is heated to, and left at, a temperature below the eutectoid for a sufficiently long period of time-for example, at about 700^0C for between *18* and *24 h*r, yet another microstructure will form. It is called spheroidite**.** Instead of the alternating ferrite and cementite lamellae (pearlite), or the

microstructure observed for bainite, the Fe_3C phase appears as sphere-like particles embedded in a continuous phase matrix. This transformation has occurred by additional carbon diffusion with no change in the compositions or relative amounts of ferrite and cementite phases. The driving force for this transformation is the reduction in α -Fe_3C phase boundary area.

6.4.3 Martensite

Yet another micro constituent or phase called martensite is formed when austenitized iron-carbon alloys are rapidly cooled (or quenched) to a relatively low temperature (in the vicinity of the ambient). Martensite is a non equilibrium single-phase structure that results from a diffusion less transformation of austenite. The martensitic transformation occurs when the quenching rate is rapid enough to prevent carbon diffusion. However, large numbers of atoms experience cooperative movements, in that there is only a slight displacement of each atom relative to its neighbors. This occurs in such a way that the *FCC* austenite experiences a polymorphic transformation to a body-centered tetragonal *(BCT)* martensite. A unit cell of this crystal structure is simply a body-centered cube that has been elongated along one of its dimensions; this structure is distinctly different from that for BCC ferrite. All the carbon atoms remain as interstitial impurities in martensite, they constitute a supersaturated solid solution that is capable of rapidly transforming to other structures if heated to temperatures at which diffusion rates become appreciable. The martensitic transformation is not unique to iron-carbon alloys. Since the martensitic transformation does not involve diffusion, it occurs almost instantaneously; the martensite grains nucleate and grow at a very rapid rate almost equal to the velocity of sound within the austenite matrix. Thus the martensitic transformation rate, for all practical purposes, is time independent. Martensite grains take on a plate-like or needle-like appearance. As already mentioned, martensite as well as other micro constituents (e.g., pearlite) can coexist. Being a non equilibrium phase, martensite does not appear on the iron-iron carbide phase diagram (Figure 6.1). Since the martensitic transformation is diffusion less and instantaneous, it is not depicted in this diagram as the pearlitic and bainitic reactions are. The beginning of this transformation is represented by a horizontal line designated *M* (start) (Figure 6.6). Two other horizontal and dashed lines, labeled *M (50%)* and *M (90%)*, indicate percentages of the austenite-to-martensite transformation. The temperatures at which these lines are located vary with alloy composition but, nevertheless, must be relatively low because carbon diffusion must be virtually nonexistent. The horizontal and

linear character of these lines indicates that the martensitic transformation is independent of time; it is a function only of the temperature to which the alloy is quenched or rapidly cooled. Consider an alloy of eutectoid composition that is very rapidly cooled from a temperature above 727^0C to, say 165^0C. From the isothermal transformation diagram (Figure 6.6) it may be noted that *50%* of the austenite will immediately transform to martensite; and as long as this temperature is maintained, there will be no further transformation.

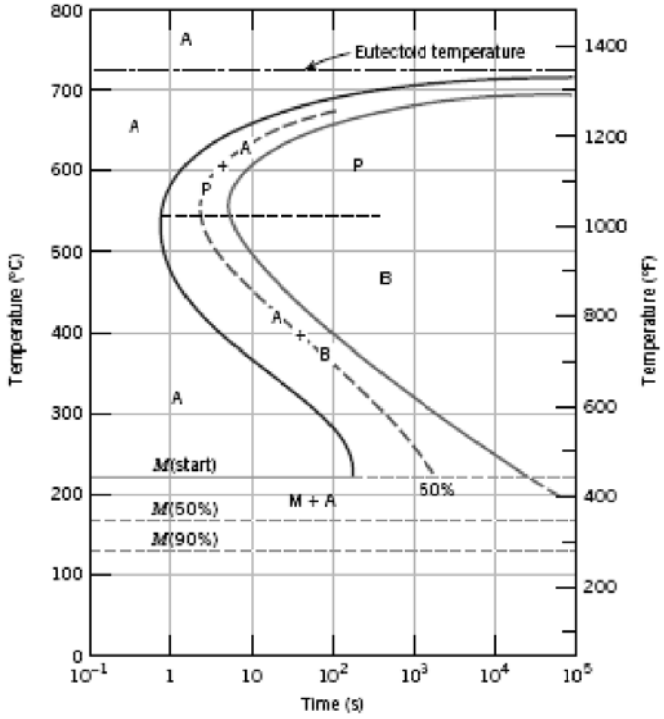

Figure 6.6: The complete isothermal transformation diagram for an iron–carbon alloy of eutectoid composition[35]

Where *A, P, B* and *M* stands for austenite, pearlite, bainite and martensite structures respectively.

6.5 Method of Sample Preparation

The objective of this study is to analyze the changes in the microstructure of *HAZ* by varying the different input parameter *i.e.* flux, current, voltage and travel speed. Before taking micrographs of the any metal sample, it is required to prepare sample for observation. In general, sample preparation of opaque materials such as metals involves obtaining a flat mirror-like finish which can be examined by reflected light. The steps taken for sample preparation are given below:

1) Cut out a section from the welded plate.
2) Grind the surface of this section by using a belt sander. Also corners and edges were beveled by grinding.
3) Using wet silicon carbide papers of successively finer grades, a finely ground surface covered with even parallel scratches from the smoothest paper was obtained. Excessive pressure is not required, because it can damage the surface finish acquired. It is important to wash the sample and fingers before moving on to a finer paper in order to avoid carrying over the coarser abrasive particles. The common rule is to grind on each paper for twice as long as it took to remove the scratches from the previous grade, turning the specimen through approx. 90^0 at each change.
4) Having thoroughly washed away all traces of grinding material, a final surface was prepared by polishing the surfaces on a polishing wheel which was covered with a fine abrasive paste or slurry.
5) To see the micrographs under the optical micrographs, etching was done with 2% nital solution.
6) Micrographs were taken with optical microscope at 200x magnification.

6.6 Method of observation

There are various methods available to count the ferrite percentage in work metal. Some of the methods are x-ray diffraction, feritscope, manual point count method etc. Manual point count method has been used to count the ferrite percentage.

In the point counting method a square grid is superimposed over the sample microstructure. The grid spacing should be similar in size, or smaller than the features being measured. The number of points to be counted depends on both the volume fraction of the phase and the desired level of precision in the result. A square grid of 50 x 50 mm^2 with total number of 2500 grids has been taken for the analysis of field. Grids were counted on the field with one repetition and mean is taken for percentage count.

The following equations should be used to calculate the volume percentage of ferrite:

P_T = Total number of points in the test grid

P_i = Point count on the i^{th} field

$P_P(i) = \frac{P_i}{PT} \times 100$= Percentage of grid points in the ferrite on the i^{th} field

There are few disadvantages of manual point count, which affect the accuracy of the results:

1. Operator bias pays a role in counting the phases falling inside the grid.
2. Specimen Preparation: Surface defects or abnormalities due to polishing or etching can lead to difficulty in distinguishing between the phases.
3. Grid Preparation: Thickness of grid lines can cause difficulty in determining whether a phase actually lies at the intersection or not.

Parent metal has approximately 49% ferrite composition as counted from the micrograph. In this study one micrograph was prepared for the parent metal as the material remained the same in all experimental trials. The grid counts, mean value and percentage of mean of field count are shown in Table 6.1.

Table 6.1: Observation Table for Field Count

Exp. No.	**flux**	**current (Amp)**	**Travel speed (m/hr)**	**Voltage (volts)**	**Field count**		**Mean count**	**%age count**
					P1	P2		
1.	I	350	27	28	309	335	322	12.88
2.	I	350	29	30	268	285	276.5	11.06
3.	I	350	31	32	289	316	302.5	12.10
4.	I	400	27	28	442	423	432.5	17.30
5.	I	400	29	30	375	344	359.5	14.38
6.	I	400	31	32	438	419	428.5	17.14
7.	I	450	27	30	388	411	399.5	15.98
8.	I	450	29	32	365	348	356.5	14.26
9.	I	450	31	28	342	331	336.5	13.46
10.	II	350	27	32	518	523	520.5	20.82
11.	II	350	29	30	507	531	519	20.76

12.	II	350	31	30	477	455	466	18.64
13.	II	400	27	30	321	337	329	13.16
14.	II	400	29	32	442	421	431.5	17.26
15.	II	400	31	28	387	398	392.5	15.70
16.	II	450	27	32	403	419	411	16.44
17.	II	450	29	28	309	320	314.5	12.58
18.	II	450	31	30	227	243	235	9.40

6.7 Observed Micrographs of HAZ

The micrographs of heat affected zone shown below have been taken at the half of width of heat affected zones. These picture have been taken after etching of specimen with 2% nital solution; with an optical microscope at 200x magnification. Figure 6.8 shows the microstructure of the parent metal and Figures 6.9 to 6.26 shows the microstructure of heat affected zones of different specimen at varied input conditions as per the treatment conditions laid out by L_{18} Taguchi design.

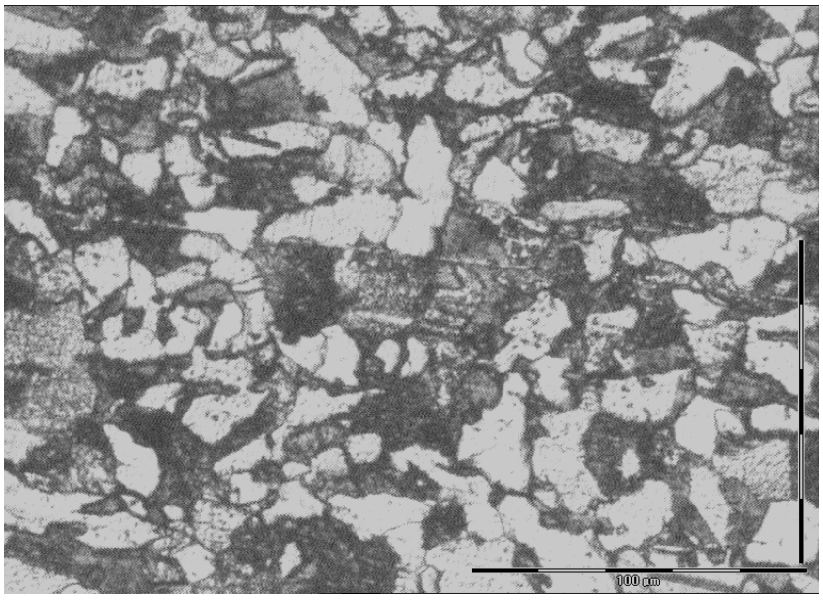

Figure 6.8: **Micrograph of Parent Metal**.

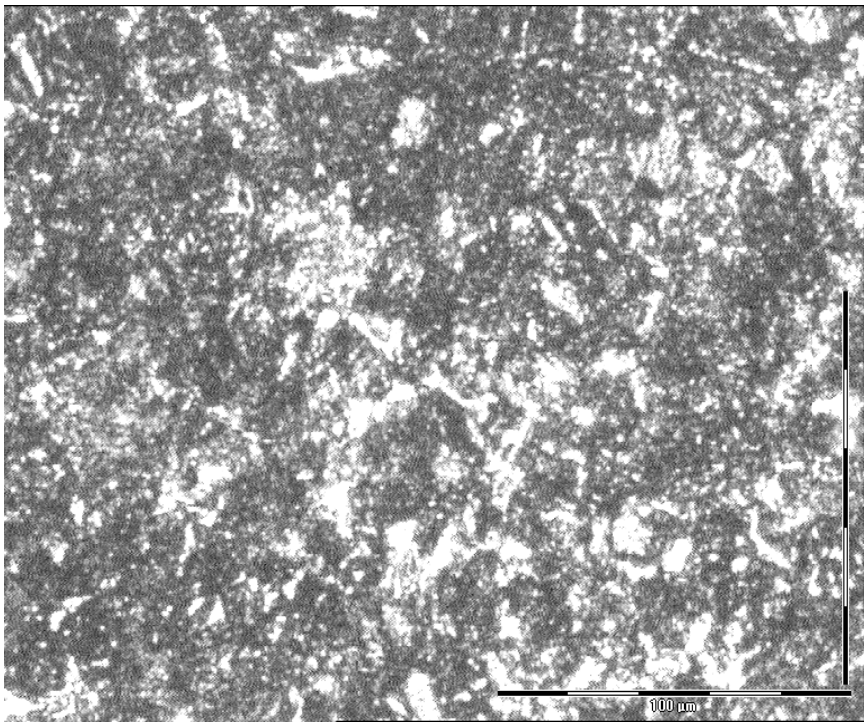

Figure 6.9 : Haz at Flux 1, Current 350 amp, Travel speed 27m/hr, Voltage 28 volts

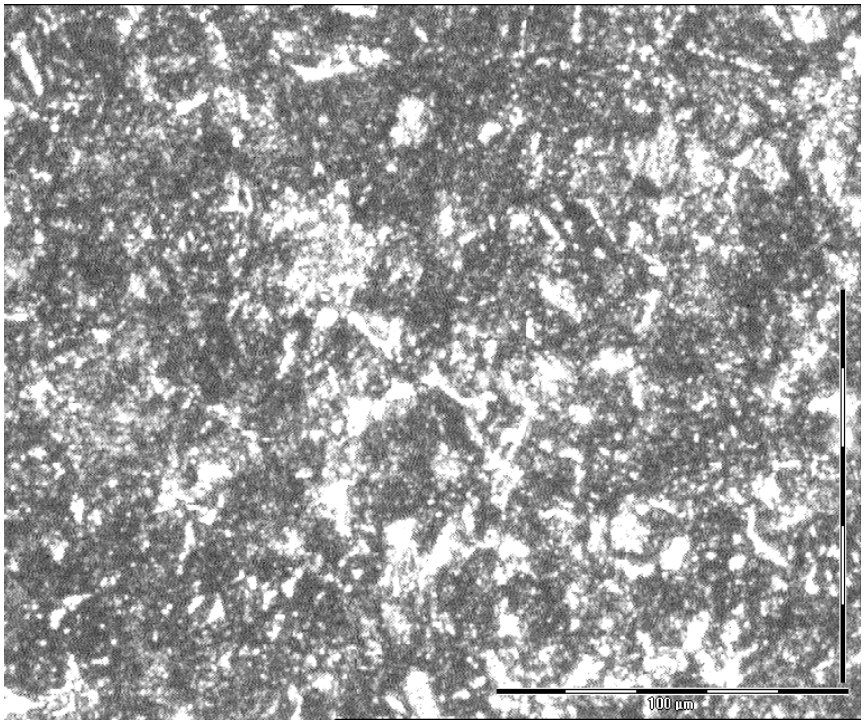

Figure 6.10 : Haz at Flux 1, Current 350 amp, Travel Speed 29m/hr,Voltage 30 volts

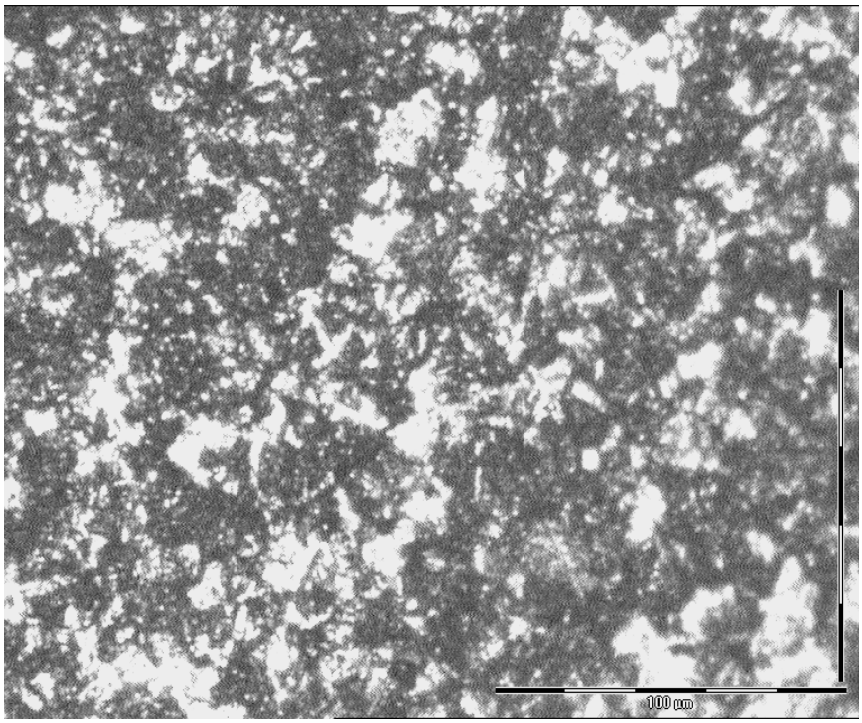

Figure 6.11 : Haz at Flux 1, Current 350 amp, Travel Speed 31m/hr, Voltage 32 volts

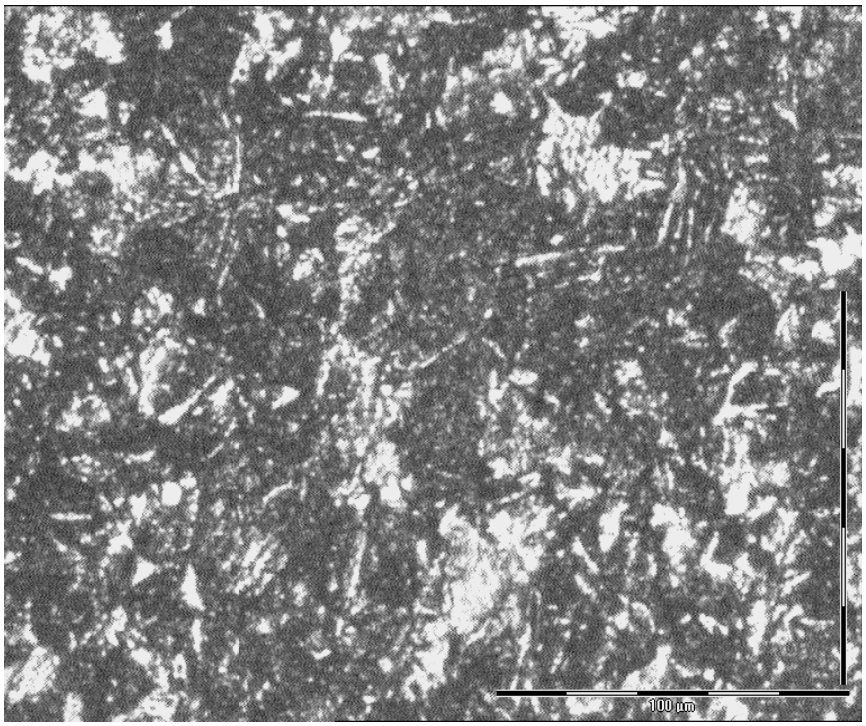

Figure 6.12: HAZ at Flux 1, Current 400 amp, Travel Speed 27m/hr, Voltage 28volts

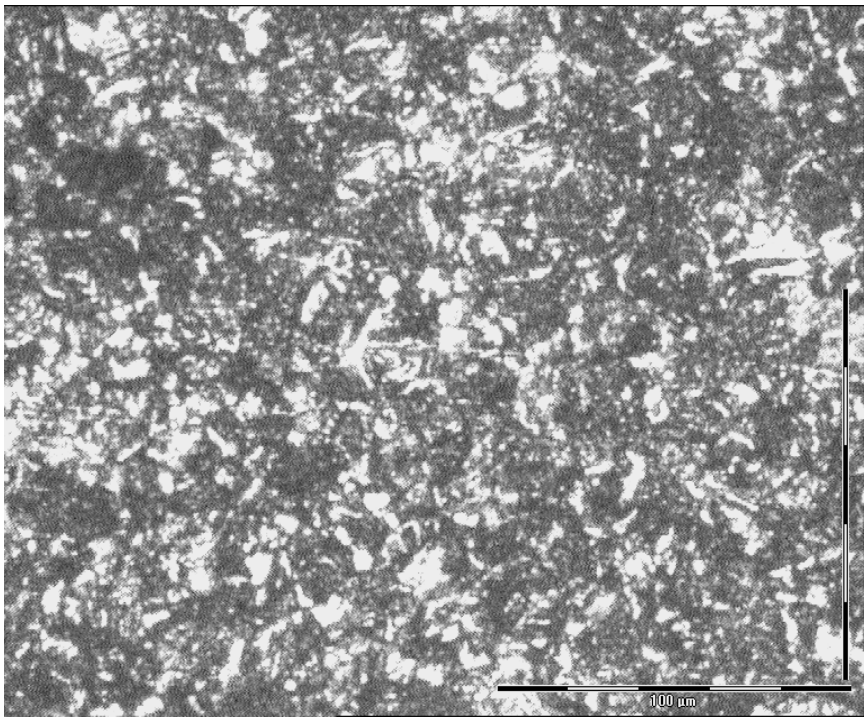

Figure 6.13: HAZ at Flux 1, Current 400 amp, Travel Speed 29m/hr, Voltage 30 volts

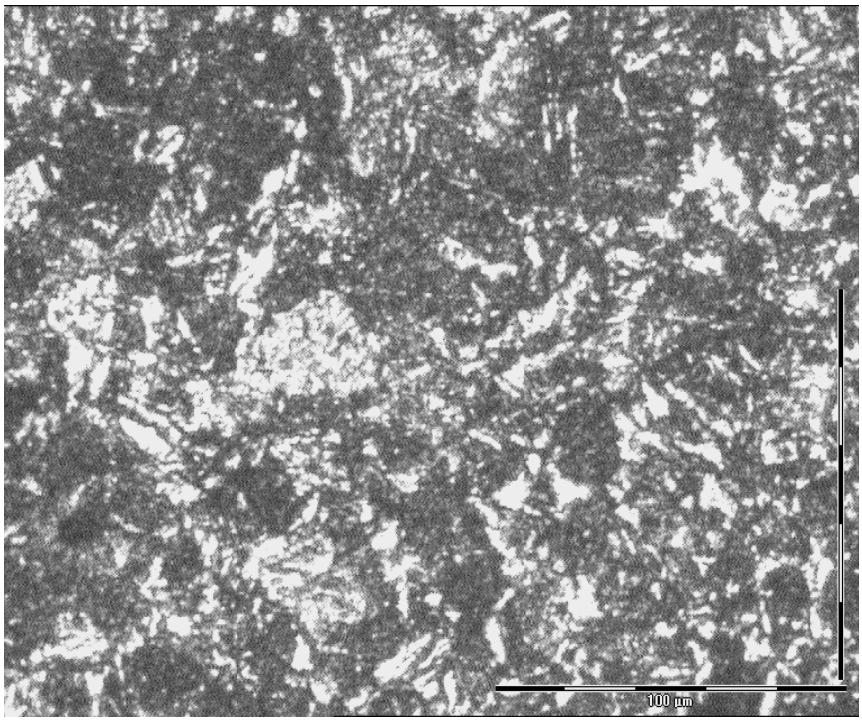

Figure 6.14: HAZ at Flux 1, Current 400 amp, Travel Speed 31m/hr, Voltage 32 volts

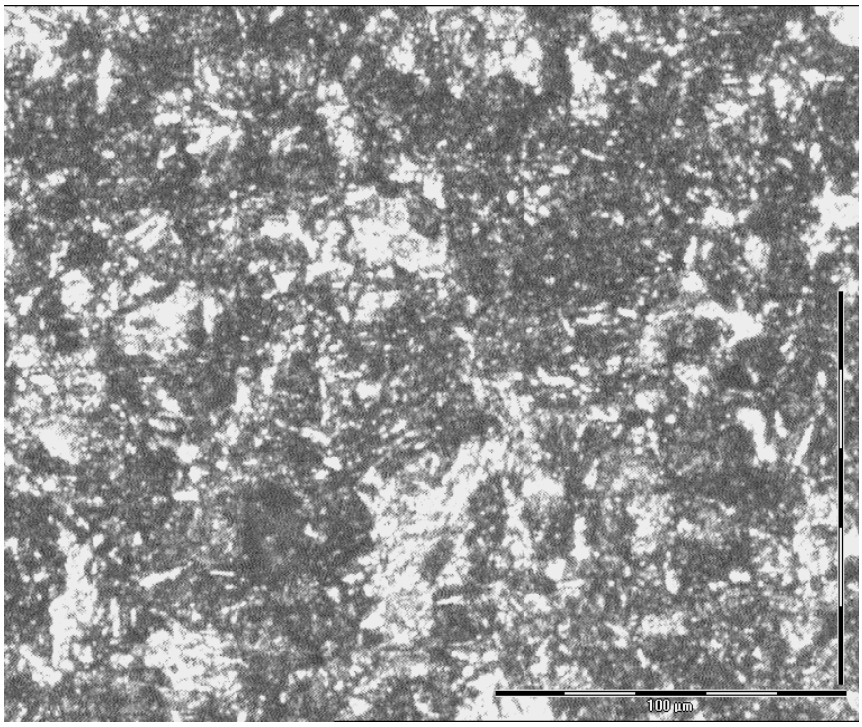

Figure 6.15: HAZ at Flux 1, Current 450 amp, Travel Speed 27m/hr, Voltage 30 volts

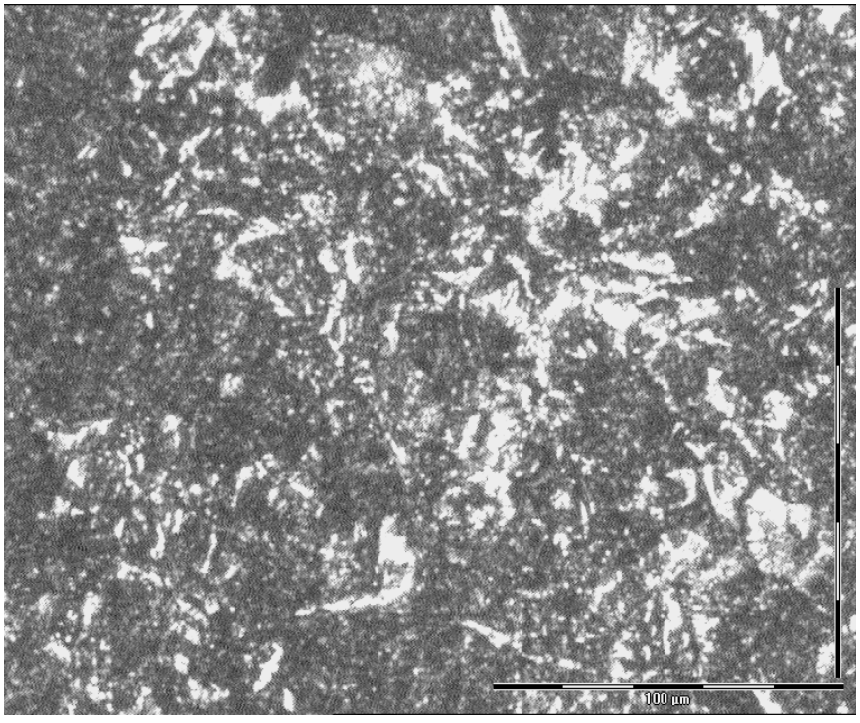

Figure 6.16: HAZ at Flux 1, Current 450 amp, Travel Speed 29m/hr, Voltage 32 volts

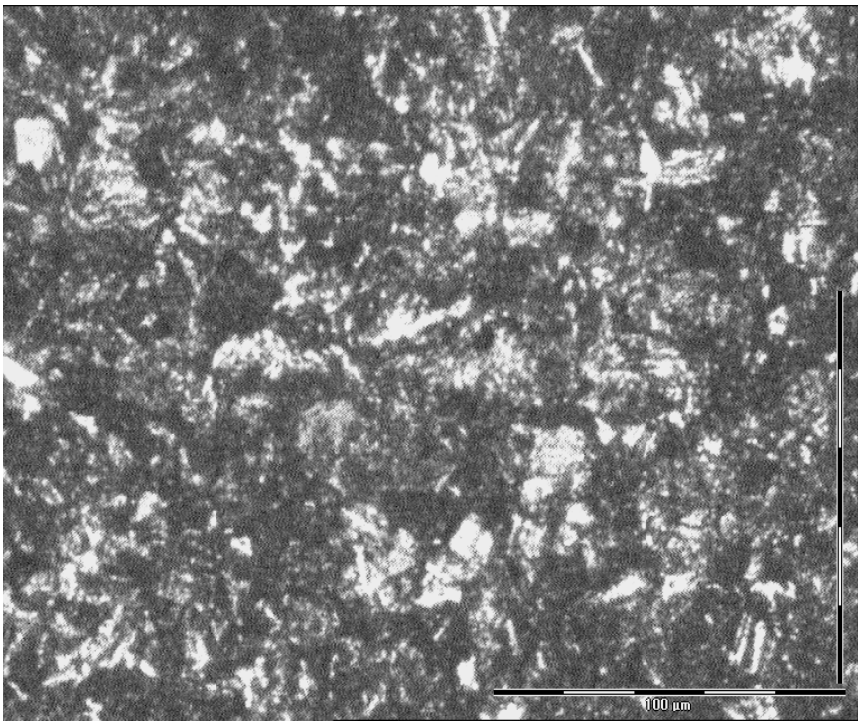

Figure 6.17: HAZ at Flux 1, Current 450 amp, Travel Speed 31m/hr, Voltage 28 volts

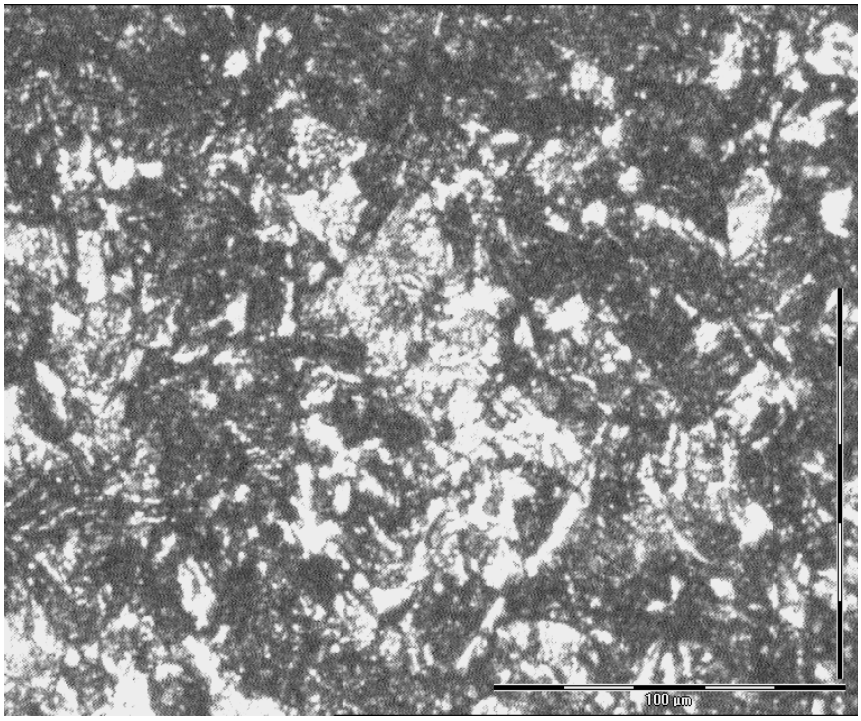

Figure 6.18 : HAZ at Flux 2, Current 350 amp, Travel Speed 27m/hr,Voltage 32 volts

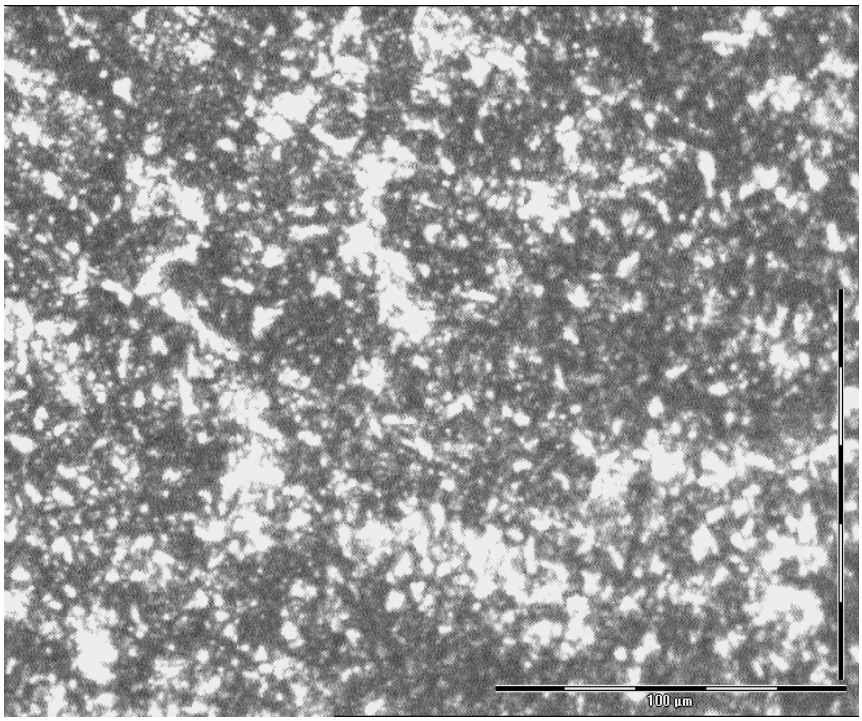

Figure 6.19 : HAZ at Flux 2, Current 350 amp, Travel Speed 29m/hr,Voltage 30 volts

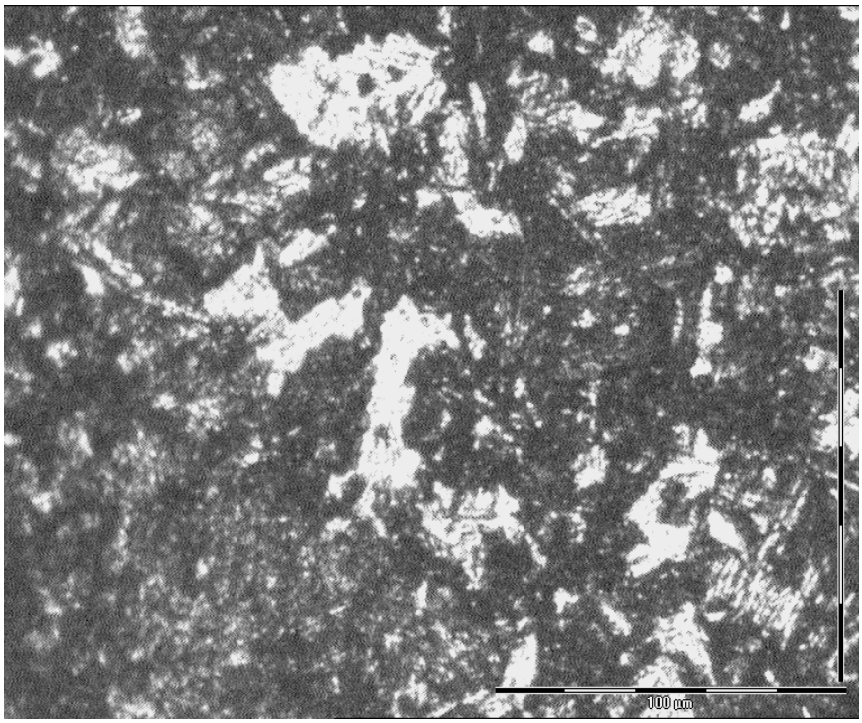

Figure 6.20 : HAZ at Flux 2, Current 350 amp, Travel Speed 31m/hr,Voltage 30 volts

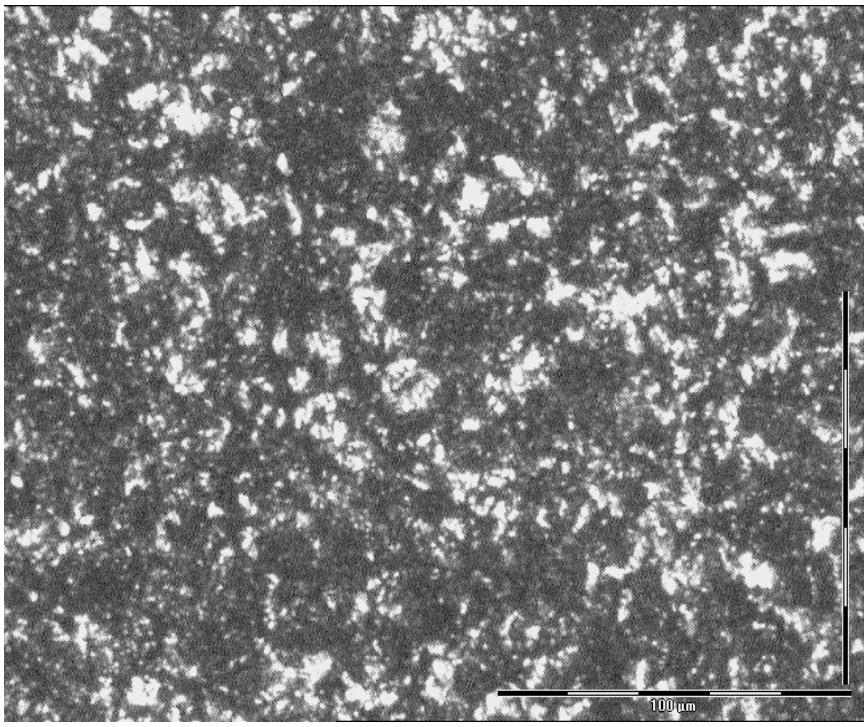

Figure 6.21 : HAZ at Flux 2, Current 400 amp, Travel Speed 27m/hr,Voltage 30 volts

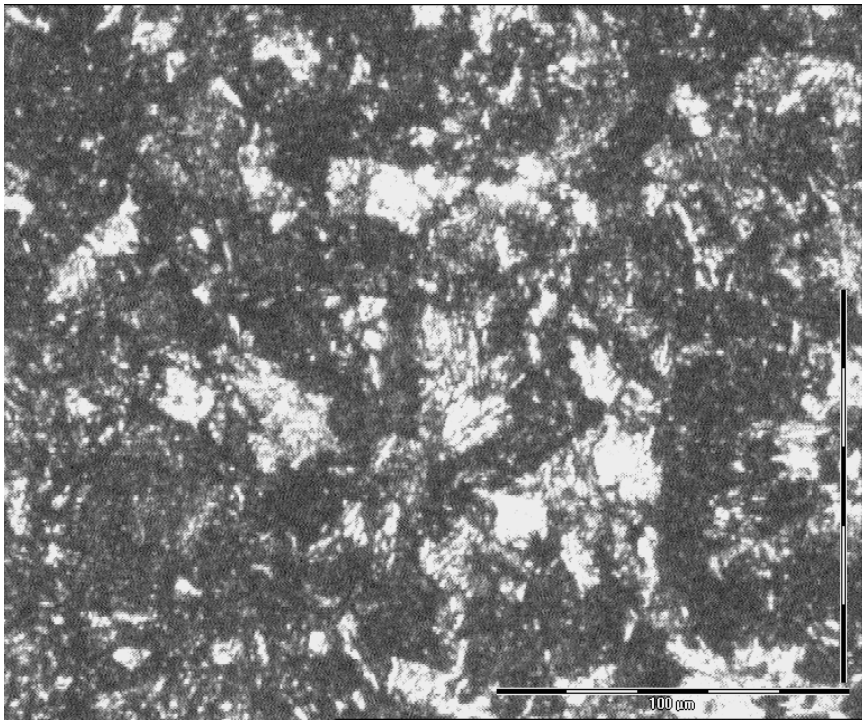

Figure 6.22 : HAZ at Flux 2, Current 400 amp, Travel Speed 29m/hr, Voltage 32volts

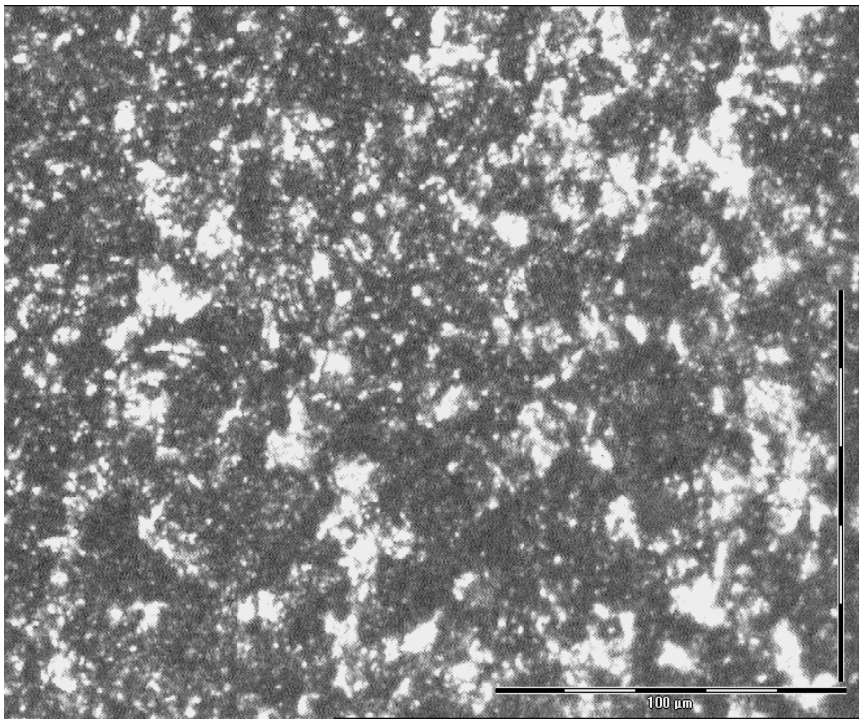

Figure 6.23 : HAZ at Flux 2,Current 400 amp, Travel Speed 31m/hr,Voltage 28 volts

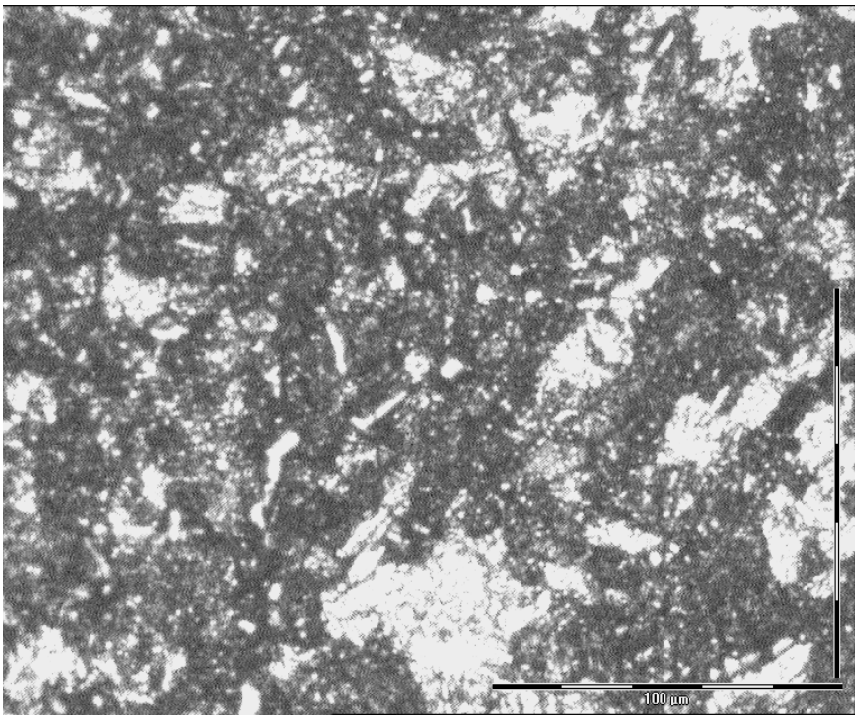

Figure 6.24: HAZ at Flux 2, Current 450 amp, Travel Speed 27m/hr, Voltage 32 volts

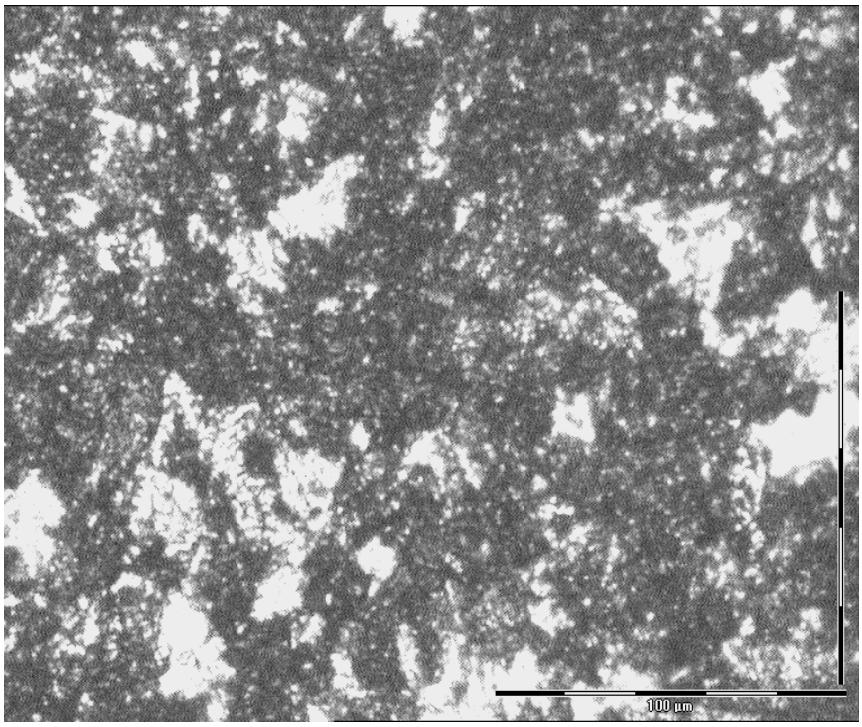

Figure 6.25 : HAZ at Flux 2, Current 450 amp, Travel Speed 29m/hr, Voltage 28volts

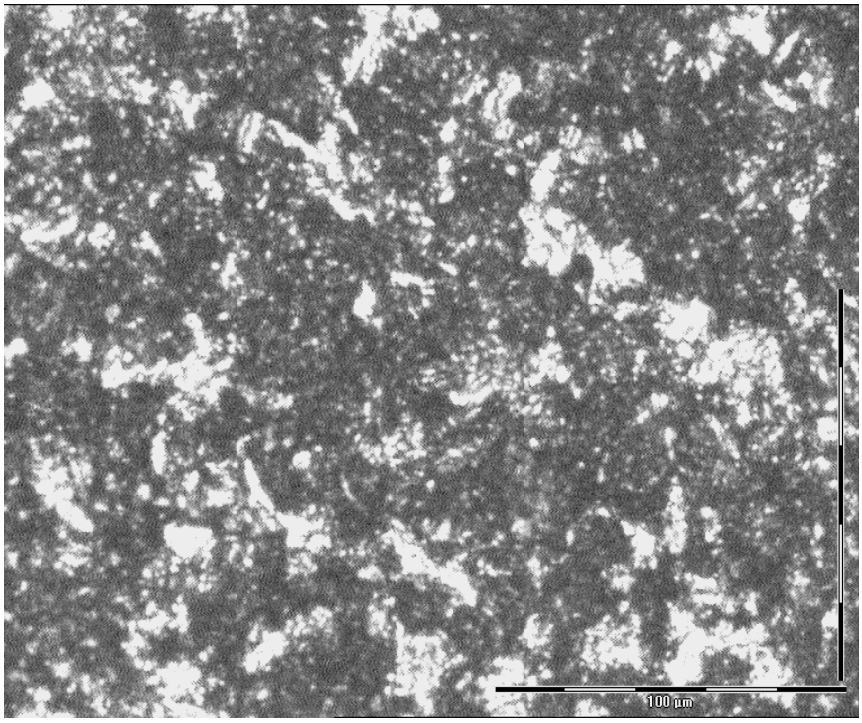

Figure 6.26: HAZ at Flux 2, Current 450 amp, Travel Speed 31m/hr, Voltage 30 volts

6.8 Discussion

Figure 6.8 shows the microstructure of the parent metal at a magnification of 200x. Two constituents are visible in the micrograph which are white and black in colour. The white and black colour indicates the presence of ferrite phase *(α-iron)* and pearlite ($\alpha+Fe_3C$) respectively. The percentage of each phase was counted with the help of manual point counting method. Figure 6.8 shows the uniform distribution of both the phases in micrograph. The percentage of ferrite composition was found to be approximately *49 %.* Figure 6.9 shows the micrograph of heat affected zone *(HAZ)* of the weld bead formed after welding at first trial input factors (given in Table 6.1). The picture of heat affected zone has been taken approximately at the middle of the of heat affected zone. It was observed from the micrograph that the metal grain size had reduced to a smaller size as compared to parent metal. Figure 6.8 shows the almost uniform distribution of both the phases in field. Some small cluster of ferrite are also visible in this micrograph. Figure 6.10 shows the micrograph of *HAZ* weld metal after 2^{nd} trial. The distribution of phases is almost equal to previous figure, but some plate shaped structures started to appear. Change in structure occurs due to increase in voltage which results in increase of heat input. Figure 6.11 shows the large clusters of ferrite and pearlite structures. The figure indicates the formation of perlitic colonies and traces of bainitic structures in the field. Figure 6.12 shows the micrograph of *HAZ* at the current and voltage settinngs of *400 amp* and *28 volts* respectively. It is clearly visible from the figure that the pearlitic proportion of the field has been increased. There are some needle shaped structures present in the field, which indicate formation of bainitic structure. The ferrite composition in this zone was found to be *17.30 %* which is significantly high. The microhardness of this zone is high as compared to the previous trials, due to presence of bainitic structures. Figure 6.13 shows the micrograph of *HAZ,* when the current , travel speed and voltage are set at *400 amp, 29 m/hr* and *30 volts* respectively. The figure shows that the ferrite phase has been distributed in the *HAZ* . Maximum area of field is covered by the pearlite phase. Except the pearlitic and ferrite structuure some traces of bainite are also present. Figure 6.14 shows the percentage ferrite count of *17.14 %.* Figure shows the lameller structures of pearlite and bainite. Ferrite can be seen in the figure in the form of clusters . Some portion of the left hand side shows the accumulation of ferrite phase iron. Figure 6.15 shows the *HAZ* at welding conditions of *450 amp, 29 m/hr, 30 volts* of current , travel speed and voltage respectively. This is a condition of very high heat input, that is why the ferrie

pecentage of this *HAZ* is lesser than the previous one. The microhardness at this condition is very high *i.e. 54.904 hvn.* This high value of microhardness is due to the formation of martensite structures in between the bainite structures. Figure 6.16 shows the *HAZ* at the maximum heat input. The ferrite percentage in this case is only *14.26%,* which is due to the very high heat input. Because in this trial the current and voltage used are at its maximum level. As in previous case the microhardness of this *HAZ* is very high *i.e.55.659 hvn* because of the presence of martensite structure in the ferrite-bainite matrix. Figure 6.17 shows the *HAZ* field after the welding at *450 amp* and *28 volts.* The percentage of ferrite phase is very less *i.e. 13.46%.* Figure 6.18 shows the *HAZ* at the lowest level of current,voltage and travel speed. Same trial condition were used in the very first trial except the flux. In this case, the flux with *1.6* basicity index has been used. The ferrite percentage in this trial was found to be *20.82%.* Probable reason for this low percentage of ferrite could be the higher percentage of *CaO+MgO* in mixture. *CaO+MgO* tendency to pick the carbon content from the weld metal pool. The figure clearly shows the formation of pearlitic colonies or the lameller structures. Figure 6.19 shows that the distribution of ferrite and pearlite phases are almost uniform.on the upper left portion of the figure symmetrical colonies of the pearlite can be seen in the picture. The ferrite percentage for this region is found to be *20.76 %.* Figure 6.20 shows the *HAZ* of the sampleproduced after the 12^{th} trial. Figure shows the cluster of ferrite in the middle portion . The bainitic growth can be seen at the lower right corner of the figure. Figure 6.21 shows the uniform distribution of ferrite in field. Figure 6.22 shows the micrograph of the *HAZ* for the 14^{th} trial's sample. The picture shows the pools of ferrites in the field with majority of needle and plate structures of pearlitic and bainitic. The ferrite percentage for this sample was found to be *17.26%* . The microhardness of this zone is *38.264 hvn* only. Figure 6.23 shows the *HAZ* of 15^{th} trial carried out during the experimented study. The percentage of ferrite and microhardness phase were found to be *15.70%* and *39.030 hvn* respectively. Figure 6.24 shows the *HAZ* at *450 amp* and *32 volts* respectively. The microhardness and ferrite percentage for this sample were found to be *43.968 hvn* and *16.44%* respectively. The picture shows the the formation of bainitic structure in the form of narrow plates distributed in the whole matrix. Percentage of ferrite was found to be higher than that of the 8^{th} trial (both having maximum level of current and voltage). This difference was caused by the higher percentage of *CaO+MgO* in *flux II* as stated earlier. Figure 6.25 indicates the high percentage of pearlitic , bainitic structures and small

percentage of ferrite phase . The microhardness for this *HAZ* was found to be *48.58 hvn* , which is quite higher than the previous trials with *flux II* which could be due to the presence of bainitic and martensitic structures. Figure 6.26 shows a very small percentage of ferrite phase in the field *(9.40%)* and microhardness of *41.470 hvn.* Micrograph shows the presence of bainitic structures in the field.

From the above disscussion it can be concluded that current and voltage plays a major role in the formation of various structures and percentage of ferrite presence. Other major factor effecting the microstructure was the composition of flux. It can be concluded that current and voltage effects effects the hardness and microstructure of the metal to a large extent, but it can not be generalized for all trials. It can also be concluded that presence of bainite and martensite has a direct relationship with the hardness of the *HAZ.*

1.1 Results

The effect of four input factors was studied on the bead geometry and micro hardness using the L_{18} Taguchi experimental design. Bead height, bead width, depth of penetration and micro hardness were measured as the response parameters. ANOVA and regression analysis was completed for all the responses to analyze the significance of the input factors. Regression equation was developed to predict the relationship amongst the dependent and independent variables. Main effect plots for mean values, S/N ratios and residual analysis has been developed and analyzed. Table 7.1 shows the value of responses measured.

Table 7.1: Table for Mean Value of Results

Experiment Number	Mean Bead Height (mm)	Mean depth of Penetration (mm)	Mean Bead width (mm)	Micro hardness of HAZ (hvn)
1.	3.405	4.915	12.235	27.045
2.	3.200	5.185	12.705	39.115
3.	3.640	4.990	14.365	50.450
4.	4.075	5.130	12.515	44.085
5.	3.655	5.695	14.440	49.815
6.	3.395	5.665	14.545	42.060
7.	4.195	6.785	13.990	54.905
8.	4.590	6.705	14.750	55.659
9.	3.645	4.810	13.330	64.635
10.	2.750	4.460	16.960	35.990
11.	3.215	4.440	13.780	32.880
12.	2.990	5.085	12.480	33.415
13.	4.010	4.960	14.045	33.850
14.	3.680	6.255	13.695	38.264
15.	3.940	4.790	12.760	39.030
16.	3.685	7.385	14.705	43.968

17.	3.620	6.050	13.090	48.108
18.	3.690	6.335	13.815	41.470

1.1.1 Bead Height

- Current is found as a significant factor with *p* value of *0.014.* Voltage, flux and travel speed did not show any significant impact on the bead height.
- Current was the only significant factor *(P=0.012)* for S/N analysis of bead height.
- The mean height using the optimal conditions would be *2.749 ± 0.165 mm* with minimum current input of *350 amp* and flux II.

1.1.2 Depth of Penetration

- For depth of penetration current and voltage would be used to be the most significant factor with *p* value of *0.002* and *0.037* respectively.
- ANOVA for S/N ratio for depth of penetration also shows the significance of current and voltage with *p* value of *0.002* and *0.042* respectively.
- For optimal value of depth of penetration, the current should be set at its higher level *(450 amp)* and *32 volts.*
- The mean depth of penetration was estimated be *6.847±1.537mm at 95%* confidence.

1.1.3 Bead Width

- Voltage was the only significant factors affecting the bead width with *p* value of *0.030.* The others factors do not show any significant effect on the bead width.
- ANOVA for S/N ratios for bead width also suggests the significance of voltage with *p* value of *0.028.*
- The predicted value of bead width with *95%* confidence in optimal design, (travel speed *31 m/hr* and *28 volts)* was *12.90 ± 0.424 mm.*

1.1.4 Microhardness

- Flux and current were the two significant factors that affect micro hardness with *p* value of *0.01* and *0.005* respectively.
- ANOVA for S/N calculations for micro hardness also shows the significance of flux and current with *p* value of *0.005* and *0.010* respectively.

- For optimal design flux with B.I. index *0.8* and high current *(450) amp* should be used to predict the micro hardness.
- The predicted value of micro hardness at optimal condition would be *55.93 ± 6.74 hvn (*at *95%* significance level).
- Micro hardness is greatly affected by the composition of flux. Contribution of flux type I is more as compared to flux II towards the micro hardness.
- Regression analysis for have been done and regression equations have been developed for all the responses.
- Micrograph for HAZ has been taken for all the eighteen samples and effects of all the input parameters have been studied and results have been compiled in chapter 6 with detailed description of every trial condition in section 6.8.

1.2 Conclusions

The present study was carried out to study the effect of four input parameters on the weld bead geometry in the submerged arc welding process. These parameters (current, voltage, travel speed and the type of flux) were varied at different levels in the range available on the machine to optimize the process parameters. The following conclusions have been drawn from the study:

- The weld bead geometry is mainly affected by the current and voltage.
- The travel speed had effect on the bead width and had little effect on the depth of penetration and bead height.
- Higher depth of penetration could be obtained at higher current and voltage, although current had no significant affect on the bead width.
- The flux basicity index did not significantly affect the bead geometry, but had a major effect on the micro hardness.
- Voltage had no significant effect on the bead height, which is contrary to the popular view.
- The flux and the current had a significant effect the microstructure. Flux with B.I. of 0.08 (Type I) showed a significantly higher micro hardness compared to flux II with B.I of 1.6. The probable reason for this could be higher presence of *CaO+MgO,* which has a tendency to pick up carbon thus lowering the micohardness in this case.

- The micro hardness was observed to have a direct relation to amount of current.
- It can be concluded that current and voltage plays a major role in the formation of various structures and percentage of ferrite presence. Other major factor effecting the microstructure was the composition of flux. It can be also be concluded that current and voltage effects the hardness and microstructure of the metal to a large extent, but it can not be generalized for all trials.
- It can also be concluded that presence of bainite and martensite has a direct relationship with the hardness of the *HAZ*.

1) S. V. Nadkarni. Modern arc welding technology, *Advani-Oerlikon limited*. 1988**.**
2) R Quintana, A Cruz, L Perdamo and G Castelannos, Study of the transfer efficiency of alloyed elements in fluxes during the submerged arc welding process, *Welding International*, Volume17 (12), pp. 958–965,2003.
3) Larry Jeffus, Welding Principles and Application, *Thomsom Delmer Learning*. 2004.
4) Eroglu M, Aksoy M, Orhan N., Effect of coarse initial grain size on microstructure and mechanical properties of weld metal and HAZ of a low carbon steel., *Material Science Eng,* Volume 269, pp. 59–66, 1999.
5) C.S. Lee, R.S. Chandel, and H.P., Seow, Effect of Welding Parameters on the Size of Heat Affected Zone of Submerged Arc Welding, *Materials and Manufacturing Processes,* Volume 15, No.5, pp. 649-666, 2000.
6) Vera Lu´ cia Othe´ro de Brito, Herman Jacobus Cornelis Voorwald, Nasareno das Neves, and Ivani de S. Bott, Effects of a Postweld Heat Treatment on a Submerged Arc Welded ASTM A537 Pressure Vessel Steel, *Journal of Materials Engineering and Performance,* Volume 10, June, 2001.
7) Keshav Prasad and D.K. Dwivedi, Application of Taguchi philosophy for parametric optimization of bead geometry and HAZ width in submerged arc welding using a mixture of fresh flux and fused flux, *Int J Adv Manuf Technology* Volume 36, pp. 475–483, 2008.
8) Eagar T.W., Oxygen and nitrogen contamination during submerged arc welding of titanium, *Proc International Conference of Welding Research*, in the 1980s, Osaka University, Osaka, Japan.
9) P. Kanjilal A, T.K. Pal and S.K. Majumdar, Combined effect of flux and welding parameters on chemical composition and mechanical properties of submerged arc weld metal, *Journal of Materials Processing Technology*, Volume 171, pp. 223–231, 2006.
10) R Quintana, A. Cruz, L. Perdomo and G. Castellanos, Study of the transfer efficiency of alloyed elements in fluxes during the submerged arc welding process, *Welding International*, Volume17 (12), pp. 958–965, 2006.

11) P.Ambroza and Lina Kavaliauskienė, Microstructure and properties of the steel subjected to overlaying welding. *Materials Science* Volume 11, No. 1, pp. 14-18. 2005.

12) A Cruz and Rquintana, Characterization of a manganese ore to define its use in the synthesis of fluxes for submerged arc welding. *Welding International*, Volume18 (3), pp. 195–201, 2004.

13) J. Jang, J.E. Indacochea., Inclusion effects on submerged-arc weld microstructure, *Journal of Materials Science*, Volume 2, pp. 689-700, 1987.

14) Ana Ma. Paniagua-Mercado, Víctor M. López-Hirata, Arturo F. Méndez-Sanchezand Maribel L. Saucedo-Munoz, Effect of Active and nonactive Fluxes on the Mechanical Properties and Microstructure in Submerged-Arc Welds of A-36 Steel Plates, *Materials and Manufacturing Processes,* Volume 22, pp. 295-297, 2007.

15) Bendell, A., 1. Disney and W. A.Pridmore, Taguchi Methods: Applications in World Industry, *IFS Publications, U.K*., pp.77-354, 1989.

16) Unal R, Dean Edwin B, Taguchi approach to design optimization for quality and cost: an overview, *Presented at the 13th Annual conference of the international society of parametric analysis*, New Orleans, 1991.

17) Elsayed E.A., Chen, A. (1993), "Optimal levels of process parameters for products with multiple characteristics", *International Journal Production Research*, Volume 31, pp.1117-32.

18) H.L.Tsai, Y.S. Tarng, and C.M. Tseng, Optimization of submerged arc welding process parameters in hardfacing, *International Journal of Advanced Manufacturing Technology,* Vo1ume l2, pp. 402-406. 1996.

19) Y. S. Tarng and W. H. Yang., Application of the Taguchi Method to the Optimization of the Submerged Arc Welding Process, *Materials and Manufacturing Processes,* Volume 13, pp. 455-467, 1998.

20) Tarng Y.S, Juang S. C, Chang C. H., The use of grey-based Taguchi methods to determine submerged arc welding process parameters in hardfacing, *J Mater Process Technology,*Volume 128, pp. 1–6, 2002.

21) Moi S.C., Bandyopadhyay A, Pal PK., Submerged arc welding with a mixture of fresh flux and fused Slag, *Proc National Seminar on Advances in Material & Processing, IIT Roorkee*, 2001.

22) Myers R, Montgomery D, Response Surface Methodology. *Wiley, New York,* NY, 1982.

23) Saurav Datta, Asish Bandyopadhyay and Pradip Kumar Pal, Solving multi-criteria optimization problem in submerged arc welding consuming a mixture of fresh flux and fused slag, *Int J Adv Manuf Technol*, Volume 33, pp. 935–942, 2008.

24) Saurav Datta and Asish Bandyopadhyay and Pradip Kumar Pal, Application of Taguchi philosophy for parametric optimization of bead geometry and HAZ width in submerged arc welding using a mixture of fresh flux and fused flux, *Int J Adv Manuf Technol,* Volume 36, pp. 689–698, 2008.

25) Saurav Datta and Asish Bandyopadhyay and Pradip Kumar Pal, Modeling and optimization of features of bead geometry including percentage dilution in submerged arc welding using mixture of fresh flux and fused slag , *Int J Adv Manuf Technol,* Volume 36, pp. 1080–1090, 2008.

26) Patnaik, A., Biswas, S. and Mahapatra, S.S, An evolutionary approach to parameter optimisation of submerged arc welding in the hardfacing process, *Int. J. Manufacturing Research,* Volume 2, pp.462–483, 2007.

27) W. Troyer and J. Mikurak, Study of Mechanical Properties of Submerged Arc Welds after metal powder addition, *Welding J.,* Volume 53, pp. 494-498, 1974.

28) J. Tanaka, T. Kitada, Y. Naganawa, Y. Kunisada and H. Nakagawa, Element transfer behaviour during submerged arc welding, *Weld. Pool Chem. and Metall. The WI, Cambridge, UK,* Volume 8, pp. 279-288, 1980.

29) M.L.E. Devis, How submerged arc flux composition influence element transfer. *Weld.Pool Chem.and Metall. The WI, Cambridge, UK,* Volume 8, pp. 289-310, 1980.

30) N.D. Pandey, A. Bharti, Effect of submerged arc welding parameters and fluxes on element transfer behaviour and weld-metal chemistry, *Journal of Materials Processing Technology,* Volume 40, 195-211, 1994.

31) N.A. Mcpherson, T.N. Baker, and D.W. Millar, A Study of the Structure of Dissimilar Submerged Arc Welds. *Metallurgical and materials transactions* Volume 29, pp. 823-832, 1998.

32) R. S. Chandel, H. P. Seow, F. L. Cheong, Effect of metal powder addition on mechanical properties of submerged arc welds. *Journal of Materials Science Letters* , Volume 17, pp. 1785-1786, 1998.

33) Abilio Manuel Pinho De Jesus, A Alfredo, S. Ribeiro A Antonio A. Fernandes, Influence of the submerged arc welding in the mechanical behaviour of the P355NL1 steel-part II: analysis of the low/high cycle fatigue behaviours, *J Mater Sci,* Volume 42, pp. 5973–5981, 2007.

34) S. Datta , M. Sundar , A. Bandyopadhyay , G. Nandi , P.K. Pal , S.C. Roy , Effect of process parameters on mechanical properties of submerged arc butt-welding experiments and statistical modeling, *Int. J. of Microstructure and Materials Properties ,* Volume 2, pp. 339-360, 2007.

35) William D. Callister, Jr., Material Science and Engineering: An Introduction, *John Wiley & Sons*, Inc. 2007.